Tools for Comparing ICON EUV Data with Different Ground-based and Space-based Proxies

Satyaki Das

Thesis submitted to the Faculty of the
Virginia Polytechnic Institute and State University
in partial fulfillment of requirements for the degree of

Master of Science
in
Aerospace Engineering

Scott L. England, Chair
Scott M. Bailey
Gregory D. Earle

May 08, 2019
Blacksburg, Virginia

Keywords: ICON, EUV, SSULI, O^+ density, NmF2, HmF2.

Tools for Comparing ICON EUV Data with Different Ground-based and Space-based Proxies

Satyaki Das

ABSTRACT

The ionosphere is the part of Earth's upper atmosphere, from about 60 km to 1,000 km altitude and contains ionized particles and plasma. In this region at about 150 kilometers above the surface of the earth starts the F region and it extends up to 500 kilometers. The Ionosphere is filled with tenuous gases and is a mixture of neutral and charged particles. These winds do not follow any flow pattern and changes with season, the day's heating and cooling, and incoming bursts of radiation from the sun. In order to study the behavior of these ions and understand this complicated region, NASA has developed the ICON mission. The satellite consists of four major instruments which are IVM, EUV, FUV and MIGHTI. This work is concentrated on the EUV instrument which measures the ionized oxygen densities in the F region of the Ionosphere. Different atmospheric model including the IRI and TIEGCM, along with data obtained from ground-based observations and the ICON FUV instrument will be compared to the ionized oxygen profile, NmF2, HmF2 and various other parameters that are obtained from the EUV. The tool developed for ICON EUV instrument is tested using SSULI data and it agrees with the IRI and TIEGCM model.

Tools for Comparing ICON EUV Data with Different Ground-based and Space-based Proxies

Satyaki Das

GENERAL AUDIENCE ABSTRACT

The ionosphere is the part of Earth's upper atmosphere, from about 60 km to 1,000 km altitude and contains ionized particles and plasma. In this region at about 150 kilometers above the surface of the earth starts the F region and it extends up to 500 kilometers. The Ionosphere is filled with tenuous gases and is a mixture of neutral and charged particles. In order to study the behavior of these ions and understand this complicated region, NASA has developed the ICON mission. This work is concentrated on retrieving the data from EUV (Extreme Ultra Violet) instrument and compares the data with previously obtained data to check how consistent it is.

Acknowledgements

I would like to thank Dr. Scott England for his guidance and patience throughout this project. I would also like to give thanks to Dr. Scott Bailey and Dr. Gregory D. Earle for helping me with their inputs throughout my research work.
The SSULI program and the original SSULI data analysis and inversions completed by Dr. Andrew Stephan at the U.S. Naval Research Laboratory were funded by the U.S. Air Force Defense Meteorological Satellite Program.
The ICON Level 2 EUV and FUV data files used in this study were generated for testing purposes and made available by the ICON team. These files do not come from actual flight data. The ICON mission is supported by NASA's Explorer's office through contract NNG12FA45C.

Table of Contents

List of Figures

List of Tables

CHAPTER 1: Introduction to the Ionosphere, its composition, electrodynamics and other features

1.1 Summary

In this chapter a brief description of the Earth’s atmosphere, the ionosphere, different layers of ionosphere and the features of the Ionosphere is discussed including the electromagnetics involved in that region of space and the different incidents that take place in Ionosphere.

1.2 Earth’s atmosphere and the Ionosphere

Earth' atmosphere is divided into five layers based on the height. They are the exosphere, the thermosphere, the mesosphere, the stratosphere and the troposphere (see Figure 1). There is a nonexistent imaginary line at about 100 km above the surface of the Earth where the environment and space meets. This line is called the Kamran line. The troposphere is the layer nearest to Earth's surface. It extends from 4 miles to 12 miles (7 to 20 km) and half of the earth’s air lies in this layer. Above troposphere lies the stratosphere. It starts at 12 miles and finishes around 31 miles (50 km) over the ground. Ozone is found in this layer and it absorbs the harmful Ultraviolet rays from the sun. The air here is exceptionally dry, and this is the place planes and weather balloons fly. The mesosphere begins at 31 miles (50 km) and stretches out to 53 miles (85 km) high. The region in theupper part of the mesosphere is called the mesopause. The thermosphere reaches out from around 56 miles (90 km) to somewhere in the range of 310 and 620 miles. This region in this layer is very warm and temperatures can get up to 2,700 degrees F. Auroras happen in this layer of atmosphere. Charged particles from space collideswith ions and atoms in the thermosphere, energizing them. The particles release the energy by discharging photons of light (Airglow), which we see as the beautiful Aurora Borealis and Aurora Australis.The exosphere, the most expansive layer, is incredibly rarefied and is the place the air overlaps with near-Earth space. It is made out of particles of hydrogen and helium that are non-uniformly distributed across the exosphere

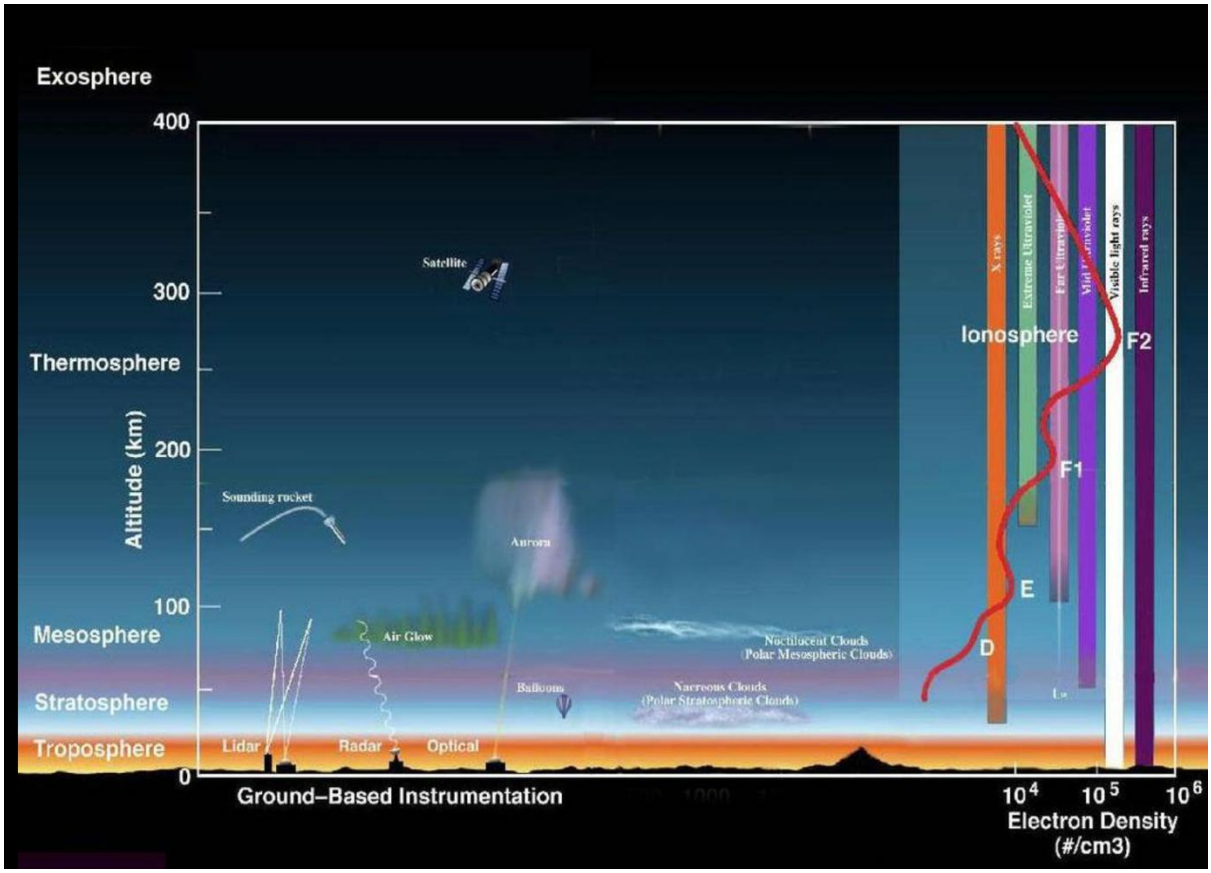

Figure 1: The Earth's atmosphere and different layers of it. The image is published by NASA on January 2013. (https://www.nasa.gov/mission_pages/sunearth/science/atmosphere-layers2.html)

At a specific altitude range, the earth's atmosphere is filled with ions, atoms and charged particles. This layer of the atmosphere is called the Ionosphere. In this region of space, X rays and Ultraviolet rays from the sun interacts with the particles and ions present. A portion of these release electrons free from the neutral particles, making electrically charged (particles or atoms with missing electrons) ions and free electrons. These electrically charged particles and electrons move uniquely in contrast to the more abundant, electrically neutral particles. There are three principle layers of the ionosphere (see Figure 2), called the D region, the E region, and the F region. These regions do not have sharp limits, and the elevations at which they are found shift over the span of multi day and from season to season. The D regionbegins around 60 or 70 km (37 or 43 miles) over the ground and stretches out upward to around 90 km (56 miles). Next is the E region, beginning at around 90 or 100 km (56 or 62 miles) up and reaching out to 120 or 150 km (75 or 93 miles). The highest piece of the ionosphere, the F region, begins around 150 km (93 miles) and stretches out up to 500 km (311 miles).The density of ionized particles, and even the presence of the distinctive regions of the ionosphere differs with time. The ionosphere is altogether different in the daytime versus night. Amid the day, X-rays an UV light from the Sun energized particles and atoms which releases the energy in the form of electrons, creating a persistent supply of particles and free electrons. In the meantime, a portion of the particles and electrons impact and recombine to produce electrically unbiased ions and atoms. During the day, a larger number of particles are made than are destroyed, so the quantity of particles in the three areas increments. Around evening time, the recombination procedure

takes over without daylight, and the quantity of particles drops. Through the span of most evenings, the D region vanishes completely, and the E regiondensity decreases. Every morning, as sunlight-based X-beams and UV light return, the D and E regions are repopulated with particles. The F region sticks around for the duration of the night, yet by and large parts into an upper F2 region and a lower F1 region during the day.

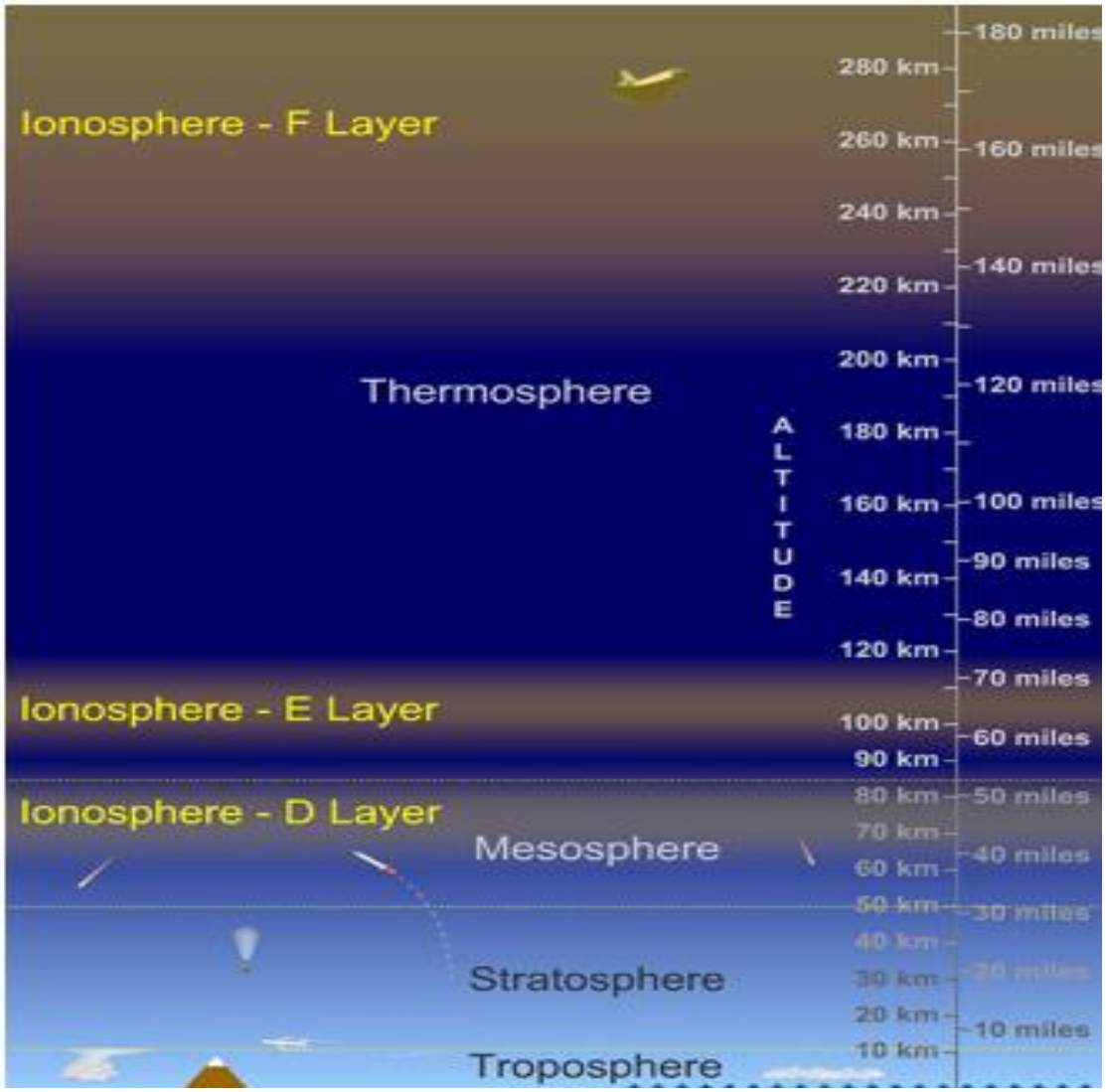

Figure 2: Different regions of the Ionosphere. The image is published by Randy Russell, UCAR (https://scied.ucar.edu/ionosphere).

The ionosphere regions can ingest or host radio signs, or they can twist radio waves, just as mirroring the signs as depicted previously. The particular conduct relies upon both the recurrence of the radio flag just as the attributes of the ionosphere regions included. Since Global Positioning System (GPS) satellites utilize radio signals, the precision of GPS can be seriously diminished when those signalsare modified as they go through ionospheric regions. So also, some radio energy interchanges with the ionosphere and can be disturbed if the frequency utilized is one that an ionosphere layer affects or absorbes completely, bringing about a debilitated or even all out loss of signal. Researchers continually measure and produce

models of the consistently changing ionosphere with the goal that individuals responsible for radio interchanges can foresee interruptions. Researchers also utilize radio waves in different approaches to test and screen the generally difficult to detect ionosphere. Different radarsand receivers, on the ground and on satellites, are utilized to screen the always changing ionosphere. Whether receiving natural signals from near-earth space, or using a transmit-receive system, a variety of radars are used to study the ionosphere. Alongside the day by day changes in the ionosphere, there are likewise occasional and longer-term varieties too in the different regions of the Ionosphere.

The following sections will detail aspects of the ionosphere, and ionospheric observations that are relevant to the work in this thesis.

1.2.1Height profile of Ionospheric state parameters

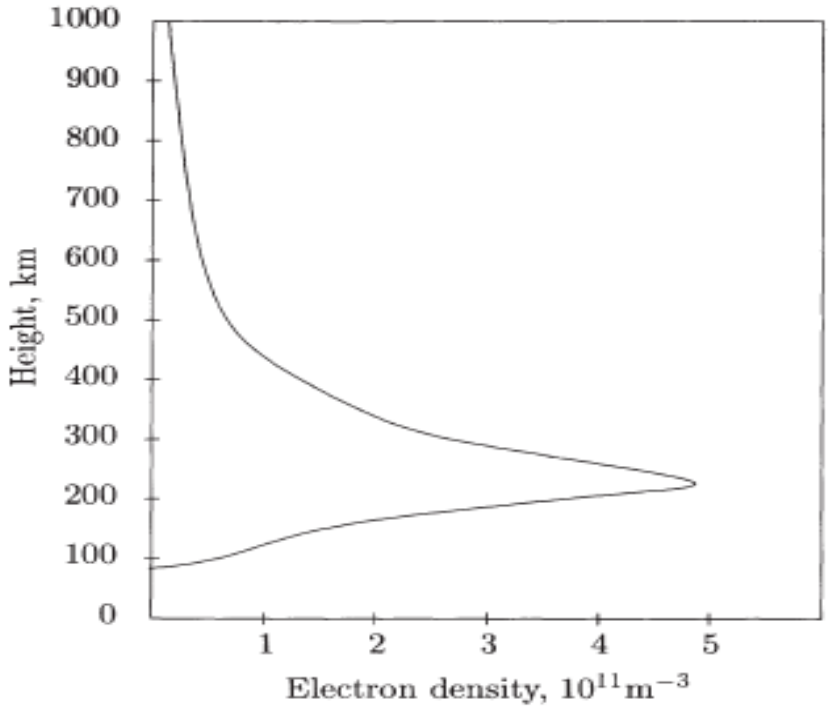

Figure 3: The above figure shows how the electron density varies with height in the Ionosphere. The image is taken from the book 'Physics of the earth and space environment' by Gerd W Prolss.

Figure 3 shows how the electron density varies with height for a day with low solar flux. In this particular case, the peak density is located at a height of about 240 km, and the value of the same is about $5 \times lO^{11}$ particles per m^3, has a thickness of about 120 km. Here, the peak

density of the profile is termed as NmF2 and the corresponding height is called as HmF2.From
figure 3 we can infer the ion density from the electron density. The ionosphere consists of a quasi- neutral mixture of species that can be ions or electrons. And total number of the positive ions in always equal to the total number of negatively charged ions.

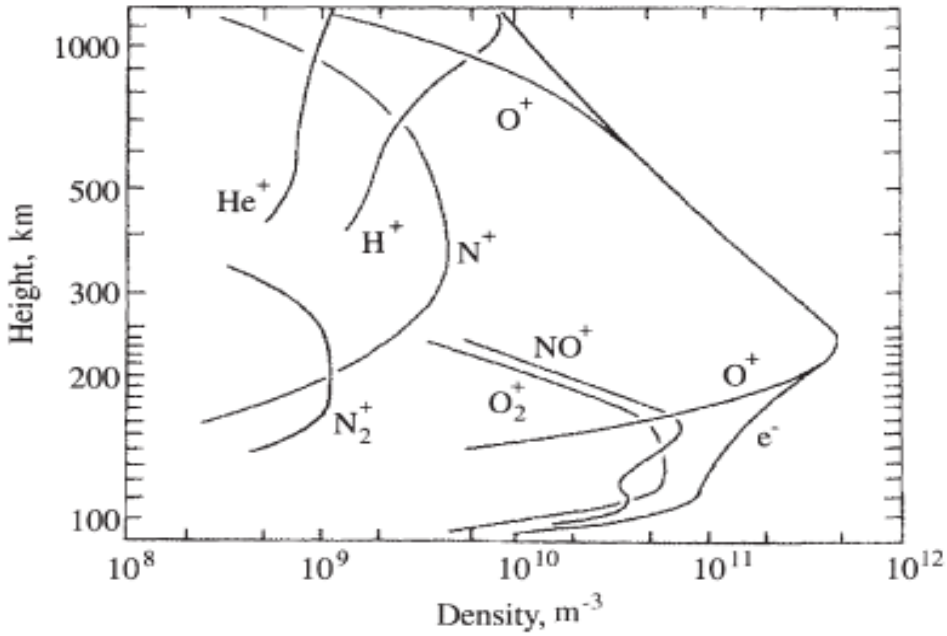

Figure 4: The above graph shows how the density varies with height for different species in the Ionosphere (Johnson et. al, 1966)

The ionic structure of the ionosphere is appeared in Fig. 4. The electron thickness profile (e-) compares to that of Fig. 3, then again, actually now the layer structure of the conveyance is not as simple to perceive with the logarithmic portrayal. It is seen that the sub-atomic particles O_2^+ and NO^+ command in the lower ionosphere, which is positively amazing for the instance of the NO^+ particles. In the district of the most extreme and in the upper ionosphere, the essential particle is O+, which appears to be sensible in perspective on the predominance of thermospheric nuclear oxygen in this district. Again, astonishing are the nonattendance of bigger He + densities and the immediate change from O^+ to H^+ as essential particle in the upper ionosphere. The lower district of the ionosphere ruled by O_2^+ and NO^+ particles is indicated the E region; the nuclear oxygen particle area over this is known as the F region. Proceeding with upward, we come tothe locale of predominant H^+ particles, the plasmasphere, which, maybe to some degree subjectively, isn't considered as a component of the ionosphere. At long last, following the letters in order, the lowermost locale of the ionosphere, where bunch particles and negative particles assume a vital job, is signified the D region.

1.3 Electrodynamics in the low and middle latitude Ionosphere

According to Heelis et. al (2004), The ion number density changes with altitude as shown in Figure 5. Even though the peak density is a function of the latitude, there is significant contrast between daytime and nighttime profile of the same. During daytime there are two peaks of ion density, one in the E region and the other in the F region of the Ionosphere. These peaks are driven by ionization balance by chemical losses and diffusion.During night time, due to chemical losses the E region peak reduces significantly but downward diffusion helps to maintain the peak in F region.

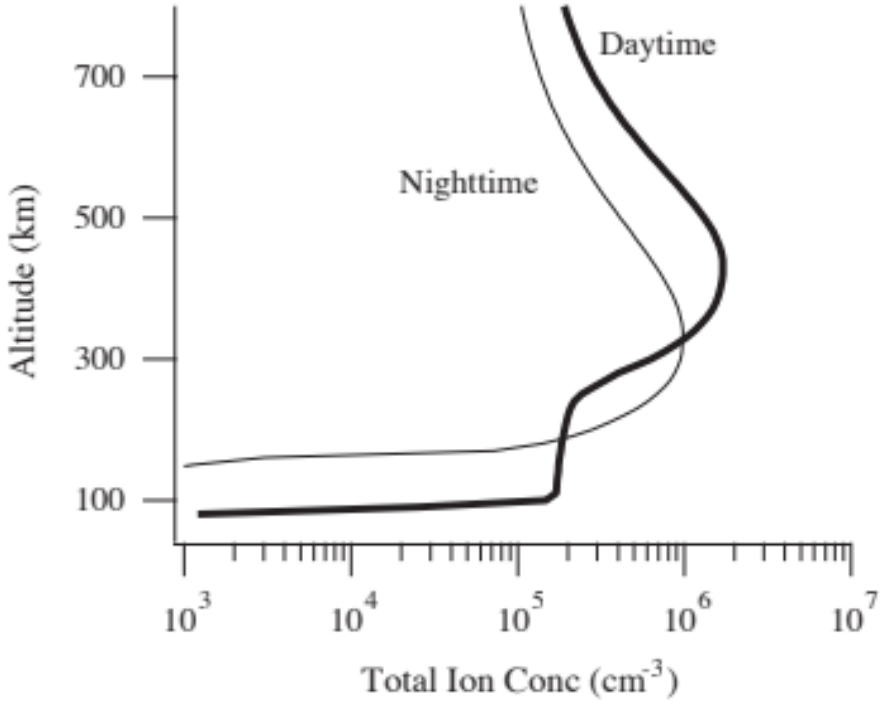

Figure 5: The above figure shows how the density varies in the atmosphere with altitude during the day and night. The image is taken from the book 'Physics of the earth and space environment' by Gerd W Prolss.

Figure 6 shows how the dipole latitude varies with altitude in the Earth's atmosphereand the region we will consider, which is definedby the dipole magnetic field. The lowerboundary in this region is chosen at an altitude where the ion density is negligible. The outer boundary is selected in such a way that it contains all the latitudes we wish to include and is defined by dipole magnetic field. The neutrals and charged particles in this region contain ionized magnetic plasma and any force that produces relative motion between the ions and electrons will drive a current. In this region the current is driven by four major factors. They are 1) collisions with neutral particles. 2) Electric fields. 3) Lorentz force. 4) Partial pressure gradients.

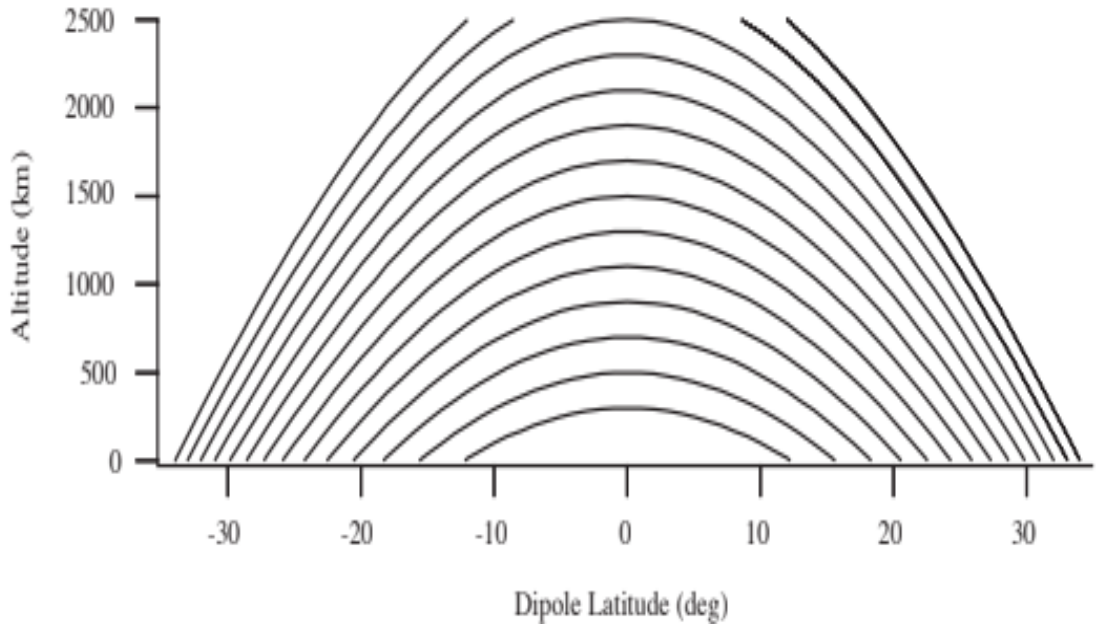

Figure 6: The above figure shows how the dipole latitude varies with altitude in the Earth's atmosphere. The figure is taken from Heelis et. al (2004)

This Ionosphere is filled with closed magnetic fields that penetrates through the region where there is negligible number of ions and thus current cannot flow.The current generated due to the forces described above electric fields needs to be divergence free. To fulfil this requirement electric fields are produced in this region. At higher latitudes, the ions move perpendicular to the wind and the magnetic field, with a small magnitude. They movein the direction of the wind at lowaltitudes.Even though the electrons move in the direction of E×B above 100 km, the ions move towards the direction of E×B at higher altitudes and in the direction of electric fields at low altitude.

The ionosphere in the low and middle latitude region possesses neutral wind motions. These motions are driven by tidal oscillations that propagatefrom below (Forbes, 1995) and by in situ heating.Tidaloscillations are influenced by the absorption of solar radiation in thestratosphere. These oscillationsplay a significant role to drive the neutral atmosphere motions inthe E-region. The upper atmosphere absorbs EUV solar radiations and it produces in situ winds in the F region of the ionosphere. The charged particles in this region is dominated by diffusion along the magnetic field lines. Figure 7shows the block diagram that explains the E and F region dynamo. The concentration of ions and neutrals determine the determine the conductivity in the E region.In the F-region, due to the transportation of plasma along the magnetic field lines, the conductivity and winds of the ionosphere is changed.

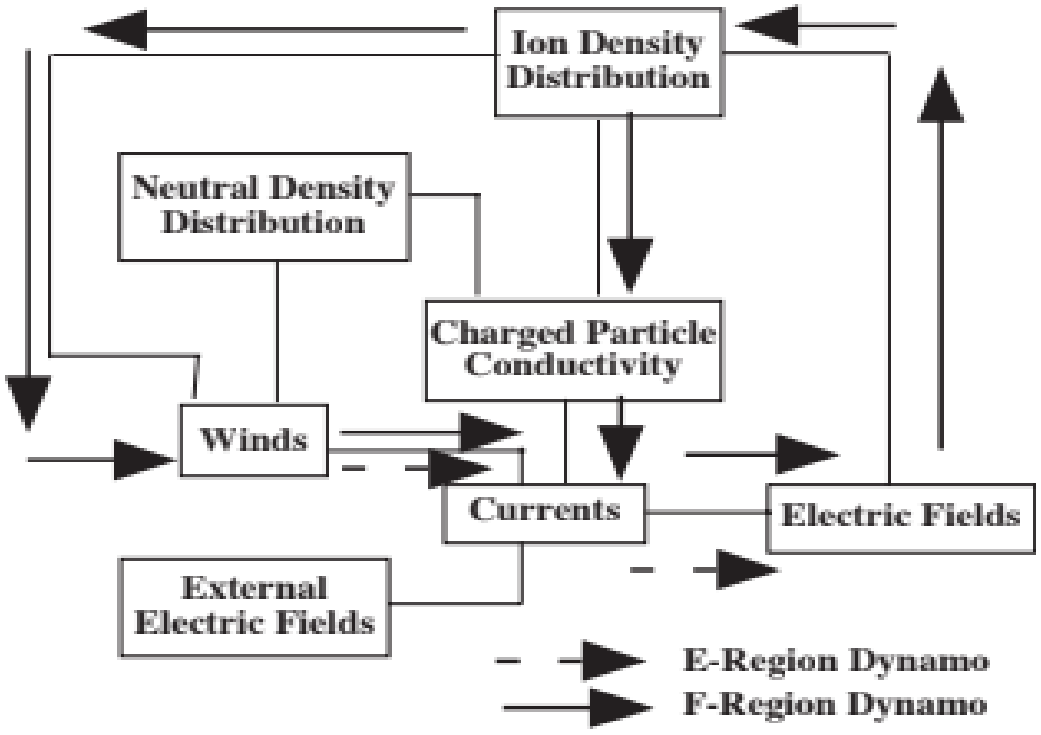

Figure 7: The above figure is a block diagram that explains the E and F region dynamos. The figure is taken from Heelis et. Al (2004)

1.3.1 F region dynamo

According to the same Heelis publication, (Heelis et. al, 2004), “in the low-latitude F-region meridional winds havea dominant component parallel to the magnetic fieldand do not drive a current. Remember that inthe F-region the Hallconductivity is negligible. Zonalwinds, which are predominantly perpendicular to the magnetic field, thus drive a current perpendicular tothe wind and the magnetic field. Near the equator thiscurrent is almost vertical. Fig. 8 illustrates the winddriven current in the Fregion and the E-region closurecurrent that will result from any divergence in the F-regioncurrent. Dashed lines illustrate field-aligned currents thatcomplete the current loop.

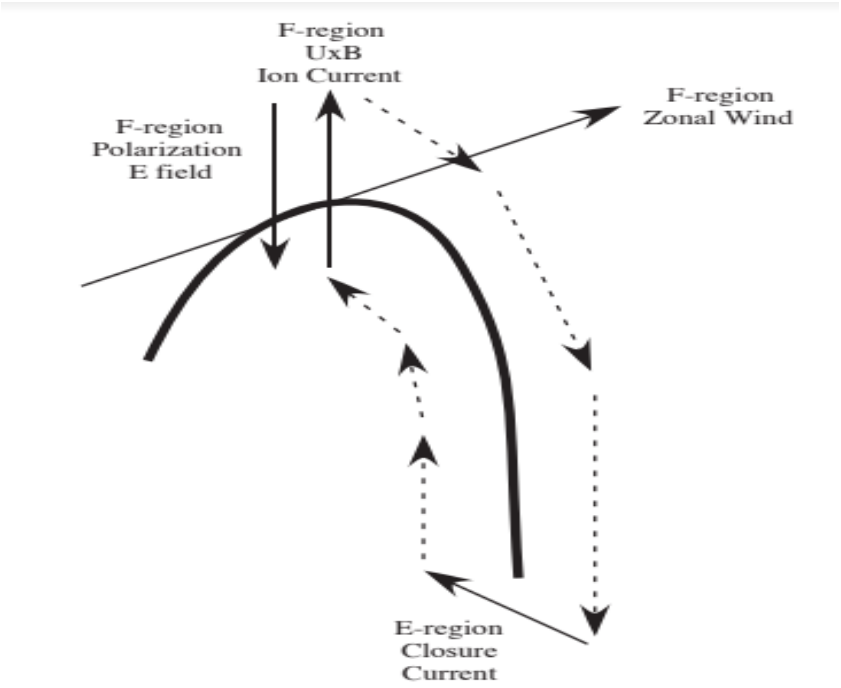

Figure 8: The above figure shows how current loops is driven by zonal neutral winds in the F region.The figure is taken from Heelis et. al (2004)

In the daytime when the E-region Pedersen conductivity is so much larger than the F-region Pedersenconductivity the polarization field from this source is negligible. However, during the nighttime when the E-regionPedersen conductivity is essentially zero, the polarization field is directly proportional to the F-region dynamo wind.The polarization field is created by a divergence in theF-region current that results from altitude gradients in the flux-tube integrated Pedersen conductivity. Fig. 9 showsthe local time distribution of the F-region zonal wind,which we assume is constant with altitude and latitude,andschematic distributions of the flux-tube integrated Pedersenconductivity as function of flux tube apex height for typicaldaytime and nighttime conditions. Signs on the nighttimeprofile indicate where polarization charges will accumulateto create the electric field. This electric field will produce adominant E × B zonal drift of the charged particles in theF-region. Furthermore, we see that the polarization field willbe the largest during the nighttime, when the E-region conductivity is smallest. Thus, eastward nighttime drifts in theF-region will be larger than expectations based on consideration of the E-region dynamo winds only (Rishbeth et.al, 1971b).Inclusion of the F-region dynamo therefore resolves one ofthe problems eluded to earlier but does so by consideringonly the polarization field in the magnetic meridian.”

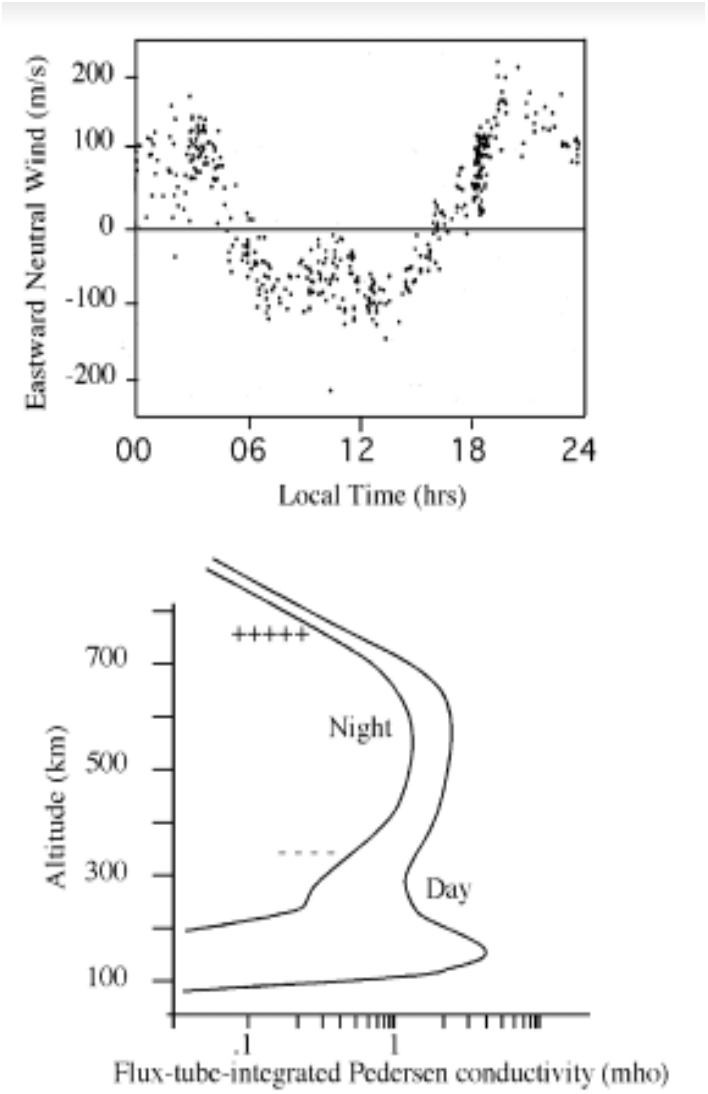

Figure 9: The figure shows the local time distribution of the F-region zonal wind (Wharton et. al, 1994)

Due to the polarization electric fields are created and it will dominate in the low and mid latitude regions. Component of the electric field in the magnetic meridian may drive currents in the E-region andgradients in these currents can change the polarization electric field.

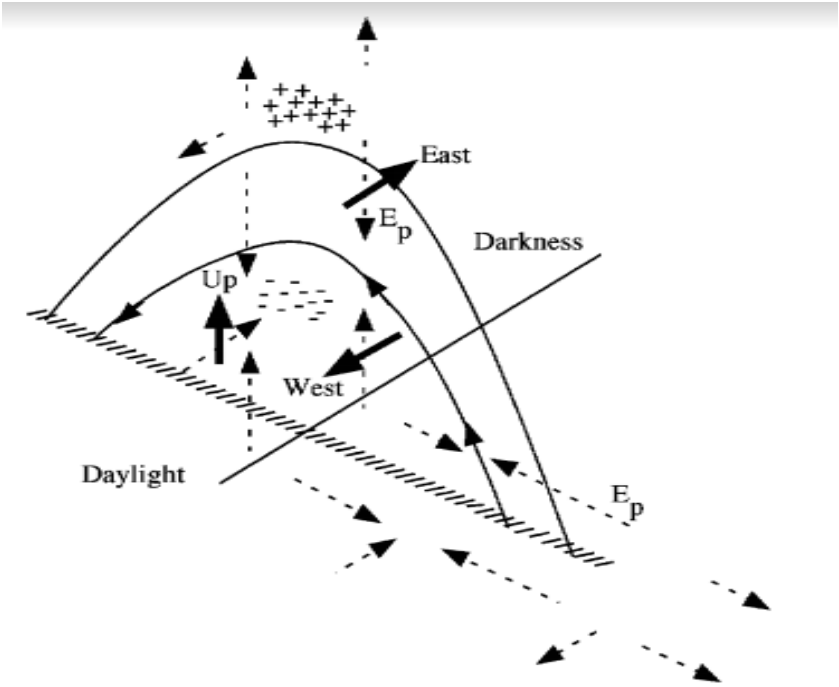

Figure 10: The above figure shows the Polarization charges and associated electric fields resulting from an eastward zonal wind in the F-region. The figure is taken from Heelis et. al (2004)

According to Heelis et. al (2004), "we illustrate the configuration of electric fieldsand currents that result from the F-region dynamo process in figure 10.In order to do this, we confine our attention to the dusk terminator where a large gradient in the conductivity of theE- and the F-regions will exist. Across this region we assume for simplicity that the F-region neutral wind blows at aconstant velocity to the east and we assume that the E-regionwinds are zero. The dashed arrows indicate the configuration of the electric field produced only the original F-regiondynamo. These fields are shown in the middle and lowerF-region and mapped to the E-region. The heavy arrows denote the direction of E × B drifts in the F-region producedby these electric fields. The most important features to noteare the nighttime eastward drift in the middle F-region andthe accompanying westward drift at lower altitudes. Thesefeatures are seen in observations (Coley and Heelis, 1989;Eccles et al., 1999), and reproduced in computational models (Heelis et al., 1974; Eccles, 1998b). Prior to sunset a vertically upward E ×B drift is produced in the lower F-regionwhich when combined with the eastward and westward driftscomprises the so-called "evening vortex". This vertical driftmay also account for the pre-reversal enhancement that isapparent in the observations of Fig. 11. The largest polarization field is the meridional field, which is established aftersunset and labeled Ep. The fields appearing before sunsethave been termed fringing fields by Rishbeth et. al (1971b) andEccles et. al (1998a). We should be aware however, that we havenot considered the modification of the field that can takeplace when the mapped field drives currents in the E-regionthat must also be divergence free. If we assume, for simplicity that the Hall conductivity dominates completely in thisregion, then the meridional polarization field drives a zonalcurrent across the terminator. If this current is not continuousthen polarization charges will accumulate at the terminator."

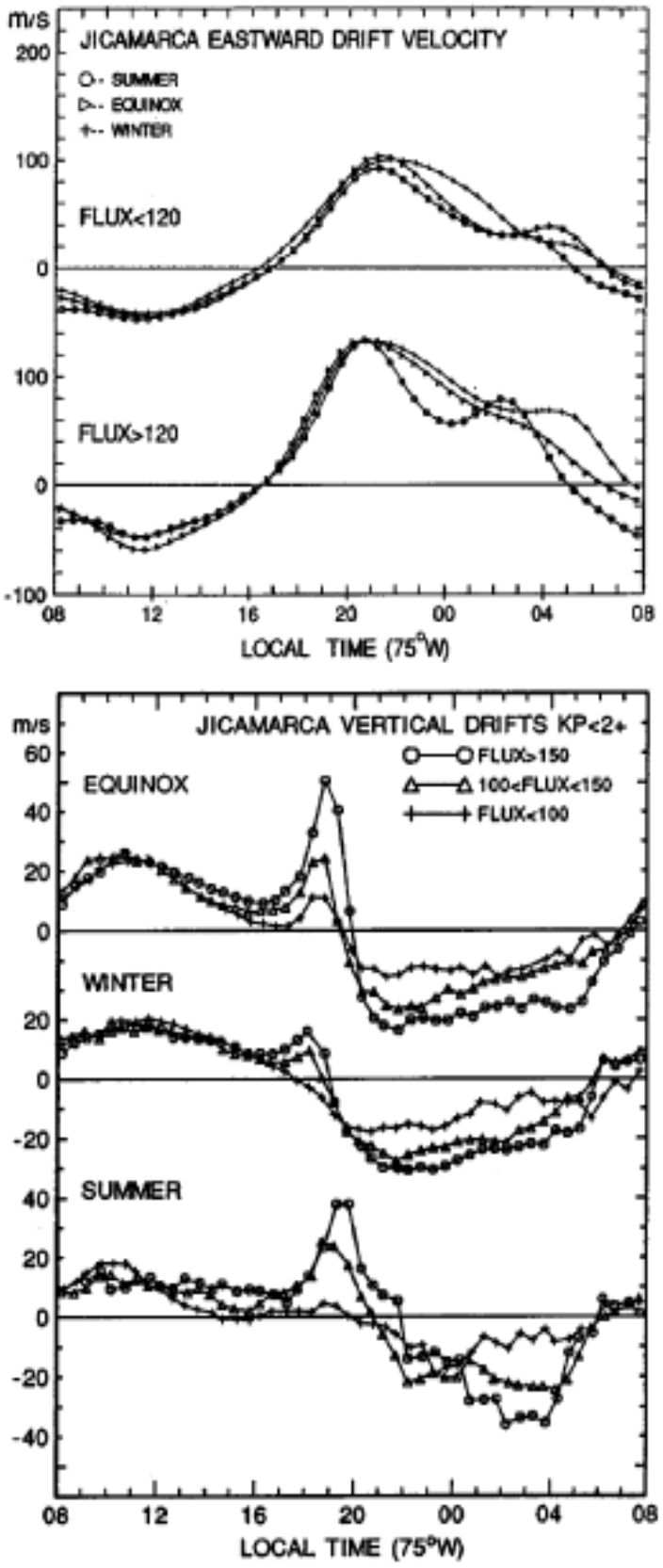

Figure 11: The above figure shows how the zonal drifts(upper panel) and vertical drifts (lower panel) change with local time observed at the equator by the Jicamarcaradar (from Fejer et al., 1991).

1.4 F-layer O^+ Airglow

Airglowis a faint emission of light by a planetary atmosphere. Due to the airglow, the atmosphere of the Earth is never completely dark even if there was no stars or diffused light from the sun.There are various reasons why airglow is produced in the Earth's atmosphere such as the recombination of atoms which were photoionized by the Sun during the day, luminescence caused by cosmic rays striking the upper atmosphere, and chemiluminescence. Due to the sunlight these airglows are not visible during the day.

Airglow at night may look bluish to the observer. Airglow emission is fairly uniform across the atmosphere even though it appears brightest at about 10° above the observer's horizon,.

Figure 12: The figure shows airglow in different layers of the Ionosphere (Courtesy: NASA).

As per the information given in Stephan et. al (2016), "measurement of atmospheric extreme and far ultraviolet (EUV/FUV) airglow is advantageous for space-based remote sensing of Earth's ionosphere and thermosphere in that absorption by molecular species in the lower thermosphere eliminates background terrestrial glow from lower atmospheric regions and isolates the measured emissions to those coming from within the upper atmospheric region of interest. For the *F* region of the ionosphere (100–500 km) these measurements focus on emissions related to the O^+ ion, which closely approximates the total plasma density in this altitude range. At night, photons produced by recombination processes are directly correlated to the species content (Meier et. al, 1991). In sunlit regions, those emissions are either overwhelmed by or intertwined with solar- driven sources.This paper presents results using the O^+ 83.4 nm feature to infer the daytime ionosphere. This feature consistsof a closely spaced

triplet (vacuum wavelengths 83.2759, 83.3330, and 83.4466 nm (Martin et al., 1993)), sharing a common singlet lower (ground) state and a triplet upper state ($2p^4{}^4P \rightarrow 2p^3{}^4S$). The primary source ofthis emission is photoionization of an inner shell electron of atomic oxygen by solar EUV ($\lambda < 43.6$ nm), leaving an O+ ion in an excited state which then returns to its ground state,along with the emission of an 83.4 nmphoton. Photoelectron impact ionization of O is a secondary source that contributes on the order of 10% tothe total column emission (Cleary et al., 1989; Meier, 1991). While the production of 83.4 nm photons fromthese two sources peaks in the lower thermosphere, below 200 km, these photons subsequently undergomultiple resonant scattering by O+, the predominant ion within the F region of the ionosphere. The resultis a measured altitude profile of the 83.4 nm emission that, when viewed from above the ionosphere andtoward Earth's limb, depends in part on the O+ ion density or equivalently the electron density in the F regionof the ionosphere. Direct scattering of solar 83.4 nm photons contributes a small amount to the measuredprofile above ~400 km, but this source has been shown to be largely insignificant for most ionospheric measurements (Feldman et al., 1981; Meier, 1990).The ion concentration in the F region of the ionosphere is 95% O^+ such that measures of O^+ are effectivelyequivalent to electron densities in that region ($O^+(z) = n_e(z)$). While this leads to the interchangeable use of"ions" and "electrons" in the description of this algorithm, it is reiterated that the radiation transport is entirelythrough the ion (O^+) population. The electron density is most simply parameterized in functional form as aChapman layer by:

$$n_e(z) = N_m \exp\left(\alpha\left(1 - \frac{(Z - Z_m)}{H} - \exp\frac{-(Z - Z_m)}{H}\right)\right)$$

where ne is the density as a function of altitude Z, Nm is the peak electron density, α is currently set equal to 0.5 but could be adjusted as a separate scaling factor in the set of model parameters, Zm is the altitude of thepeak electron density, and H is the topside scale height. It is these three Chapman parameters, Nm, Zm, and H,that are adjusted in the forward model in order to provide the match to the measured profile and that specifythe electron density profile that is returned by the algorithm."

1.5 Prior results

In this section of the chapter we will look at some of the results obtained by previous missions and then see the results obtained by the SSULI instrument in chapter 3.

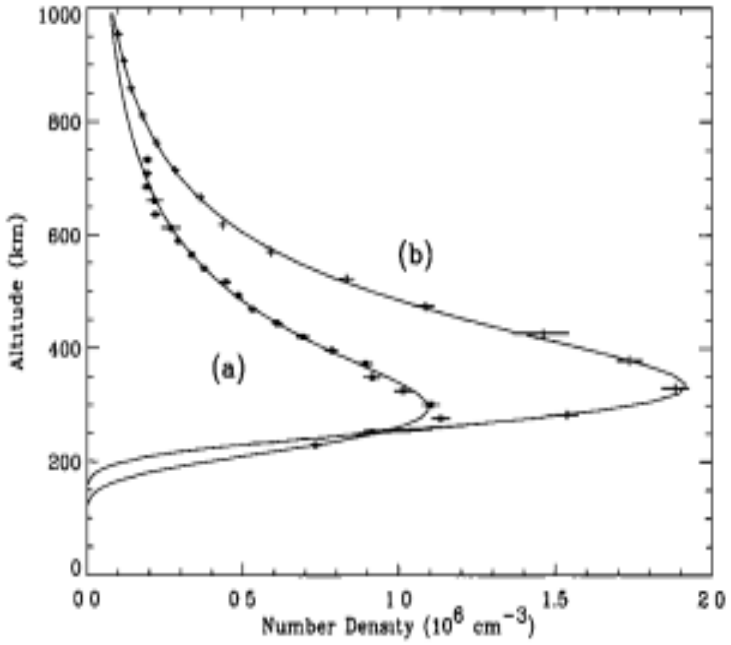

Figure 13: The above graph shows the variation of O^+ density with altitude for a) 13.99 UT and b) 17.25 UT. The data is collected from the Millstone Hill incoherent scatter radar from March 18, 1990.

It can be observed from figure 13 that plot (a) is taken during the afternoon period and plot (b) during the sunset. The peak density is much higher during sunset compared to afternoon and the height in which it occurs also rises up. We will learn more about this trend in the third chapter where we can see similar observation for the SSULI data as well and look into some of the reasons behind this feature.

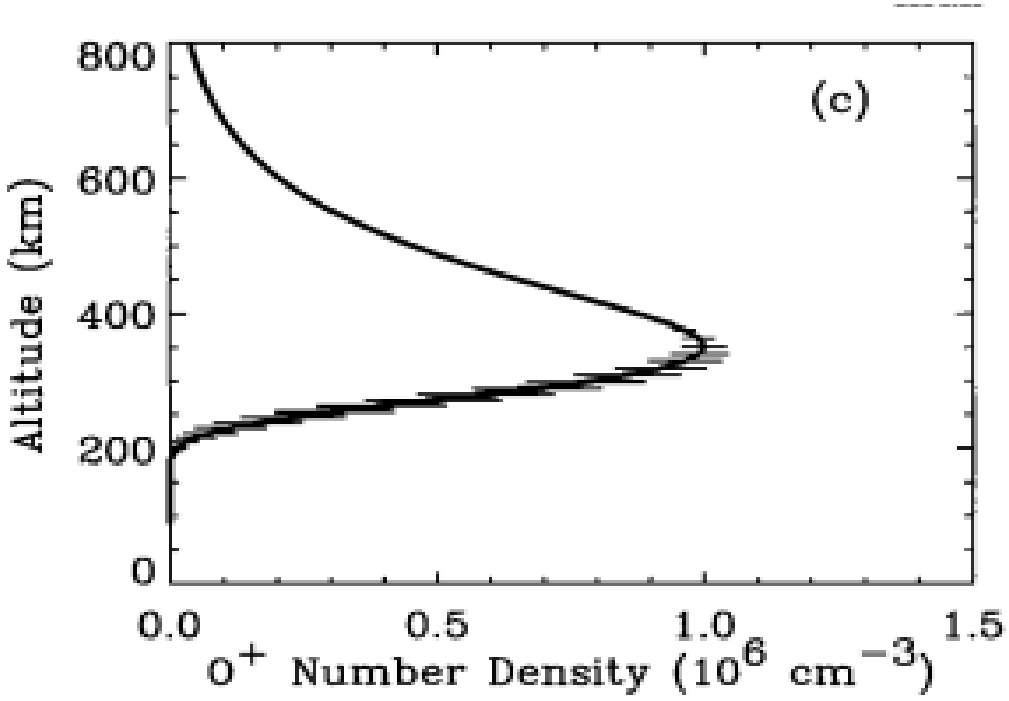

Figure 14: The above graph shows the variation of O^+ density with altitude for Zmax= 350 km. The data is collected from DIT retrieval of chapman layer. (Picone et. al, 1997).

Figure 14 is quite similar to the profile we got in figure 13. Though the peak density matches with plot (a), the height at which it occurs (HmF2) is different. There can be several reasons behind it. The solar flux may be different between the two days or the time when the data is taken is different that led to a different value of HmF2.

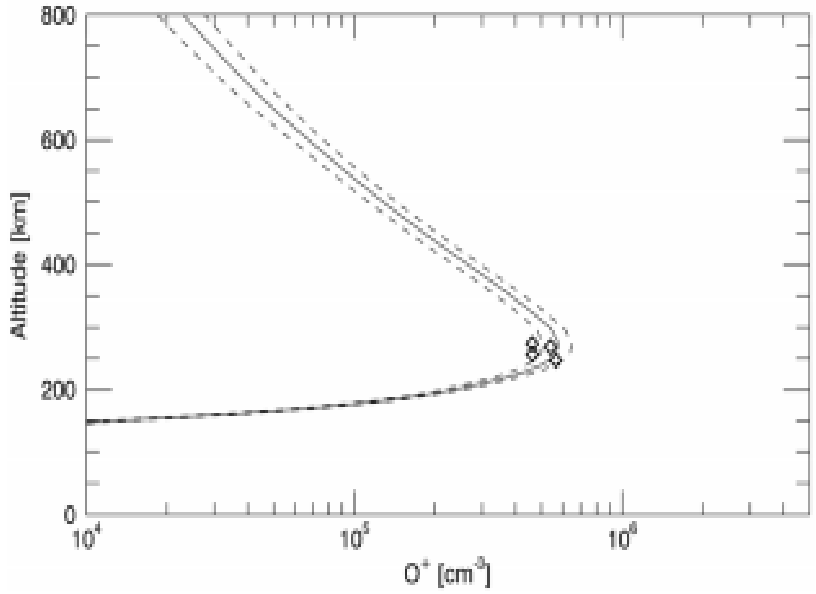

Figure 15: The graph shows the variation of O^+ density with altitude. The data is collected from SSULI instrument of DSMP F19 satellite on September 6, 2014(Stephan et. al, 2016)

Out of the three results discussed above, the peak density value of O^+ ion (NmF2) is the lowest and so as the HmF2. One reason behind this can be the data is taken much before the time afternoon period which caused the NmF2 and HmF2 values to be less. A lower solar flux value can be another reason behind it.

In chapter 2 we will discuss about the methods we have developed to retrieve data from ICON EUV instrument and in chapter 3 we will see how the method works to read SSULI data and compare it with different space-based models. This chapter will also give us a glimpse of whether the SSULI data behaves similarly with the results discussed in chapter 1 or not.

CHAPTER 2: Methods and tools to retrieve and validate the ICON EUV data

2.1 Summary

In this chapter a brief description of the methods used to develop the algorithm and code that will retrieve the data from ICON EUV (Extreme Ultraviolet) instrument is discussed. Also, a brief description about the IRI (International Reference Ionosphere) model and TIEGCM (Thermosphere Ionosphere Electrodynamics General Circulation Model) and FUV (Far Ultraviolet) instrument is discussed along with the methods used to retrieve the data from them and compare those with the data obtained from the EUV spectrometer, in order to help validate early results from ICON mission.

2.2 EUV spectrometer: Instrument, observation and geometry of observed data from the instrument

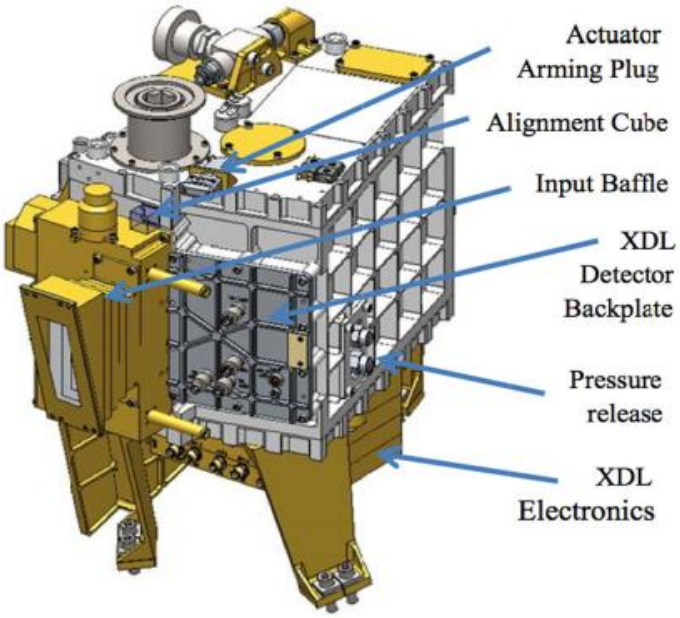

Figure 16: ICON EUV spectrometer after, Sirk et. al (2017)

The ICON EUV instrument is a 1-dimensional spectrometer (Bowyer et. al 1997) which measures the ionized oxygen density (O^+ 61.7 and 83.4 nm of wavelength) and Helium 58.4 nm line in the ionosphere of earth's atmosphere. The instrument is required to measure the 58.4 nm line to differentiate this wavelength of light is different from the 61.7 nm wavelength. The instrument design is based on heritage of four UC_Berkeley 'EURD-class' astrophysical space flight instruments and consists of an entrance aperture, a diffraction grating and a micro-

channel plate (MCP) detector. The instrument is a 1-dimensional spectrometer and builds up a 2-dimensional image of the sky. At a specific time, the EUV spectrometer captures the vertical profile of the sky it is looking at that point of time. As the captured image is one dimensional, it is called 1D spectrometer. Even though the EUV captures the vertical profile of the sky it is looking at, over the time it captures several such vertical profile and hence adds one more dimension to the image. Hence, it captures 2D image of the sky. The instrument takes data every 12 seconds and does not operate during the night. EUV takes readings from 72 different altitudes for every time step. There are total around 2630 time-steps in a day and observes the HmF2, NmF2, ionized oxygen density for every time step over 72 different altitudes.The complete description of the EUVinstrument is provided in theSirk et al. (2017),and the retrieval method is described by Stephan et al. (2017a).

2.3 EUV data content

The simulated EUV Level 2 data file which is being used for my research contains simulated data in order to test our code developed in IDL programming language. The data contains all the necessary variables that are used to retrieve the EUV data. A list of the different parameters that are used to analyze the EUV data are given below:

1) **icon_l2_euv_daytime_op_ut_sec**: This variable in the EUV data file tells us the universal time when the measurement is taken.
2) **icon_l2_euv_daytime_op_retrieval_latitude**: This variable indicates the geographical latitude of the measurement.
3) **icon_l2_euv_daytime_op_retrieval_longitude**: This variable indicates the geographical longitude of the measurement.
4) **icon_l2_euv_daytime_op_retrieval_altitude**: The variable gives the altitude at which the measurement is taken.
5) **icon_l2_euv_daytime_op_retrieval_oplus**: The variable gives the density of O^+ ion corresponding to the altitude at which the measurement is taken.
6) **icon_l2_euv_daytime_op_retrieval_NmF2**: The variable indicates the highest density of O^+ at a certain point of time.
7) **icon_l2_euv_daytime_op_retrieval_HmF2**: The variable indicates the height in which the highest density of O^+ occurs at a certain point of time.
8) **icon_l2_euv_daytime_op_retrieval_sza:**This variable in the EUV data file tells us the solar zenith angle when the measurement is taken.

The EUV spectrometer takes around 2630 measurements over a day. As the instrument does not work during the night, the data is obtained only during the daytime. The EUV instrument takes measurements from 13 degrees S to 44 degrees N when the spacecraft is in its normal orientation. For every timestep of EUV data, 72 brightness measurements are measured corresponding to the 72 different altitudes. Change in timestep results in change in position of the spacecraft and thus the latitude and longitude of measurement also changes. A forward model is used and iteratively adjusted to calculate the value of O^+ densities (Stephan et. al, 2017a) until the output produces the best match to the ICON EUV measurements. The initial

volume excitation of the 83.4 and 61.7 nm emissions by solar photoionizationof atomic oxygen in the lower thermosphere, the number of excitations per second per atom,is calculated. Theforward model calculates this excitation at a discrete set of altitudes, that are then usedto complete the radiative transfer and absorption calculations, and the integration along theline of sight.This volume emission rate field is then used to integrate along the line of sight and calculate the measured emission intensity. This emission intensity is being used to calculate the O^+ density at a particular altitude.

2.4 Comparison of EUV data with IRI and TIEGCM models

In this section, the data obtained from the simulated EUV LEVEL 2 data files are represented through different plots and graphic charts and compared with different models such as IRI and TIEGCM.

2.4.1 EUV data content

In order to write the code that will retrieve the data from the EUV instrument, a simulated data file was created which contains one day of data. The plots generated from the simulated EUV data are given below.

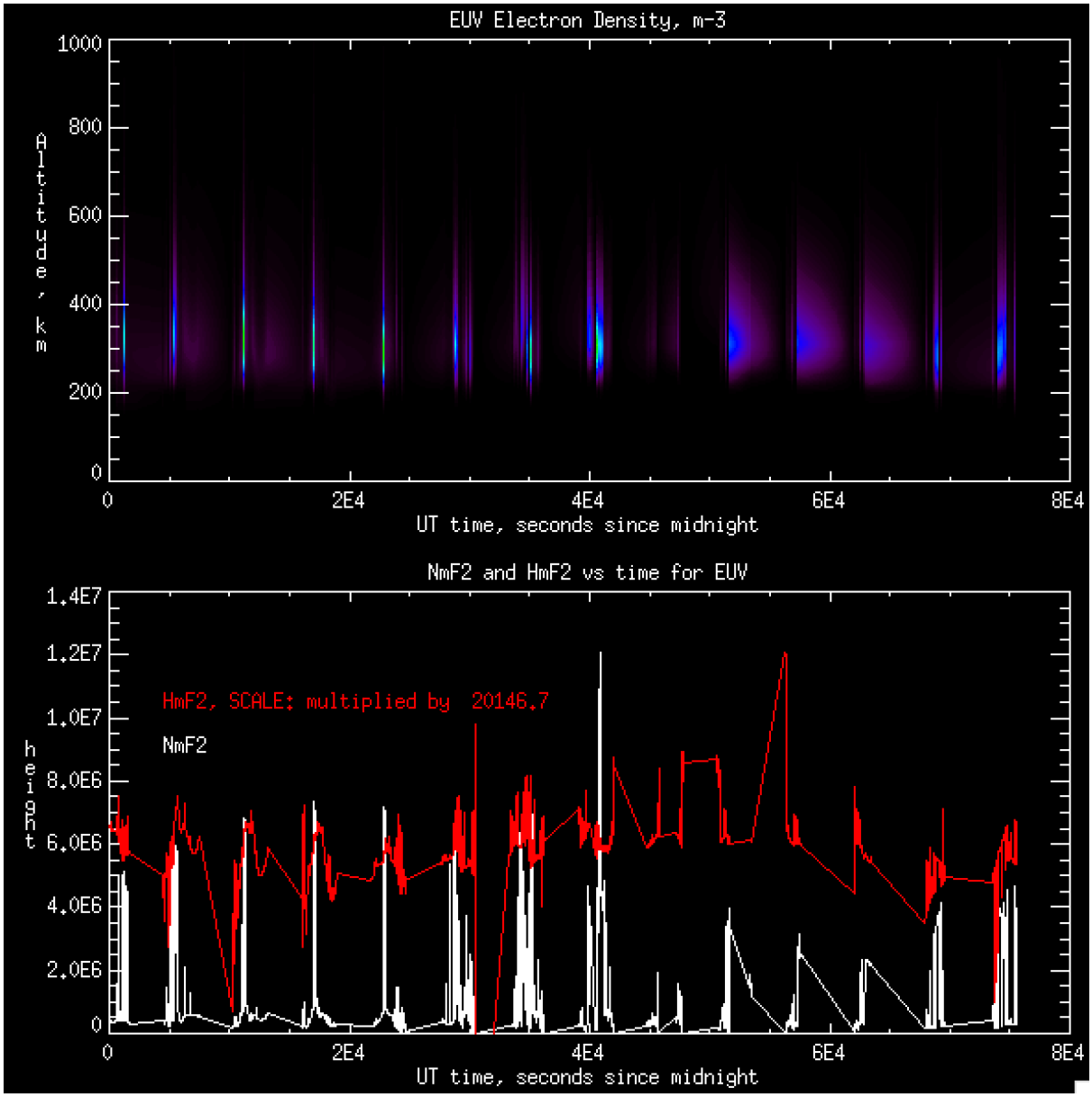

Figure 17: The first plot in the figure shows a contour plot of how O^+ density varies with altitude and time for a single day. The second plot shows the variation of HmF2(in red) and NmF2with time. The HmF2 is being scaled by a factor of 20146 to put it on the same axis.

2.4.2Comparison of EUV data and IRI data

In this section, the data obtained from EUV is compared with IRI model to check how consistent the data is. Again, for the comparison we have divided the data into two parts. In the first part, we took the data from one orbit. In the second part we included data from all the seven days.

2.4.2.1IRI model geometry and algorithm used to compare IRI data with EUV data

The International Reference Ionosphere (IRI, Bilitza et. al, 2001) is a worldwide undertaking supported by the Committee on Space Research (COSPAR) and the International Union of Radio Science (URSI). These associations shaped a Working Group in the late sixties to create an experimental standard model of the ionosphere, in view of every single accessible datum sources sanction. A few consistently improved versions of the model have been discharged. For given area, time and date, IRI depicts the electron thickness, electron temperature, particle temperature, and particle sythesis in the elevation run from around 50 km to around 2000 km; and furthermore the electron content. It gives month to month midpoints in the non-auroral ionosphere for attractively calm conditions. The real information sources are the overall system of ionosondes, the amazing disjointed dissipate radars (Jicamarca, Arecibo, Millstone Hill, Malvern, St. Santin), the ISIS and Alouette topside sounders, and in situ instruments on a few satellites and rockets. IRI is refreshed yearly amid uncommon IRI Workshop, e.g., amid COSPAR general get together). More data can be found in the workshop reports. A few augmentations are arranged, including models for the particle float, depiction of the auroral and polar ionosphere, and thought of attractive tempest impacts. Electron density, electron temperature, ion temperature, ion composition (O^+, H^+, He^+, NO^+, O^+_2) and ion drift are some of the outputs of the IRI model.

In order to retrieve the data from the IRI-2007 model, there nine inputs that we need to provide and those are year, day of the year, utsecs, geographic latitude, geographic longitude, jmag, F107A, nalt and altitude. For each timestep of EUV data the inputs are given to the IRI data where jmag is zero and it signifies that we are using the geographic latitude and longitude instead of magnetic and nalt is the number of altitudes present in that timestep (This is constant, and the value is 72). In return the IRI data gives the O^+ density at those 72 altitudes as output. We run the code for 2630 timesteps of EUV data and get the corresponding IRI values of O^+ densities at different time and altitudes. As, IRI model does not return the values of NmF2 and HmF2 we derive their values for every timestep assuming that they follow Gaussian-like profile near the F-layer peak. The algorithm is given below:

1) Extract the data from EUV file.
2) Use a for loop to iterate the timestep of EUV instrument.
3) For each time step, input the year, day of the year, utsecs, geographic latitude, geographic longitude, jmag, F107A, nalt and altitude for that time step of EUV data as input of IRI model To get the O^+ density as output.
4) Estimate the value of HmF2 and NmF2 from the O^+ density obtained for that time step.

5) Repeat the last two steps to get the IRI data corresponding to EUV data for the entire day.
6) Analyze and compare the two data using different graphs and plots.

2.4.2.2Comparison of EUV and IRI data

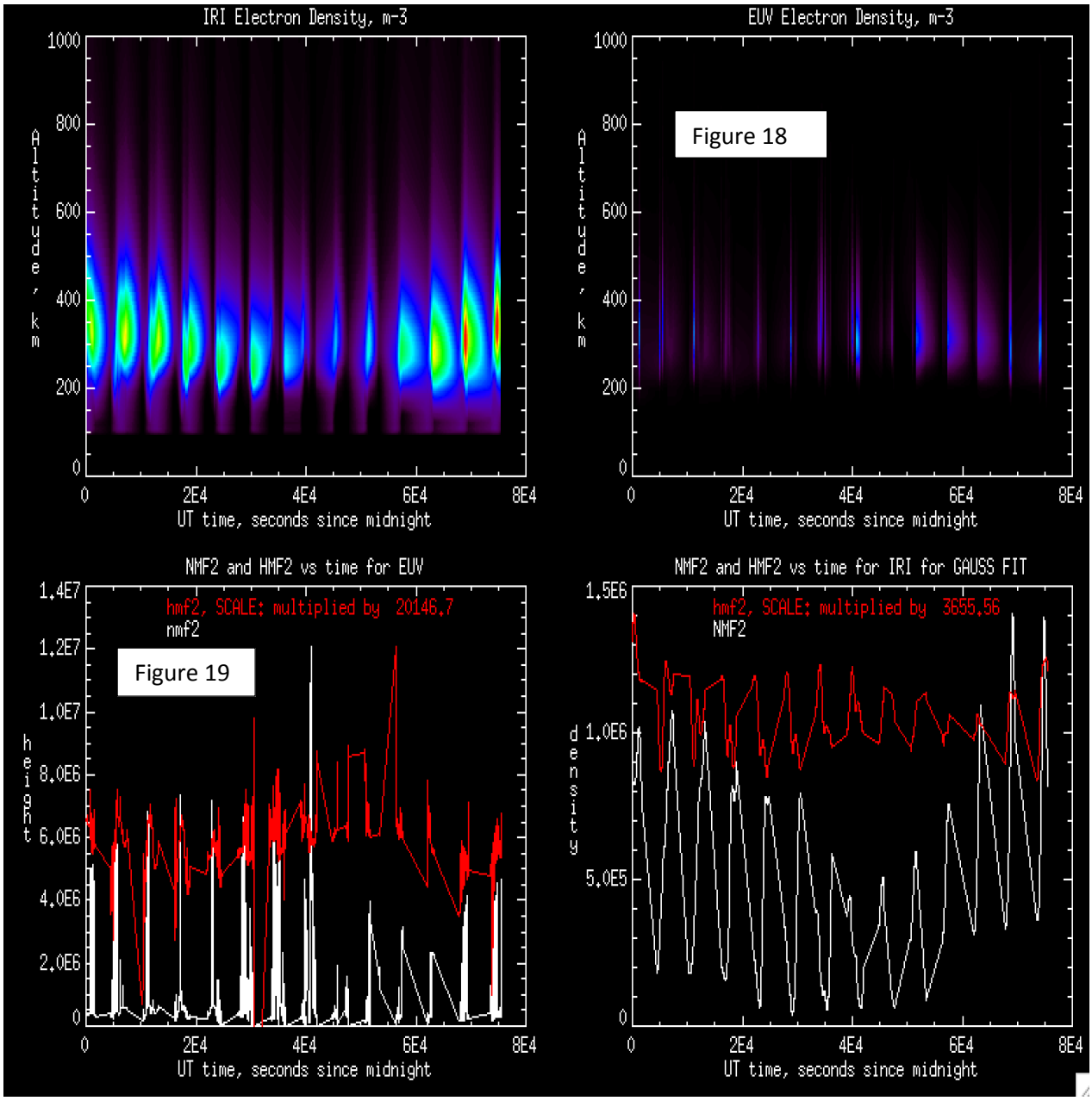

Fig 18: It shows how the O^+ density changes with time and altitude. The left plot shows the variation of the same for IRI and the plot on the right shows for EUV. This is a contour plot

where time is plotted in the x axis in seconds since midnight and altitude is plotted on the y axis in km. **Fig 19:** It shows how the NmF2 and HmF2 varies with time for EUV(The plot on left) and IRI model. In order to display the HmF2 on the same plot, it is scaled by a factor of 2064.7 for EUV and 3655.4 for IRI data. To get a better comparison of the two data, the IRI time steps has been filtered and only the reading corresponding to the seconds that EUV data has is being selected.

2.4.3 Comparison of EUV and TIEGCM data

2.4.3.1TIEGCM model geometry and algorithm used to compare TIEGCM data with EUV data

The NCAR Thermosphere-Ionosphere-Electrodynamics General Circulation Model (TIE-GCM, Maute et. al, 2017) is a thorough, first-standards, three-dimensional, non-direct portrayal of the coupled thermosphere and ionosphere framework. The model understands the three-dimensional force, vitality and congruity conditions for unbiased and particle species at each time step, utilizing a semi-understood, fourth-request, focused limited contrast conspire, on each weight surface in a stunned vertical matrix. It has 57 consistent pressure levels in the vertical, reaching out from around 97 km to 500 km in interims of one-half scale stature, and a 5° x 5° scope longitude matrix, in its base design. The time step is 120 s, but output is saved every hour.Hydrostatic harmony, consistent gravity, unfaltering state particle and electron vitality conditions, and incompressibility on a steady weight surface, are accepted. Particle speeds are gotten from the potential field made by consolidating the forced magnetospheric potential with the low-scope dynamo potential, and afterward computing particle speeds from E × B floats, as opposed to fathoming the particle energy conditions expressly. Some minor species are not as of now incorporated into the model, including hydrogen and helium and their particles, and argon. A few parameterizations are utilized in the TIE-GCM: an observational model is utilized to determine photoelectron warming; the creation of auxiliary electrons is incorporated utilizing an experimental model got from two-stream computations, the impacts of blending by gravity waves are incorporated utilizing a vortex dissemination definition; CO_2 is incorporated by indicating a lower limit condition and expecting that it is in diffusive harmony. The upper limit conditions for electron heat exchange and electron number transition are observational plans. At the lower limit, air tides are indicated utilizing the Global Scale Wave Model (GSWM, Hagan et. al, 1997).

TIEGCM data structure is almost similar to that of EUV but the timestep in the saved file is 30 minutes. So in order to compare the data with EUV data we first retrieve the data from EUV data file and then for each timestep, we convert the EUV time in seconds since midnight to the nearest minute since midnight and then retrieve the corresponding TIEGCM time in minutes since midnight and the latitude, longitude, altitudes, O^+ densities, NmF2, HmF2 and solar zenith angle for that timestep. We follow the same procedure for the remaining timesteps of EUV data as well to get the complete day profile. The algorithm is given below:

1) Retrieve the data from EUV file.
2) Use a for loop to iterate the timestep of EUV instrument.
3) For each time step, convert the EUV time in seconds since midnight to the nearest minute since midnight and then retrieve the corresponding TIEGCM time in minutes since midnight and the latitude, longitude, altitudes, O^+ densities, NmF2, HmF2 and solar zenith angle for that timestep.
4) Repeat the last two steps to get the TIEGCM data corresponding to EUV data for the entire day.
5) Analyze and compare the two data using different graphs and plots.

2.4.3.2Comparison of EUV and TIEGCM data

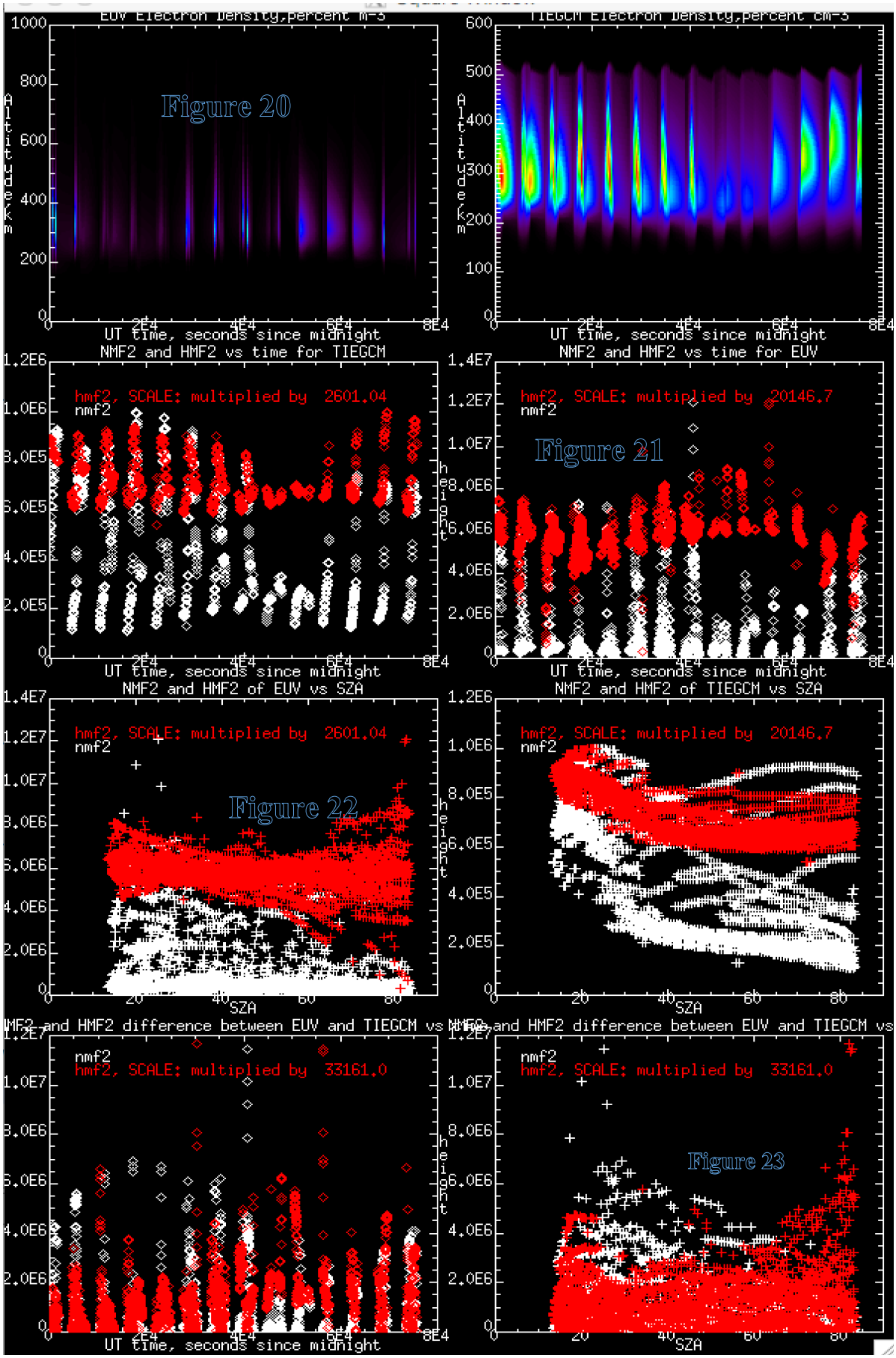
EUV Electron Density,percent M-3
Figure 20
TIEGCM Electron Density,percent CM-3
Altitude km
UT time, seconds since midnight
NMF2 and HMF2 vs time for TIEGCM
hmf2, SCALE: multiplied by 2601.04
nmf2
UT time, seconds since midnight
NMF2 and HMF2 vs time for EUV
hmf2, SCALE: multiplied by 20146.7
nmf2
Figure 21
height
UT time, seconds since midnight
NMF2 and HMF2 of EUV vs SZA
hmf2, SCALE: multiplied by 2601.04
nmf2
Figure 22
SZA
UT time, seconds since midnight
NMF2 and HMF2 of TIEGCM vs SZA
hmf2, SCALE: multiplied by 20146.7
nmf2
SZA
NMF2 and HMF2 difference between EUV and TIEGCM vs
nmf2
hmf2, SCALE: multiplied by 33161.0
UT time, seconds since midnight
NMF2 and HMF2 difference between EUV and TIEGCM vs
nmf2
hmf2, SCALE: multiplied by 33161.0
Figure 23
SZA

Fig 20: It is a contour plot which shows the $variation\ of\ O^+$ density with time and altitude. The left plot shows the variation for EUV data and the plot on the right shows for TIEGCM data. This is a contour plot where time is plotted in the x axis in seconds since midnight and altitude is plotted on the y axis in km. **Fig 21**: The diagram shows how the NmF2 and HmF2 varies with time for EUV(The plot on right) and TIEGCM data. **Fig 22:** It represents the same thing but instead of time since midnight, the NmF2 and HmF2 is plotted against the solar zenith angle. **Fig 23:** It shows the difference of NmF2 and HmF2 in between the two data against 1) time (plot on the left) and 2) Solar zenith angle. To fit the plot for HmF2 in the same graph the HmF2 values are scaled accordingly to fit it on the same plot.

The data which we have used to plot the EUV parameters are simulated data and as there is match with this data with the real conditions there is nothing to infer from the plot other than the procedure, which will act as a template for analysis after ICON is launched. We will follow on to a comparison of the EUV data with TIEGCM data.

2.5Comparison of EUV data FUV data

2.5.1FUV spectrometer

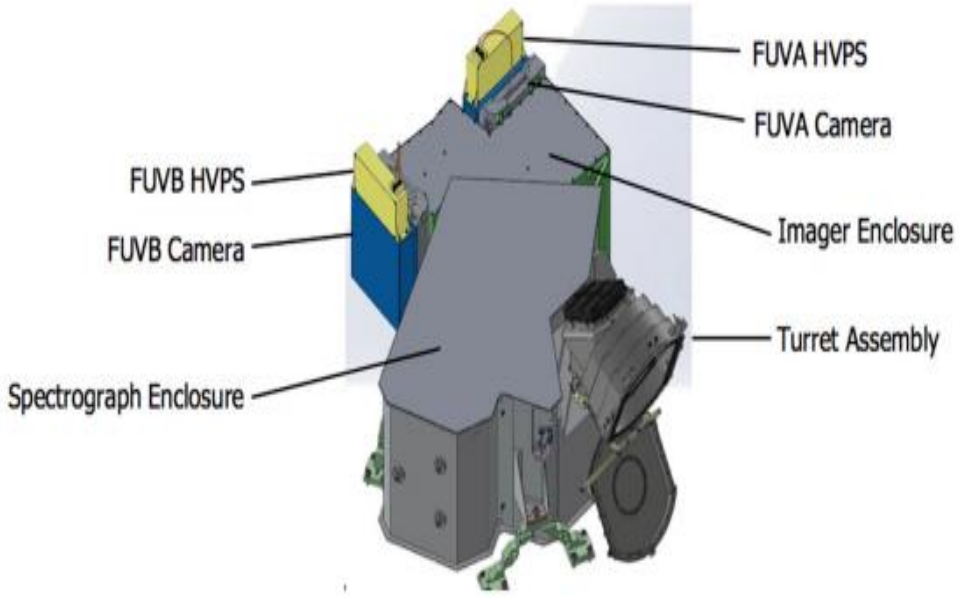

Figure 24: The FUV imager (Mende et. al, 2016)

The ICON FUV (Far ultraviolet) instrument is a 2-dimensional imager (Mende et al. 2000; Mende 2016). The instrument will quantify the brightness of both the 135.6-nm emission of O and the LBH outflow of N_2 almost 157 nm on the appendage amid the day. This helps to estimate the density of O and N_2 during the day (Stephan et. al, 2018) and the density of O^+

during night (Kamalabadi et. al, 2017)).A brief description of the instrument is given in Immel et al. (2017). During the night, the steerable turret of the instrument contains a mirror which permits the reorientation of the field of view over ±30° in the flat plane, in 13 discrete advances isolated by 5°. The instrument is given an advanced picture handling ability situated in the Instrument Control Package (Sect. 5.1) to decrease the haze due to movement of the shuttle amid imaging mixes. This movement pay, named Time-Delay Integration (TDI) rectifies for the clear movement of highlights in the imaged scene, from plate sees beneath the appendage out to the uttermost limb tangent points.

2.5.2FUV spectrometer Geometry, data content and algorithm to compare EUV and FUV data

The data obtained from FUV instrument has a different geometry compared to EUV spectrometer. Instead of 72 altitudes the FUV instrument retrieves the density at 22 altitudes only (Stephan et. al, 2018). Also, it gives the universal time and so we have to separate the hours, minutes and seconds separately and then convert it into utsecs since midnight. Also, the FUV instrument measures 135.6 nm emission which is released by both O atom and the O^+ ion and there is no way to separate the two and thus the values of O^+ obtained from FUV imager is more difficult to determine. On the other hand, as EUV spectrometer only measures the O^+ density it is very accurate. Even though the data is not accurate for FUV instrument we consider comparing the FUV data with EUV data as both the instruments are on the same mission and the data obtained from the instruments will be similar conditions and thus contamination of data due to different conditions such as season, solar flux, year etc. is eliminated. Just like EUV, FUV instrument too gives the O^+ densities, HmF2, NmF2, universal time and altitudes as output even though the data geometry is different.

2.5.3FUV and EUV data comparison

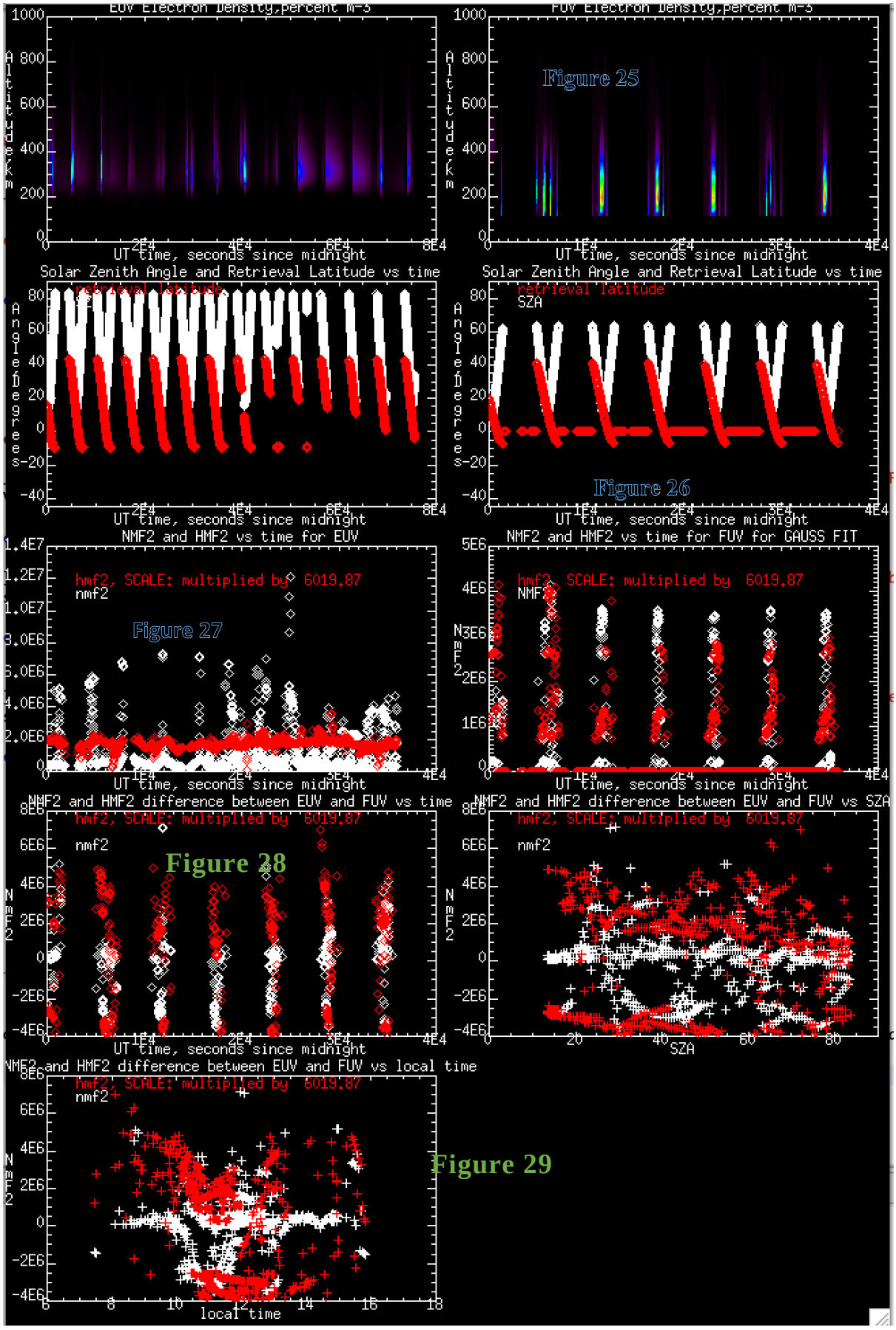
EUV Electron Density,percent M-3
FUV Electron Density,percent M-3
Altitude,km
UT time, seconds since midnight
Figure 25
Solar Zenith Angle and Retrieval Latitude vs time
retrieval latitude
SZA
Angle Degrees
Figure 26
NMF2 and HMF2 vs time for EUV
NMF2 and HMF2 vs time for FUV for GAUSS FIT
hmf2, SCALE: multiplied by 6019.87
nmf2
Figure 27
NMF2 and HMF2 difference between EUV and FUV vs time
NMF2 and HMF2 difference between EUV and FUV vs SZA
Figure 28
NMF2 and HMF2 difference between EUV and FUV vs local time
local time
Figure 29

Fig 25: It is a contour plot which shows the $variation\ of\ O^+$ density with time and altitude. The left plot shows the variation of the same for EUV data and the plot on the right shows for FUV data. This is a contour plot where time is plotted in the x axis in seconds since midnight and altitude is plotted on the y axis in km. **Fig. 26:** It shows how the solar zenith angle and Retrieval latitude varies with time for EUV and FUV data. Fig **27:** The diagram shows how the NmF2 and HmF2 varies with time for EUV(The plot on left) and FUV data. **Fig 28:** It shows the difference of NmF2 and HmF2 in between the two data against 1) time (plot on the left) and 2) Solar zenith angle. **Fig 29:** It shows the difference of NmF2 and HmF2 in between the two data against local time. To fit the plot for HmF2 in the same graph the HmF2 values are scaled accordingly to fit it on the same plot.

The data which we have used to plot the EUV parameters are simulated data and as there is match with this data with the real conditions there is nothing to infer from the plot other than the procedure, we will follow to compare the EUV data with FUV data.

2.6Comparison of EUV data Ground based data

A ground station, earth station, or earth terminal is an earthbound radio station intended for extra-planetary media transmission with shuttle (establishing some portion of the ground section of the rocket framework)or gathering of radio waves from cosmic radio sources. Ground stations might be found either on the outside of the Earth, or in its atmosphere. Earth stations speak with shuttle by transmitting and accepting radio waves in the too high recurrence or amazingly high recurrence groups (e.g., microwaves). At the point when a ground station effectively transmits radio waves to a shuttle (or the other way around), it sets up a broadcast communications interface. A foremost broadcast communications gadget of the ground station is the explanatory radio wire.

In order to know which, ground station will look at the same part of the earth's atmosphere as ICON EUV instrument is looking at specific time, we developed a code that will tell us how many times and when the ICON EUV instrument will look at a certain part (fixed longitude and latitude). As per the information received by the code, we will choose a ground station in that latitude and longitude range and look at the same time to get the data for similar conditions as of EUV data.

The below plot is taken from such a ground station.

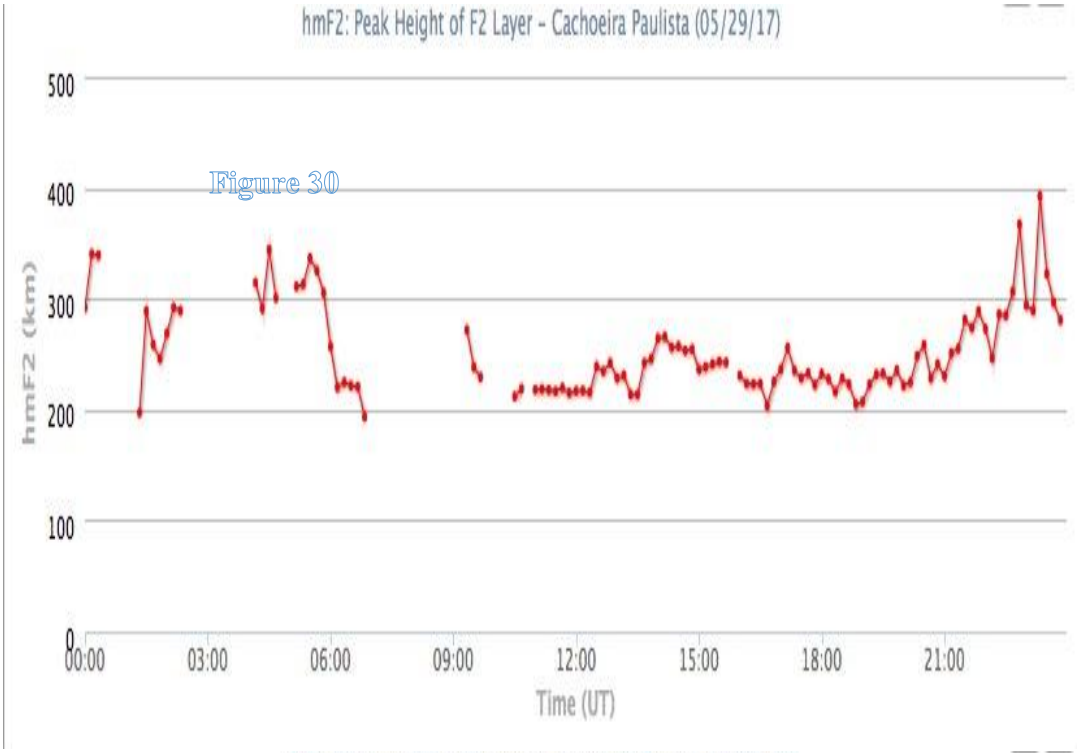

Figure 30

Figure 31

. **Fig 30:** It shows the variation of HmF2 with time for the same ground station. **Fig 31:** It shows the variation of FOF2 with time. This data is collected from the ground station of Cachoeira Paulista, Brazil. To compare this data with the EUV data, the O^+ density profile can be converted into FOF2 profile. The other ground stations that are working and can provide with data for comparison are: Boa Bista, Sao Luis and Fortaleza. These ground stations were selected based on a code developed that will tell us the time of when ICON will be looking at a particular position within a given time window.

2.7Overview of next chapter

In this section we learnt about the tools developed to extract and process EUV data and to compare it with different ground based and space-based proxies. But ICON is not yet launched and in order to test the tools developed ICON EUV we took data from another instrument named SSULI which is already in space and observes the same 83.4 nm emission that ICON EUV instrument is focused on. In the next chapter we will see how the tools works for extracting the Level 2 data from SSULI and then compare it with IRI and TIEGCM models to analyze it using the same approach outlined here for ICON EUV instrument.

CHAPTER 3: Overview, results and analysis of SSULI (Special Sensor Ultraviolet Limb Imager) data and comparison of it with different space-based proxies

3.1 Summary

In this chapter a brief description of the SSULI instrument, it's working principle geometry is discussed. Apart from that seven days of data obtained from the imager is retrieved and analyzed thoroughly and compared to the IRI (International Reference Ionosphere) model and TIEGCM (Thermosphere-Ionosphere Electrodynamics General Circulation) model.

3.2 Instrument description, geometry and orbit of Spacecraft

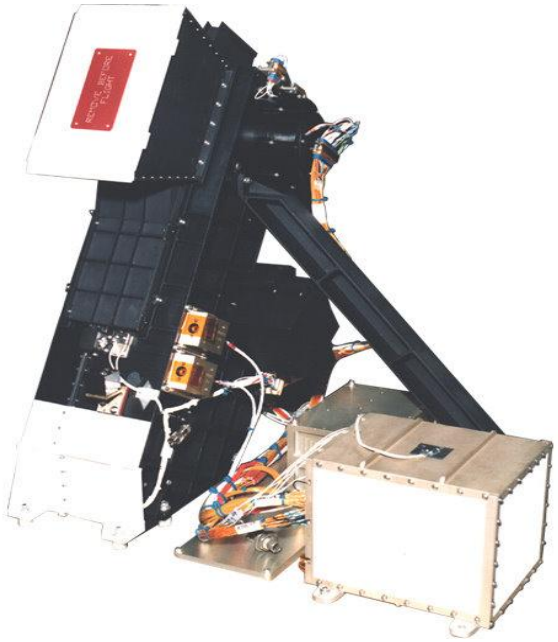

Figure 32: SSULI components (Dymond et al., 2017)

The Special Sensor Ultraviolet Limb Imager (SSULI) is an imaging spectrometer that is utilized to watch the world's ionosphere and thermosphere. These sensors give vertical power profiles of airglow that falls in the range of 800 to 1700 Angstrom (80 to 170 nanometer) and sweep from 75 km to 750 km altitude. The information from these sensors will be utilized to induce elevation profiles of particle, electron and ion density.The Naval Research Laboratory (NRL) created five remote detecting instruments for the Air Force Defense Meteorological Satellite Program (DMSP). These instruments known as SSULI (Special Sensor Ultraviolet Limb Imager) propelled on board the DMSP block of 5D3 satellites, which began in 2003. SSULI measures vertical profiles of the common airglow radiation from particles, atoms and particles in the upper environment and ionosphere by review the Earth's appendage at a digression height of roughly 50 km to 750 km.

The DMSP F19 spacecraft was launched on April 3, 2014 into a sun-synchronous 0800-2000 LT, 830 km altitude orbit. Estimations are produced using the EUV spectrum to the far ultraviolet (FUV) over the wavelength scope of 80 nanometers to 170 nanometers. The satellites will be propelled in a close polar, sun-synchronous circle at a height of roughly 830 km. The Low-Resolution Airglow and Auroral Spectrograph (LORAAS), a SSULI prototype, was propelled on board the Advanced Research and Global Observation Satellite (ARGOS_(satellite)) on February 23, 1999.

The sensor has a field-of-view of 2.4°x0.15° and sweeps out a 2.4°x17° field-of-regard during each 90 second scan, with wavelength coverage between 800Å and 1700Å at 23Å. The field of view scans ahead of the spacecraft in the orbital plane through a 17° field of regard, corresponding to approximately 75–750 km altitude. The spacecraft covers a wide range of longitude from 0 degrees to 360 degrees and hovers in the mid latitude range from 5 degrees south to 65 degrees north.

The data that we are using comes from the DMSP F19 satellite.

3.3 SSULI data content

The SSULI data file which is being used for my research contains seven consecutive days of data starting from August 01, 2014 to August 07, 2017. The data contains the output products of the NRL retrieval, which describe the best fit to the ionospheric parameters and their location (Dymond et al., 2017). A list of the different parameters that are used to analyze the SSULI data are given below:

9) **Ut_sec**: This variable in the SSULI data file tells us the universal time when the measurement is taken.
10) **Glat**: This variable indicates the geographical latitude of the measurement.
11) **Glon**: This variable indicates the geographical longitude of the measurement.
12) **Zopl**: The variable gives the altitude at which the measurement is taken.
13) **Opl**: The variable gives the density of O^+ ion corresponding to the altitude at which the measurement is taken.
14) **NmF2**: The variable indicates the highest density of O^+ at a certain point of time.
15) **HmF2**: The variable indicates the height in which the highest density of O^+ occurs at a certain point of time.

Unlike EUV spectrometer which takes 2630 measurements over a day SSULI takes around 200 measurements every day. The number varies slightly from day to day with a range spreading from 196 to 205. Also, where EUV instrument takes measurements from 13 degrees S to 44 degrees N, SSULI covers a wider range of latitude from 5 degrees S to 68 degrees N. Apart from this the measuring factors and conditions of the data are similar. For every timestep of SSULI data, 72 ionized oxygen densities are measured corresponding to the 72 different altitudes. Change in timestep results in change in position of the spacecraft and thus the latitude and longitude of measurement also changes.

3.4 Data representation and results

In this section, the data obtained from the SSULI data files are represented through different plots and graphic charts and compared with different models such as IRI and TIEGCM.

3.4.1 SSULI data content

3.4.1.1SSULI data conditions and filters

The data that is analyzed is of seven consecutive days starting from August 01, 2014 to August 07, 2014 i.e. from the 213^{th} day to the 219^{th} day of the year. The days have a F107 flux of 160, 172.5, 159.5, 156, 145 and 142.5. A graphical representation of how the solar flux and Ap index varies over the day is given below. The F107 can get as low as 50 and as high as 300. AP index can range from 2 to 400 and even more. So, the days which we are analyzing the SSULI data for have moderate F107 and AP index and the range of the two indices are small.

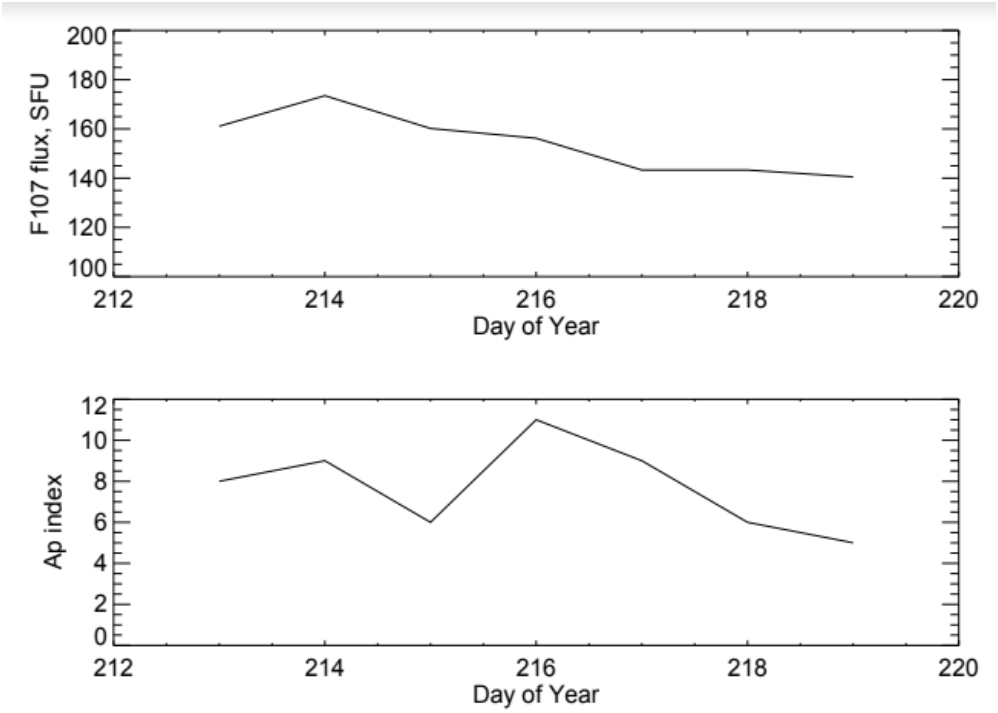

Figure 33: The variation of F107 flux and Ap index with days is shown in the above graph.

It can be seen from the above graph that the solar flux does not change much in the given seven days of data and thus will have little influence on the HmF2, NmF2 results. Also, as the data is concentrated in the northern hemisphere mostly and is taken in the month of August, it mainly represents the summer.

We did a plot of latitude with the local time (derived from the UT secs given in the data) and saw all the data is gathered either during the sunrise or during the sunset consistent with the orbit of DMSP. So, to get a better understanding about the data we decided to divide into two parts based on the local time of the data taken- sunrise data and sunset data. we will also control for latitude by using the range 35 - 50 degrees only.More is being discussed about this in later part of this section.

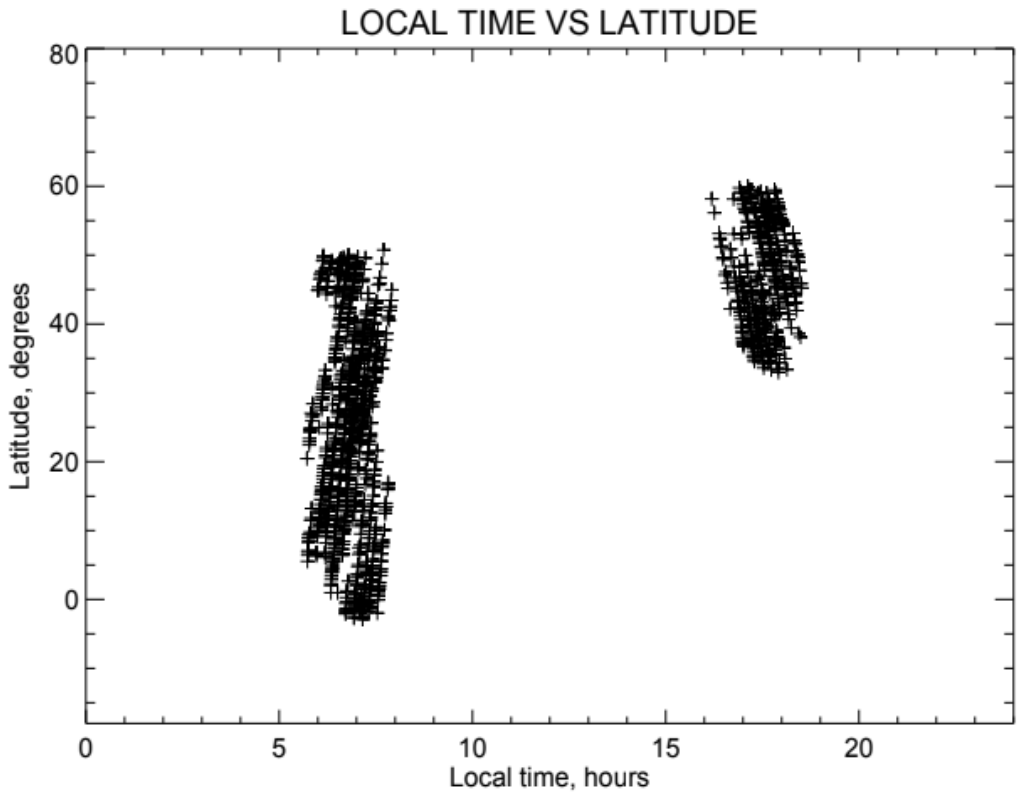

Figure 34 The above graph represents the variation of latitude with local time from all seven days

The data retrieved from the seven days is represented in three different ways. One where only an orbit is selected randomly. In the second case a day of data is selected and in the last case All the data from the seven days is considered using a filter of sunset/sunrise.

3.4.1.2SSULI data for one orbit

The spacecraft makes about 14.5 orbits in a day and we have divided each days of data into 29 segments (each either sunrise or sunset). Each orbit has four to ten timesteps to read the data from. For the ease of our work we chose one such orbit which has a good amount of data. The orbit we chose initially was from the first day and it represents the second orbit of the spacecraft. The different conditions of the orbit are represented using visuals and graphs which are given below.

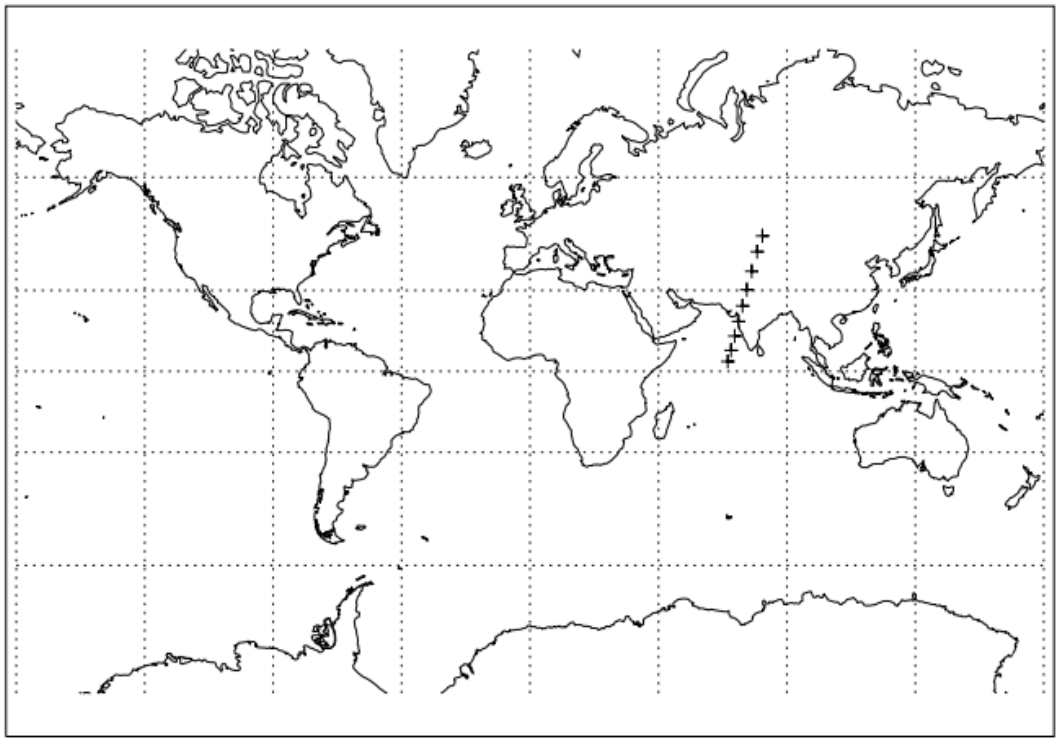

Figure 35: The figure shows the geographic latitude plotted against the geographic longitude in a map for the orbit chosen for our analysis.

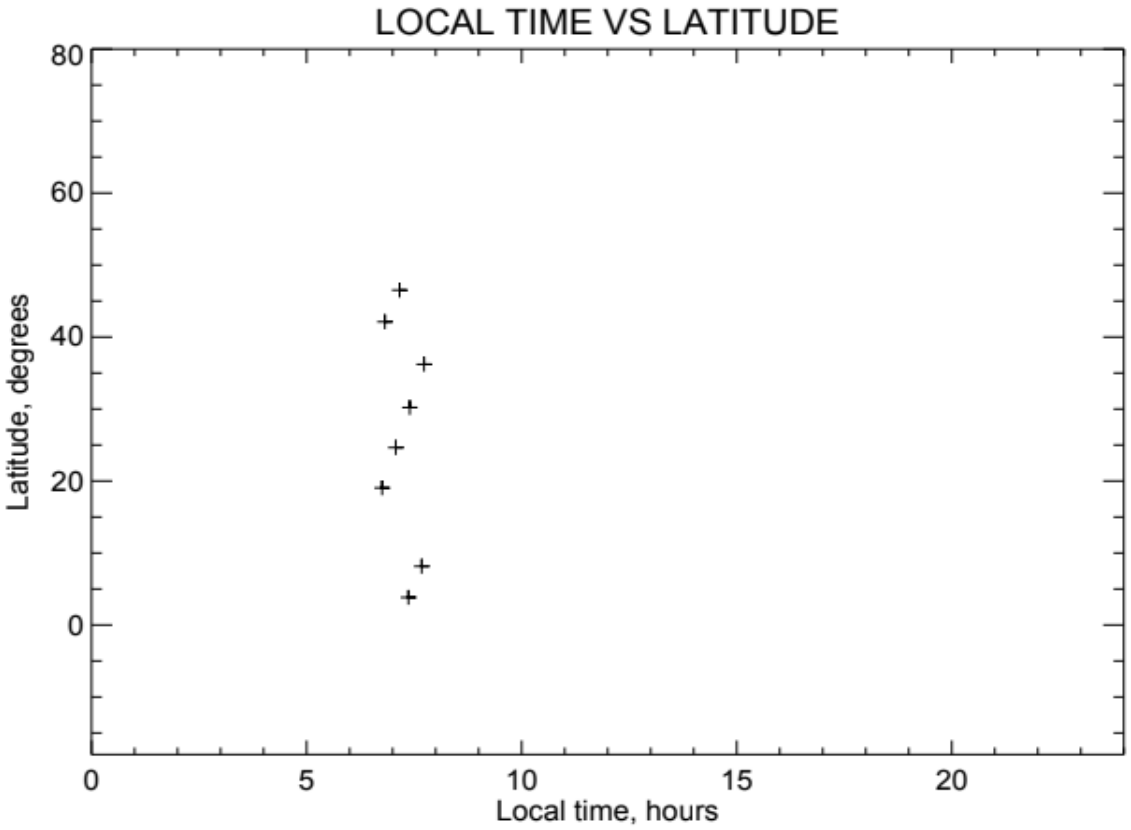

Figure 36: The figure shows how the latitude changes with local time for the chosen orbit.

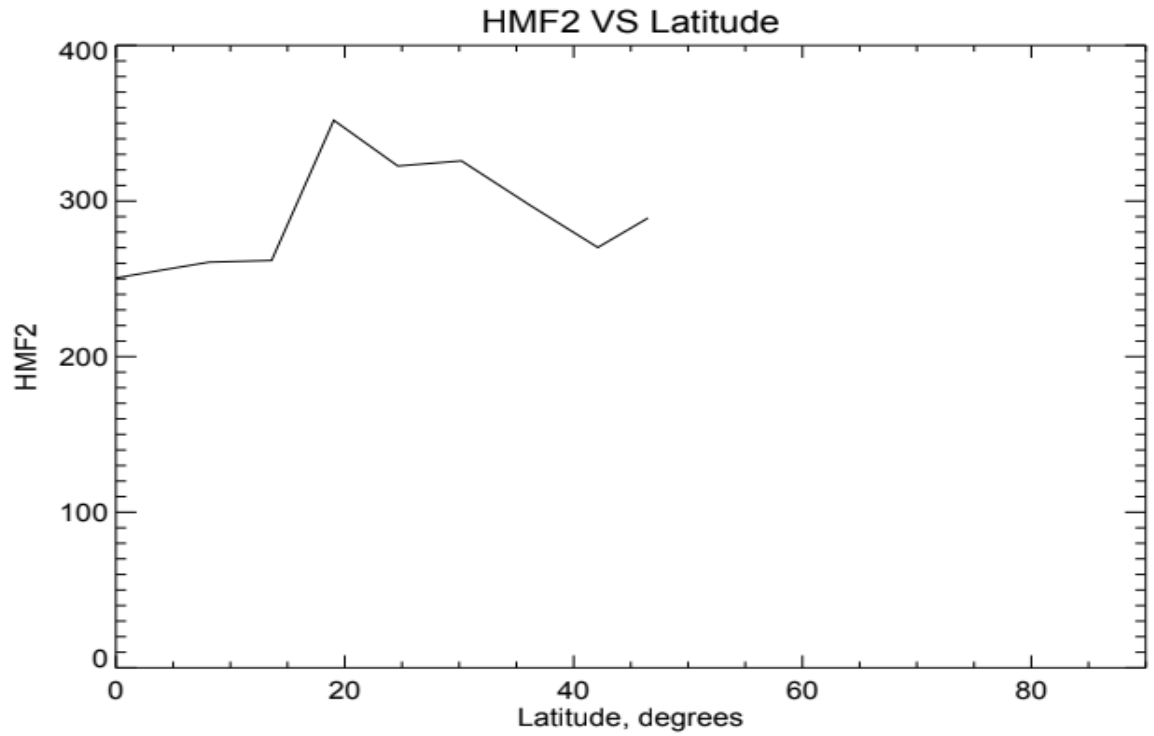

Figure 37: The above figure shows how the HmF2 changes with latitude for the chosen orbit

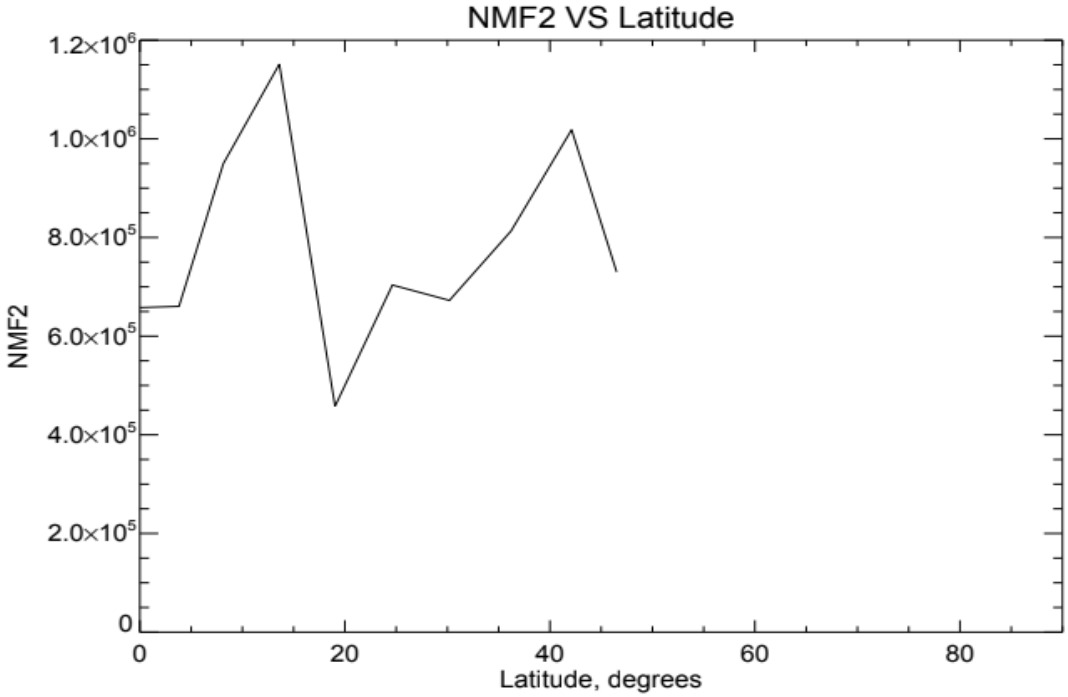

Figure 38: The figure shows how the NmF2 changes with latitude for the chosen orbit

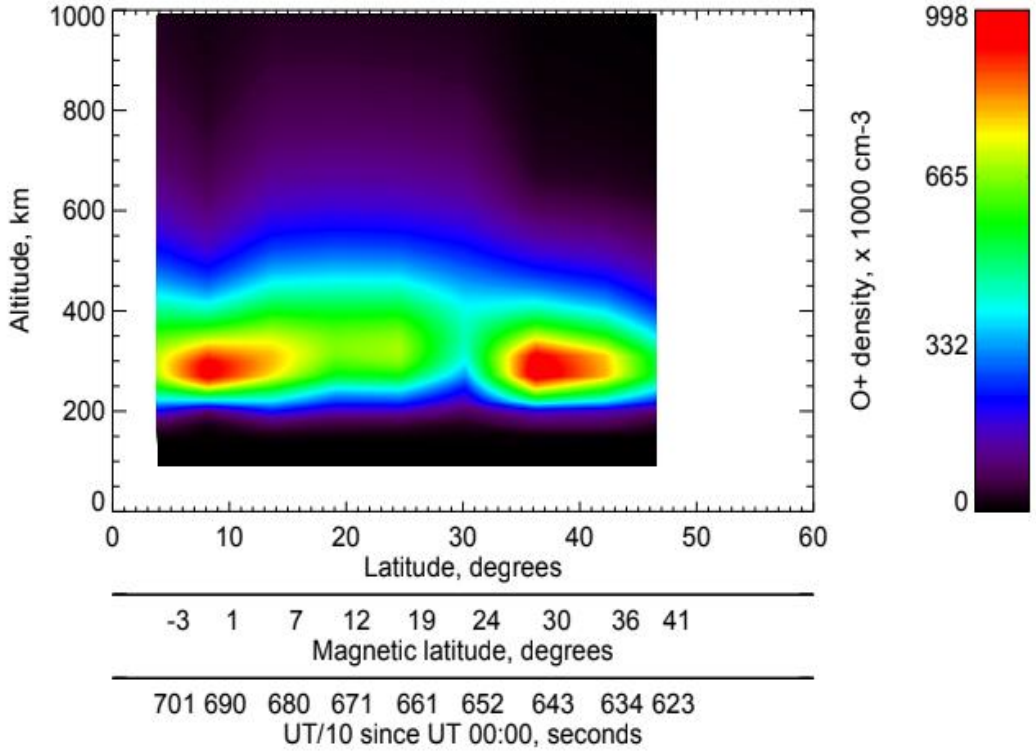

Figure 39: This figure is a contour plot which shows how the O^+ density varies with altitude as well as latitude for the chosen orbit.

From figure 35 to figure 38 it is seen that the orbit chosen has eight data points and all the data are taken during the sunrise. The latitude varies from 3 degrees north to 50 degrees north and the longitude ranges from 67 degrees east to 86 degrees east. As the data is taken during sunrise, the HmF2 values are quite low due to the lack of ionization of ions during the sunrise. From the contour plot in figure 39, we can see that there are two peaks of O^+ densities, one at 10 degrees north and the at around 40 degrees north. This observation is confirmed by the NmF2 plot against the latitude in figure 38 but the reason of the two peaks is unknown. We discuss about the same in later part of this section.

3.4.1.3SSULI data for one day

For our research, we have used seven days of data. As the days are in the same month and all have a similar solar flux, we picked a day randomly (in this case the first day i.e. August 01,2014) and analyzed its data. The day has a F107 flux of 160 and Ap index of 8.

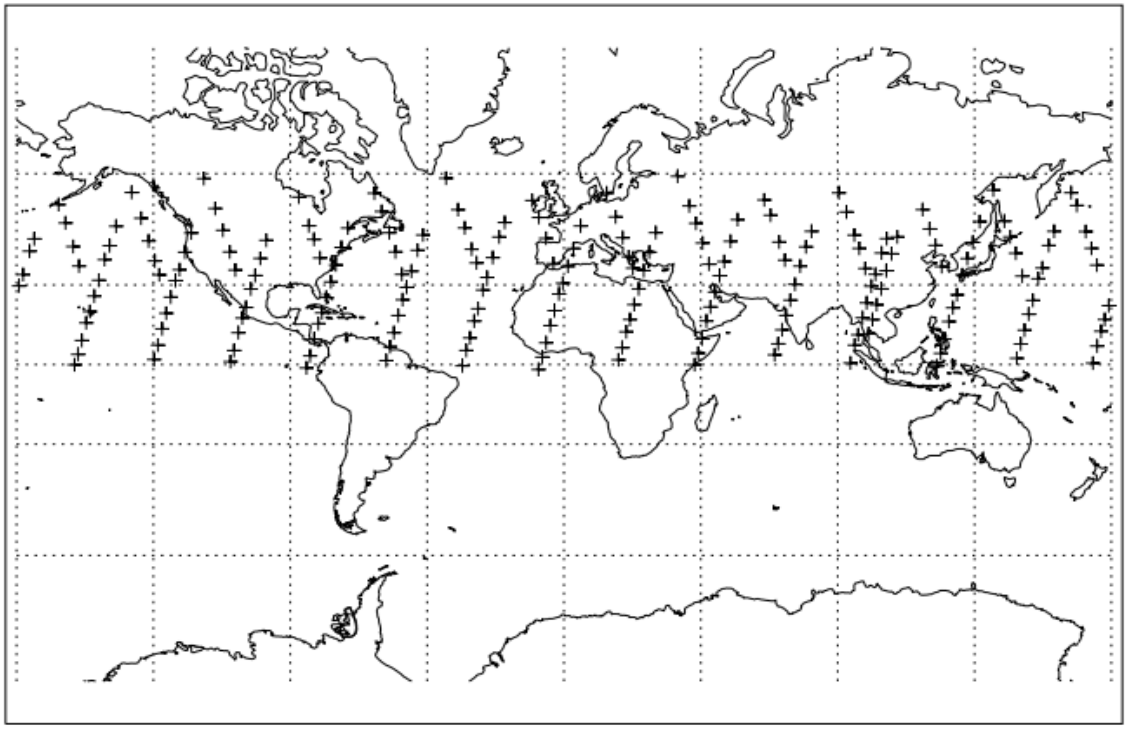

Figure 40: The figure shows the geographic latitude plotted against the geographic longitude in a map for the day chosen for our analysis.

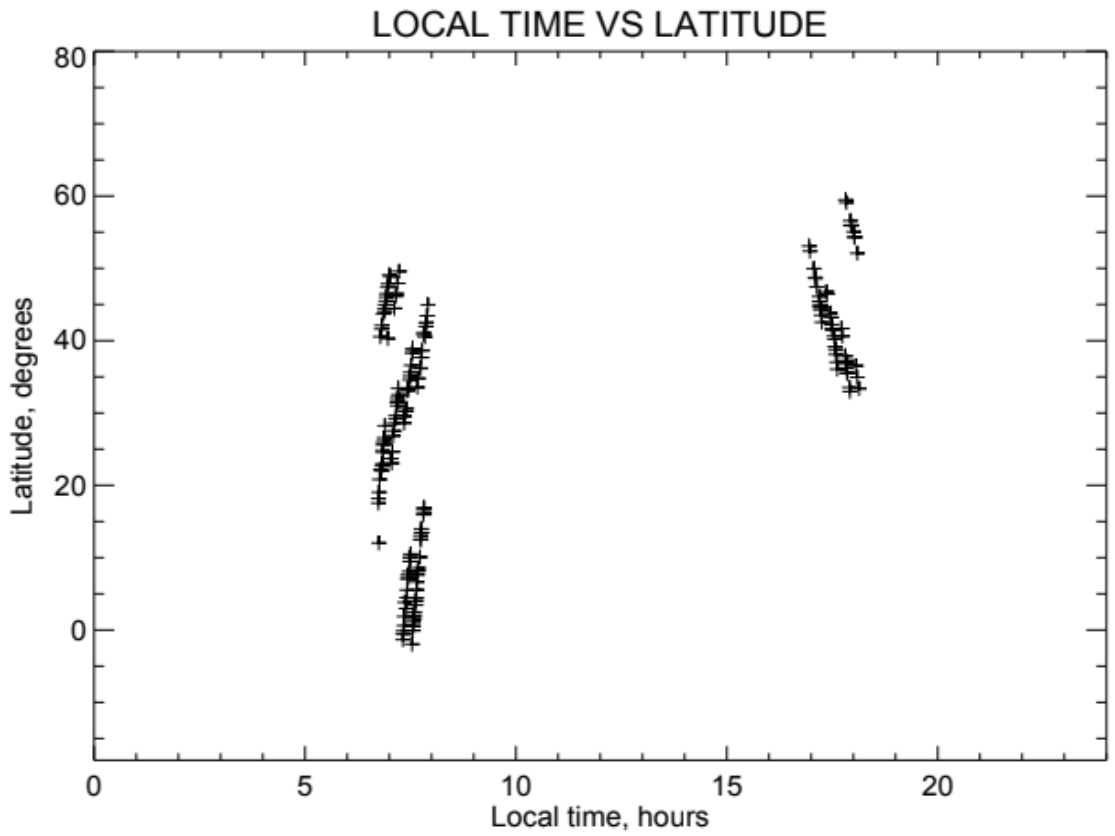

Figure 41: The figure shows how the latitude changes with local time for the chosen day.

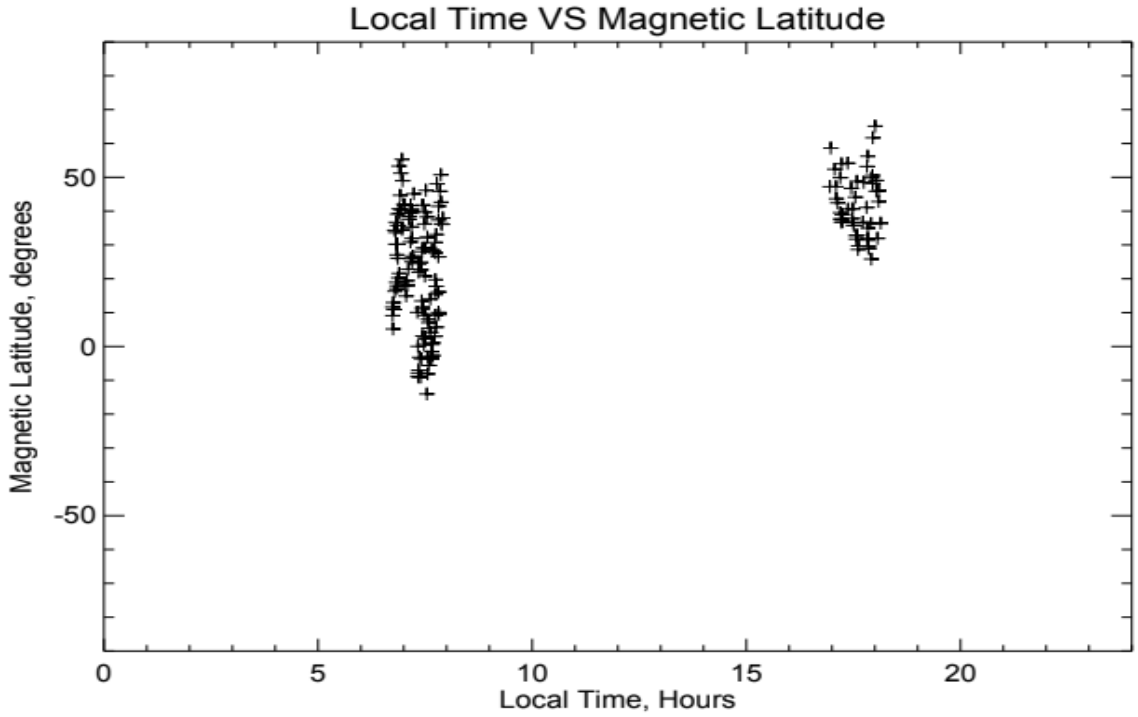

Figure 42: The figure shows how the magnetic latitude changes with local time for the chosen day.

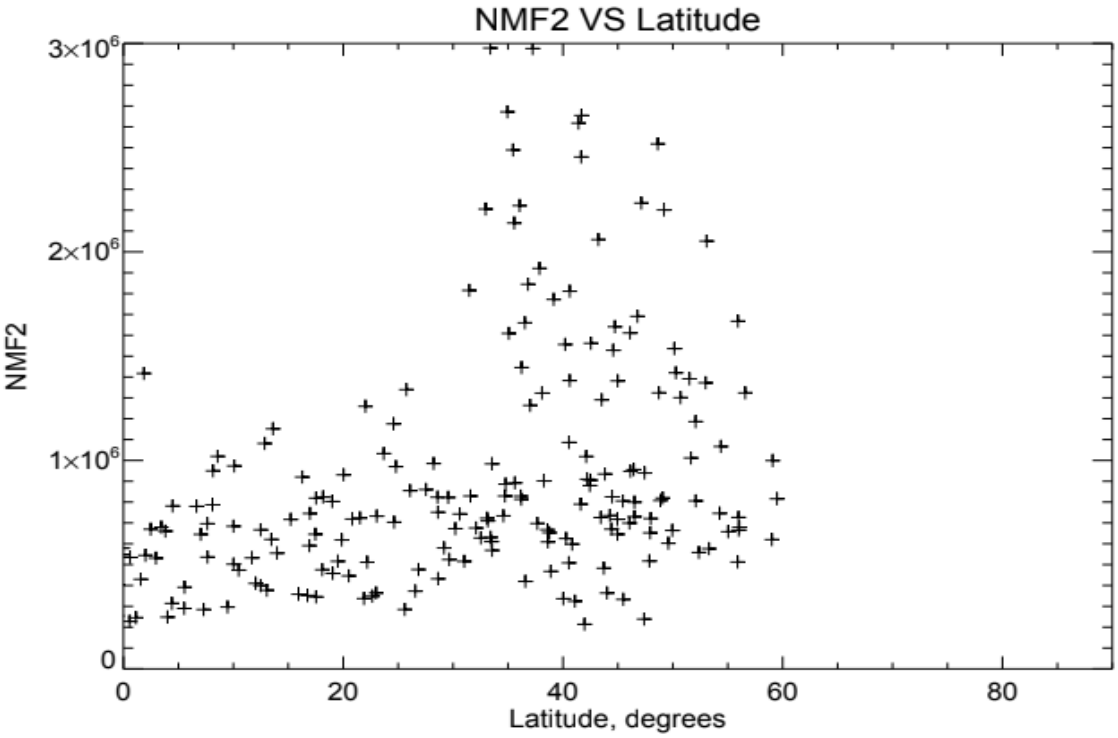

Figure 43: The figure shows how the NmF2 changes with latitude for the chosen day

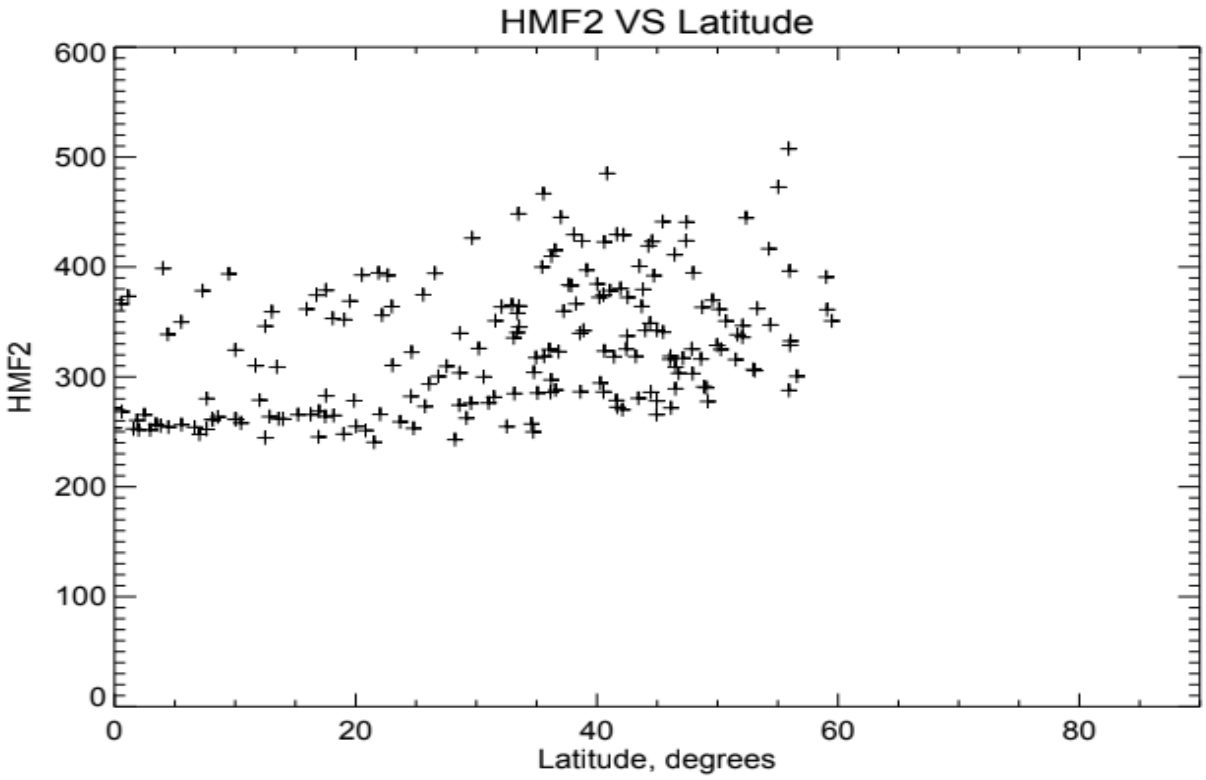

Figure 44: The figure shows how the HmF2 changes with latitude for the chosen day.

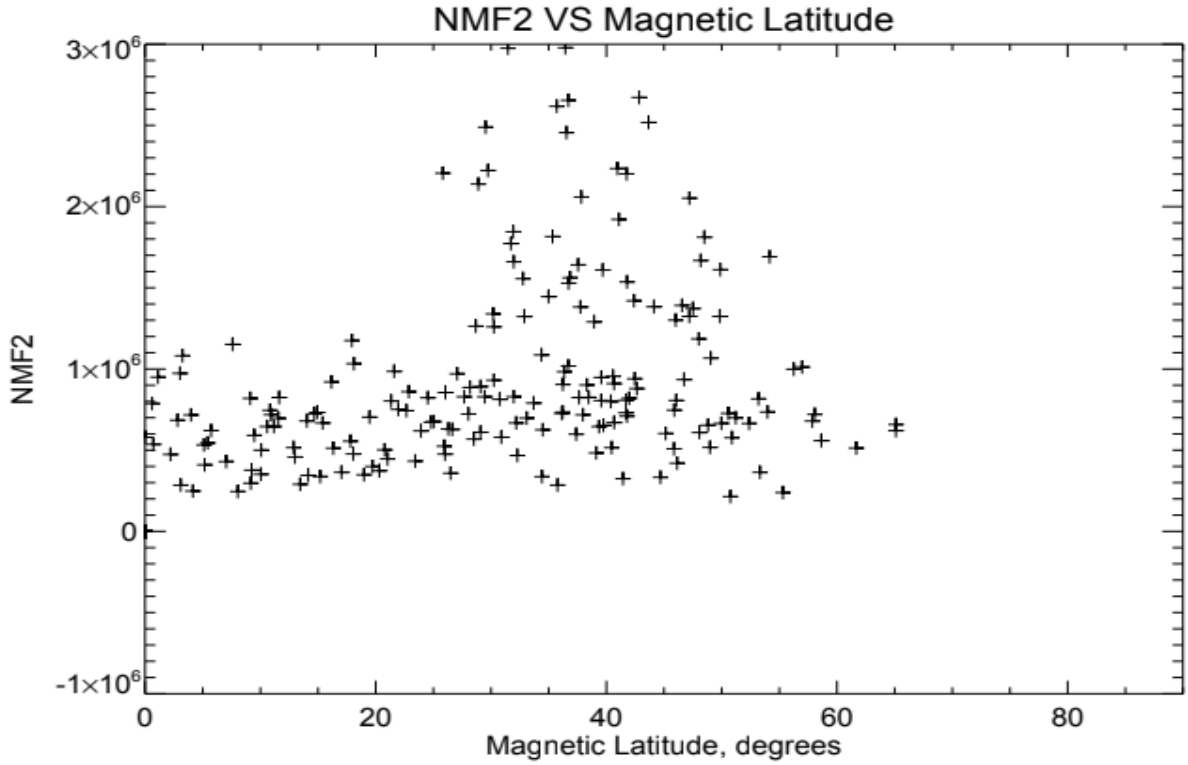

Figure 45: The figure shows how the NmF2 changes with magnetic latitude for the chosen day

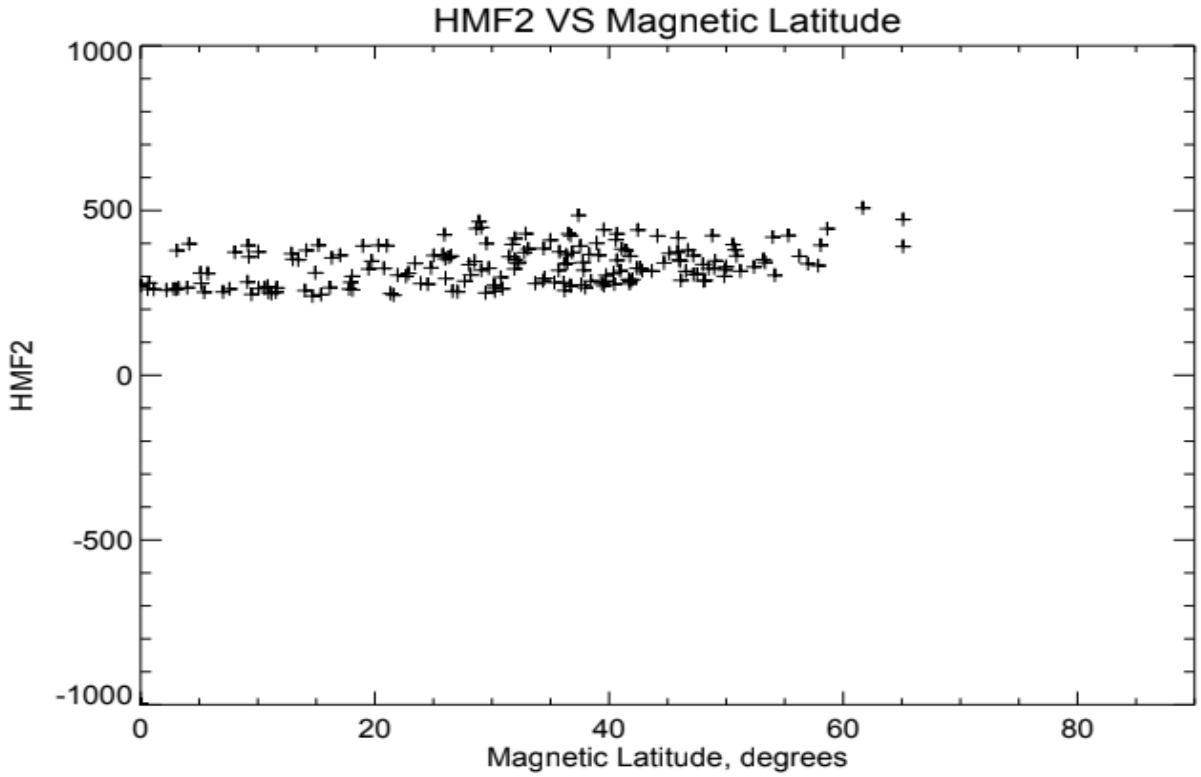

Figure 46: The figure shows how the HmF2 changes with magnetic latitude for the chosen day.

From figures 40 to 46, it is seen that the data is taken in the mid latitude region. The spacecraft makes 14.5 orbits in the day. The time of the data taken is either during the local sunrise or during local sunset. The NmF2 values are quite scattered in both the cases. First, when we plot against the geographical latitude and second, when we plot it against the magnetic latitude. But in case of HmF2, the data is more spread in case of geographical latitude compared to the HmF2 when we plot it against the magnetic latitude. This observation gives us an indication that the HmF2 does not change much over the magnetic latitude throughout the day compared to the geographical latitude. In figure 12 and figure 14 the variation of NmF2 with latitude is shown. In later part of this section, we have separated the sunset data from the sunrise data and observed that the higher values of NmF2 usually happens during the local sunset time and the lower values during the local sunrise time.

3.4.1.4 SSULI data for all seven days

In this part of the report, all the data obtained from the seven days are represented using graphs and plots. In order to obtain seven days data, data from each day is retrieved and clubbed together into a singular array. This array has a dimension of 7*29*15*72 in case of O^+ density where the first digit of the array represents the number of days, the second digit represents number of segments each day has, the third digit points to the number of timestep each segment has, and the fourth digit corresponds to the 72 different altitudes where the data is measured. One thing needs to be noted here that not all the segments has 15 timesteps of data. So, to get the timesteps where valid data is present, either we have filtered the data or assigned the empty data to large values so that it does not fall in the graph. Below are the graphs we obtained from the data.

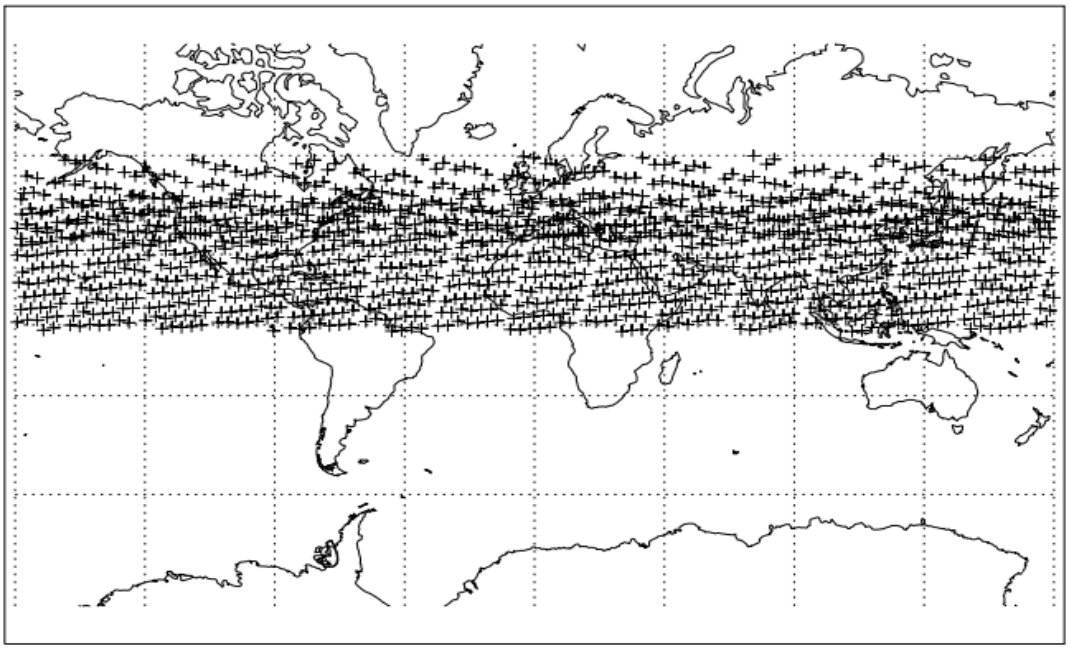

Figure 47: The figure shows the geographic latitude plotted against the geographic longitude in a map for the days chosen for our analysis.

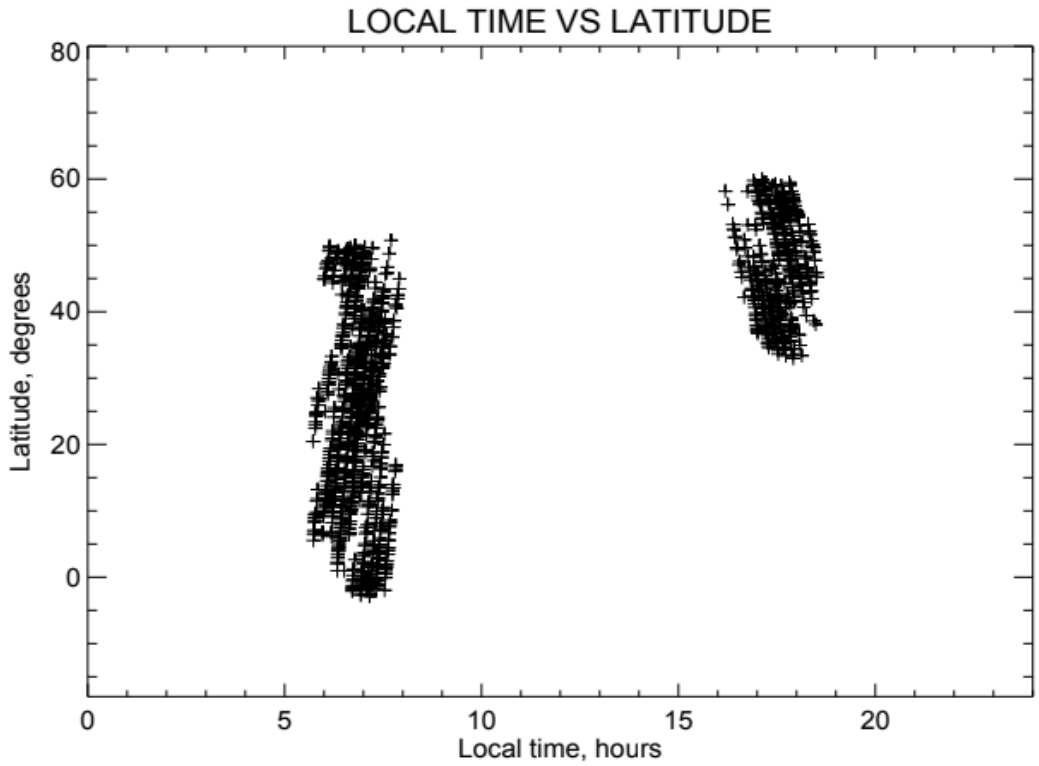

Figure 48: The figure shows how the latitude changes with local time for the chosen days.

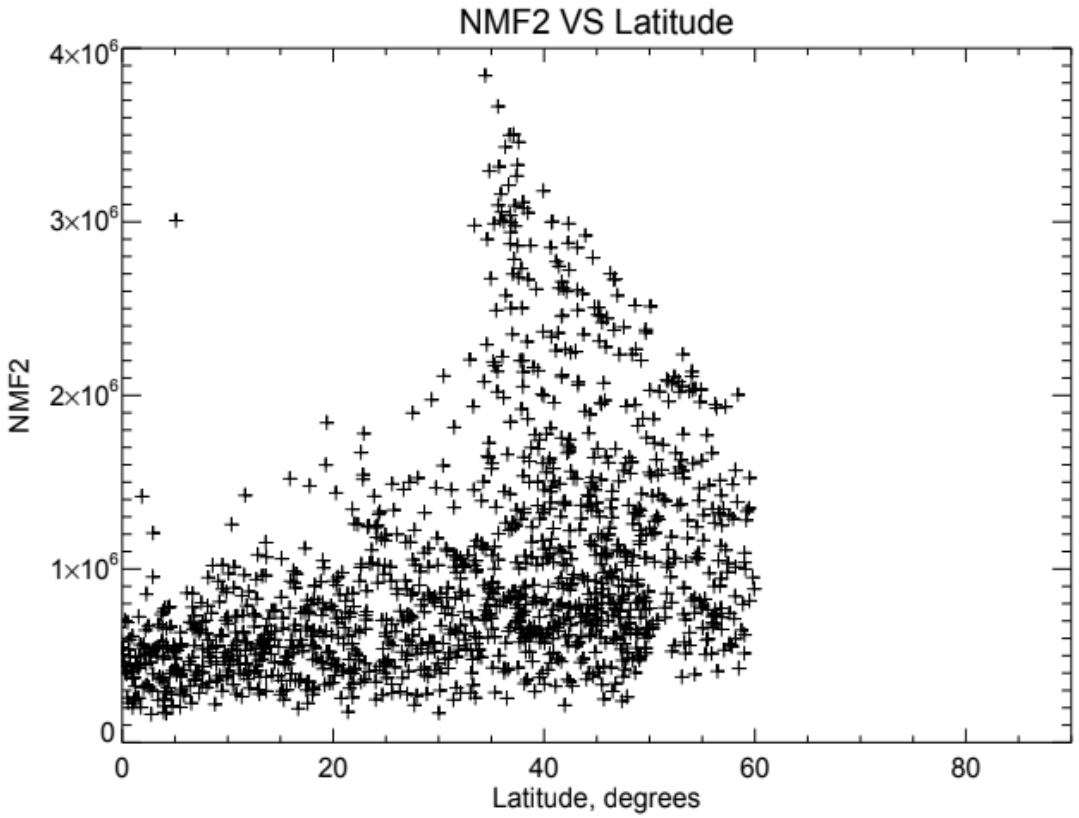

Figure 49: The figure shows how the NmF2 changes with latitude for the chosen days

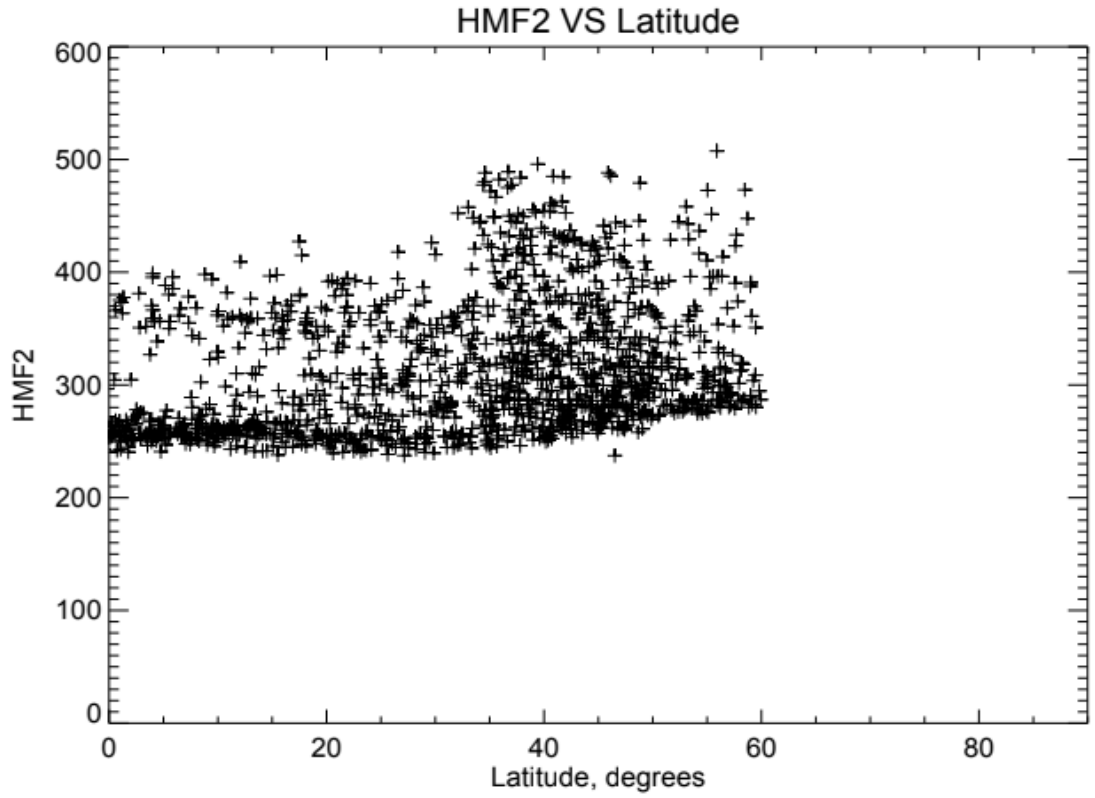

Figure 50: The figure shows how the HmF2 changes with latitude for the chosen days

From figures 16 and 17 we can know about the geographical locations and the time in which the SSULI observations are made for the given seven days of data. The spacecraft collects data in the mid latitude region and either during the local sunrise or local sunset. Figure 18 and 19 shows how the NmF2 and HmF2 varies with latitude but as the spread for both the parameters are significantly high, we divided the seven days of data into two parts. One for the sunrise and the other part represents the data taken during sunset. The graphs and plots obtained after that are given below.

3.4.1.4.1Case 1: SSULI data during sunrise

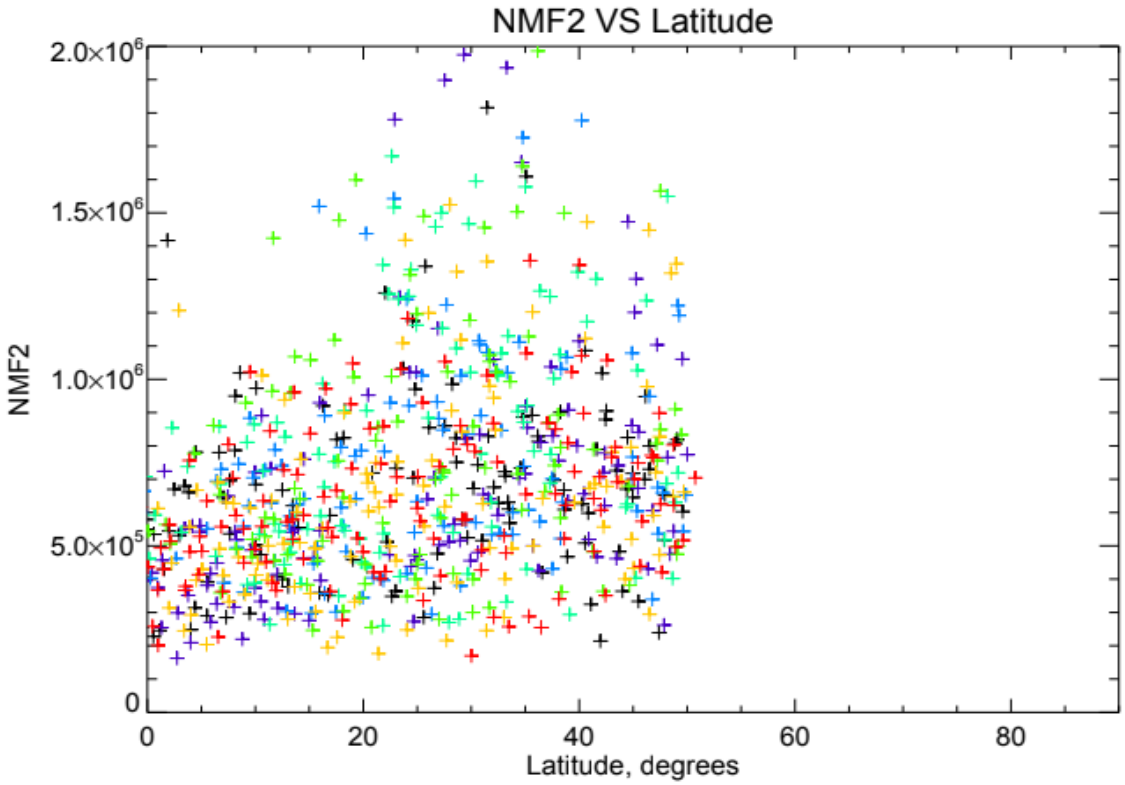

Figure 51: The figure shows how the NmF2 changes with latitude for the chosen days. The different color in the graph represent data from different days. The above figure shows how the NmF2 changes with latitude for the chosen days. The different color in the graph represent data from different days, starting from black and running through red.

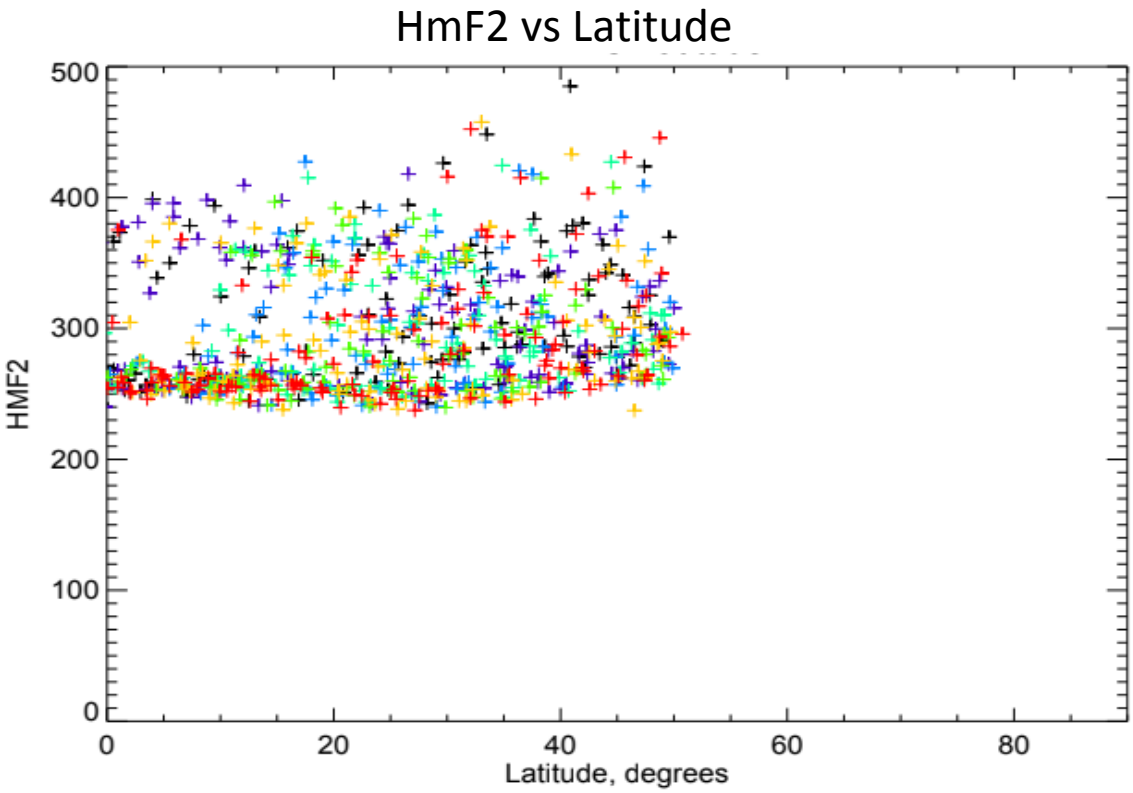

Figure 52: The figure shows how the HmF2 changes with latitude for the chosen days. The different color in the graph represent data from different days.

3.4.1.4.2Case 2: SSULI data during sunset

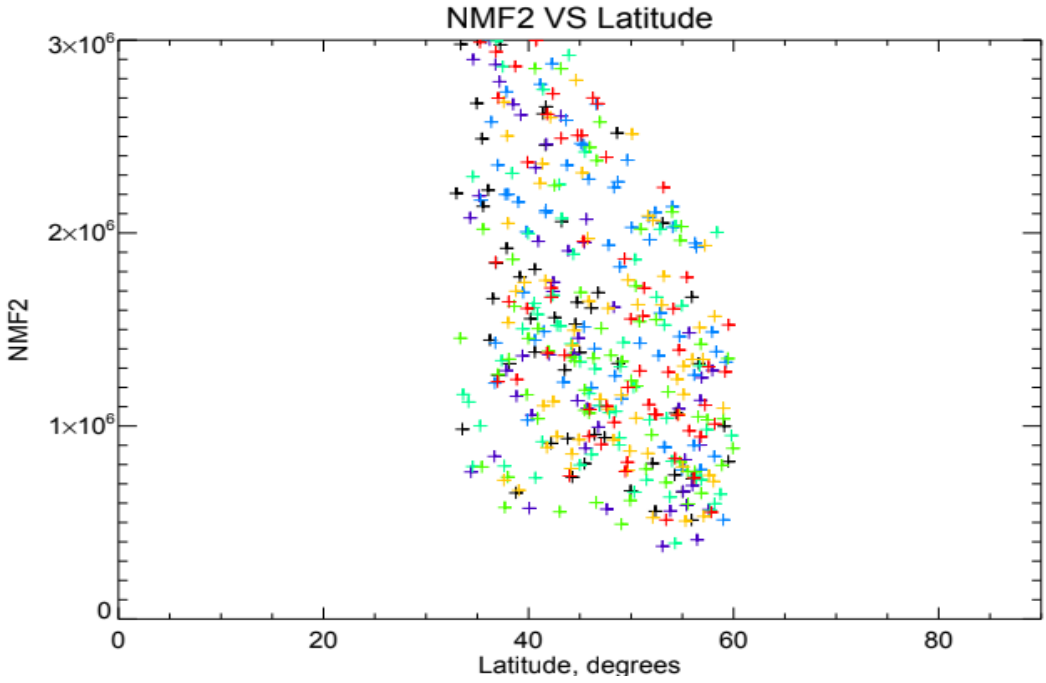

Figure 53: The figure shows how the NmF2 changes with latitude for the chosen days. The different color in the graph represent data from different days.

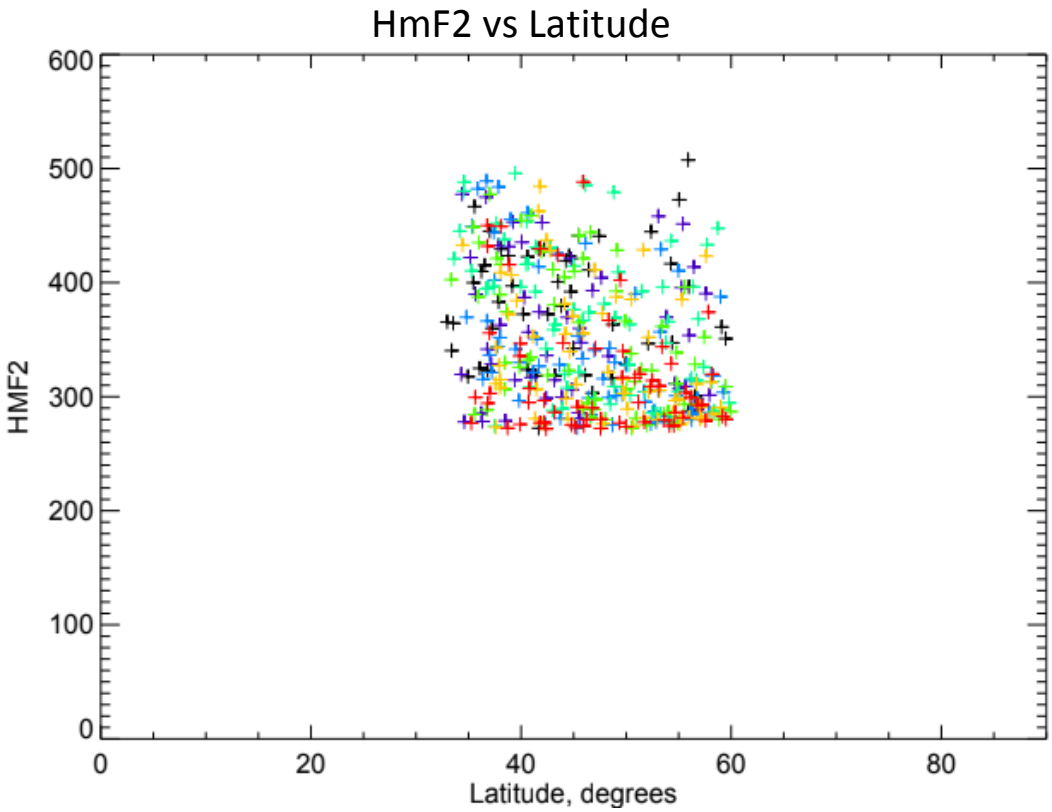

Figure 54: The figure shows how the HmF2 changes with latitude for the chosen days. The different color in the graph represent data from different days.

From Figure 51 to figure 54 it is seen that, during sunrise the satellite takes data from wide range of latitude over the seven days compared to sunset. Also, the NmF2 values of the data taken during sunrise are lower than the NmF2 values than the ones taken during sunset. This is mainly because of the ionization process over the day, the ions of different species tend to move upwards and hence the higher value of NmF2. During sunrise due to lower ionization process, the nmF2 values are generally lower than at sunset. Another observation that can made from Figure 52 and Figure 54 is that the HmF2 value is higher during sunset time compared to value of HmF2 during the sunrise. This tells us the ions move upwards throughout the day and then moves down after the sunset. Also, the days with higher solar flux tend to have higher HmF2 values compared to the days with low solar flux. The more the difference between the solar flux, the more difference will be in the HmF2 values.

In order to know more about the data, we segregated the data as per four different conditions and calculated the mean NmF2, mean HmF2 and the total vertical O^+ ions present for that category. Each category has four letters in it which corresponds to four different criteria.

Letter 1	This indicates the Solar activity. H for high solar flux and L for low solar flux.
Letter 2	This letter indicates to the time of the day when the measurement is the taken. S stands for Sunset and R stands for Sunrise.
Letter 3	This letter indicates what type of geographical latitude range the data falls into. L for low latitude (0 to 20 Degrees N), M for mid latitude (20 to 40 Degrees N), and H for high latitude (40 to 60 Degrees N).

Letter 4	This letter indicates what type of magnetic latitude range the data falls into. L for low latitude (0 to 20 Degrees N), M for mid latitude (20 to 40 Degrees N) and H for high latitude (40 to 60 Degrees N).

Table 1

In the table below, the different values obtained from the data after the separation of data in the above mentioned four different categories are given below.

	Mean NmF2	Mean HmF2	Vertical O^+
LRLL	604334.5	276.93	1.891e13
LRLM	541426.44	308.83	1.348e13
LRLH	NO DATA	NO DATA	NO DATA
LRML	709647.69	287.76	1.5316e13
LRMM	794681.25	295.07	1.3477e13
LRMH	576860.69	326.4	1.104e13
LRHL	NO DATA	NO DATA	NO DATA
LRHM	718769.25	317.09	9.399e12
LRHH	756735.2	291.8	8.663e12
LSLL	NO DATA	NO DATA	NO DATA
LSLM	NO DATA	NO DATA	NO DATA
LSLH	NO DATA	NO DATA	NO DATA
LSML	NO DATA	NO DATA	NO DATA
LSMM	2240247.5	368.3	2.8098e13
LSMH	1681154.2	342.4	2.1536e13
LSHL	NO DATA	NO DATA	NO DATA
LSHM	1951685.8	358.2	3.593e13
LSHH	1319905.6	317.6	4.5728e13
HRLL	553797.75	304	2.165e13
HRLM	438059.8	342	1.4124e13
HRLH	NO DATA	NO DATA	NO DATA
HRML	817168.44	304.2	2.0068e13
HRMM	886273.69	310.7	1.4556e13
HRMH	607997	296.6	1.254e13
HRHL	NO DATA	NO DATA	NO DATA
HRHM	940203.2	296.2	1.0655e13
HRHH	659482.12	319.5	9.641e12
HSLL	NO DATA	NO DATA	NO DATA
HSLM	NO DATA	NO DATA	NO DATA
HSLH	NO DATA	NO DATA	NO DATA
HSML	NO DATA	NO DATA	NO DATA
HSMM	2335309.5	381.9	2.262e13
HSMH	1610674.1	372.79	2.298e13
HSHL	NO DATA	NO DATA	NO DATA
HSHM	1899032.4	359.04	4.257e13
HSHH	1355508.6	339.4	5.3e13

Table 2

We can see from the above table that the highest NmF2 values occur in the mid latitude region. We will talk more about this in the conclusion section of this chapter.

3.4.2Comparison of SSULI data and IRI data

In this section, the data obtained from SSULI is compared with IRI model to check how consistent the data is. Again, for the comparison we have divided the data into two parts. In the first part, we took the data from one orbit. In the second part we included data from all the seven days.

3.4.2.1Comparison of data from one orbit

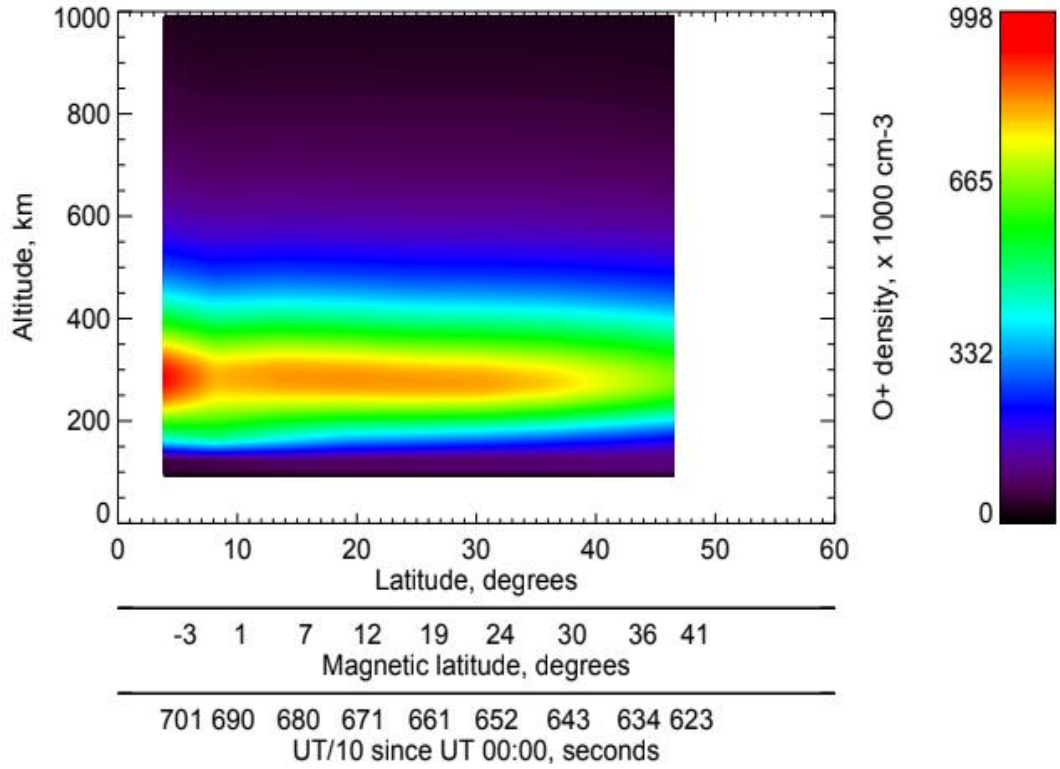

Figure 55: This figure is a contour plot which shows how the O^+ density varies with altitude as well as latitude for the chosen orbit.

In order to compare the data IRI model we have used the same orbit which we chose to represent the SSULI data. But unlike the SSULI data the IRI contour plot does not have two peaks even though the densities match quite well. So, get deeper understanding of whether the two data is agreeing or not we took three more orbits to compare. The first orbit is chosen from the first day and the next two from the fourth day.

Orbit 2

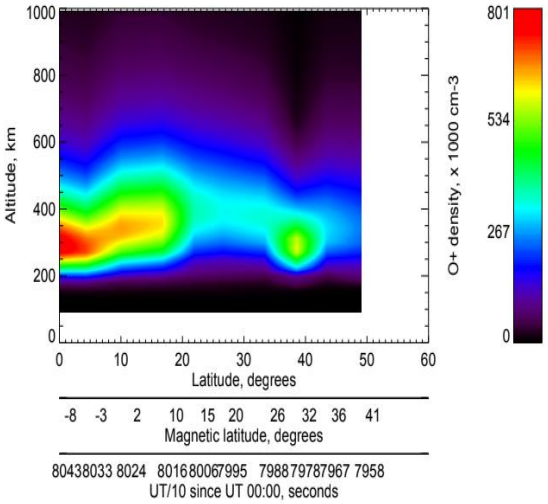

Figure 56: O^+ density contour plot for SSULI data

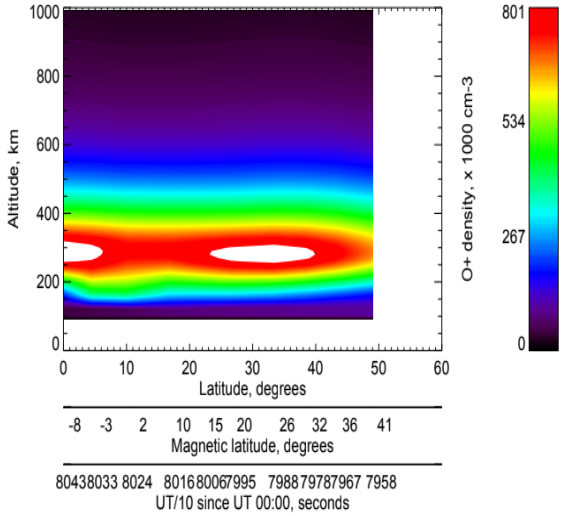

Figure 57: O^+ density contour plot for IRI data

Orbit 3

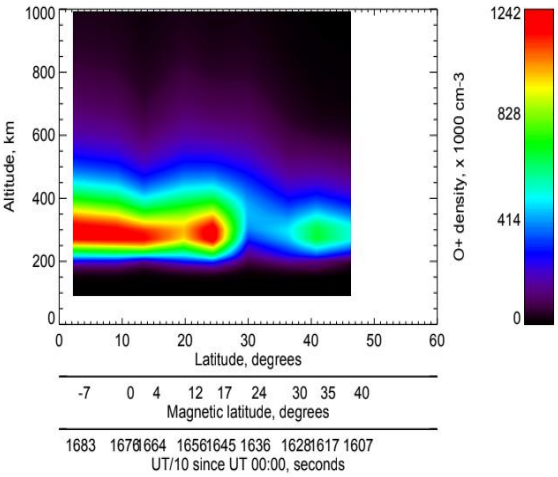

Figure 58: O^+ density contour plot for SSULI data

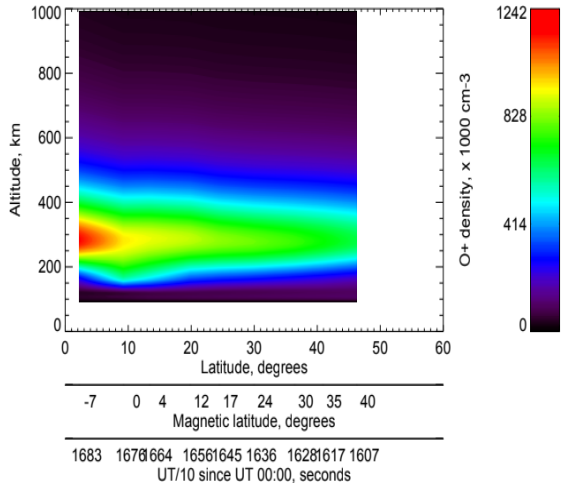

Figure 59: O^+ density contour plot for IRI data

Orbit 4

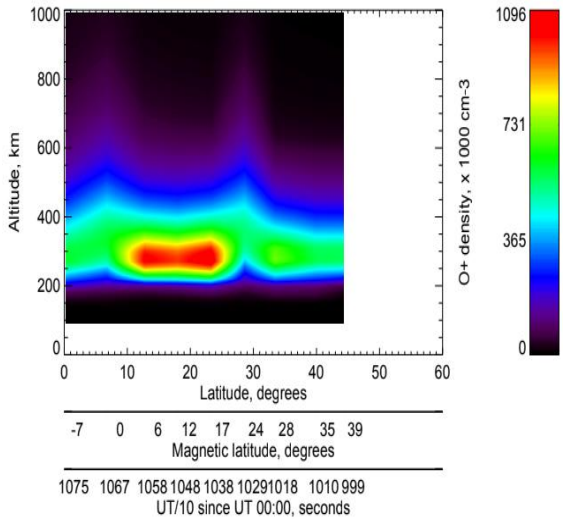

Figure 60: O^+ density contour plot for SSULI data

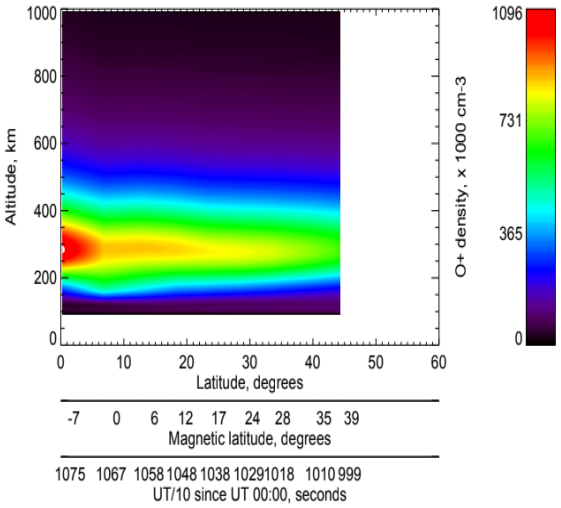

Figure 61: O^+ density contour plot for IRI data

Figures 56,58 and 60 represents the SSULI data and Figures 57, 59 and 61 represents the IRI data for the corresponding SSULI orbits. Even though for orbit 2 the IRI data does not match with the SSULI data, for orbit 3 and 4 both the data agrees with each other. It can also be observed that the altitude corresponding to the peak values of O^+ densities are quite similar in both types of data. The SSULI O^+ density is consistent with the IRI O^+ density.

3.4.2.2Comparison of data from all seven days

In order to compare the SSULI data with IRI data we divided the data from seven days into two parts. One for the sunrise and the other for the sunset just like we did it while analyzing the SSULI data.

3.4.2.2.1Comparison of sunrise data

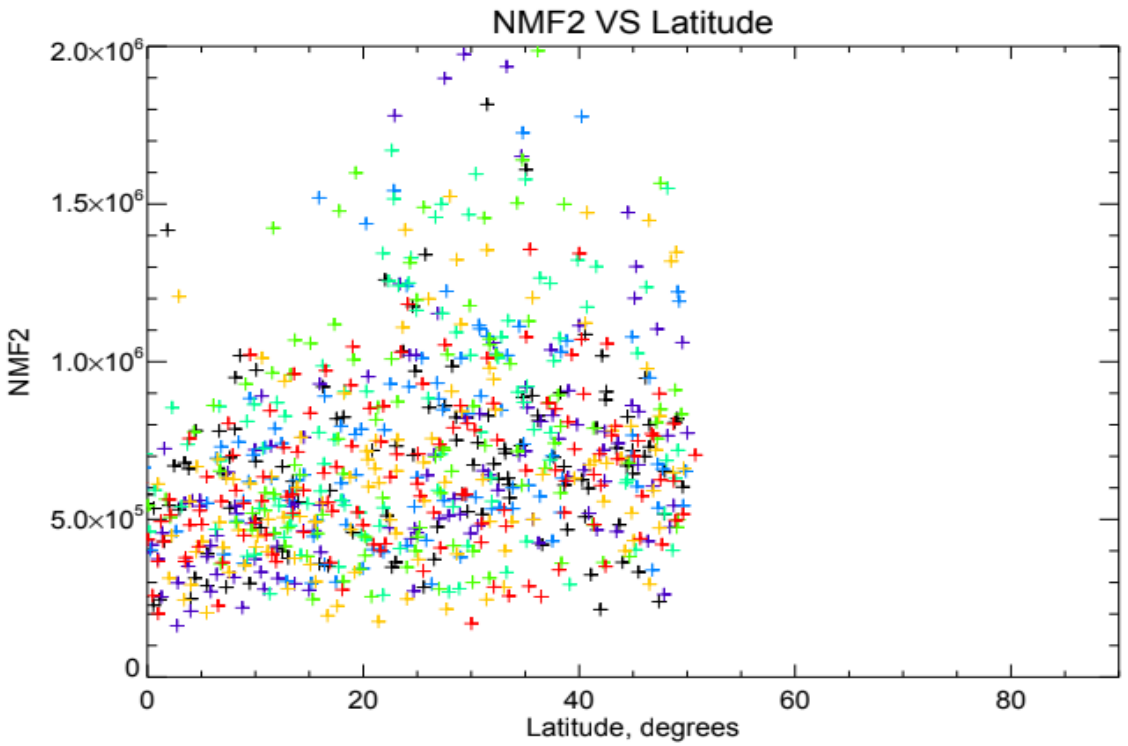

Figure 62: The figure shows how the SSULI NmF2 changes with latitude for the chosen days. The different color in the graph represent data from different days.

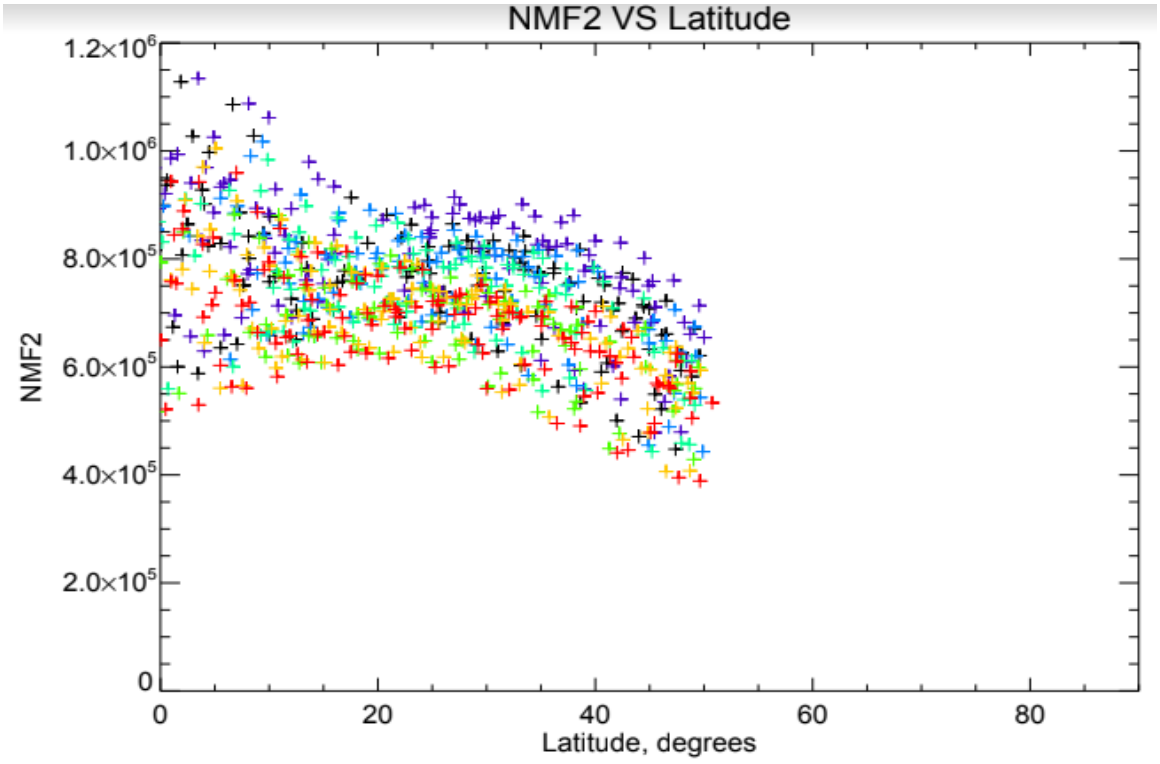

Figure 63: The figure shows how the IRI NmF2 changes with latitude for the chosen days. The different color in the graph represent data from different days.

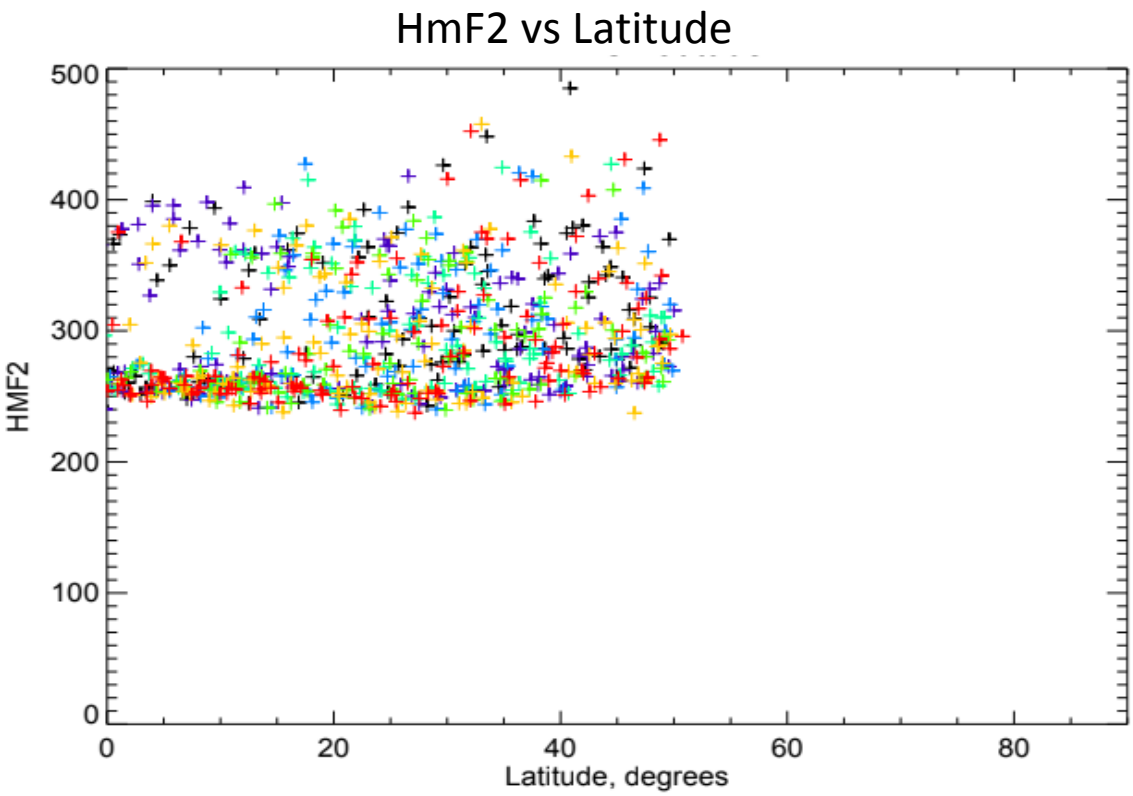

Figure 64: The figure shows how the SSULI HmF2 changes with latitude for the chosen days. The different color in the graph represent data from different days.

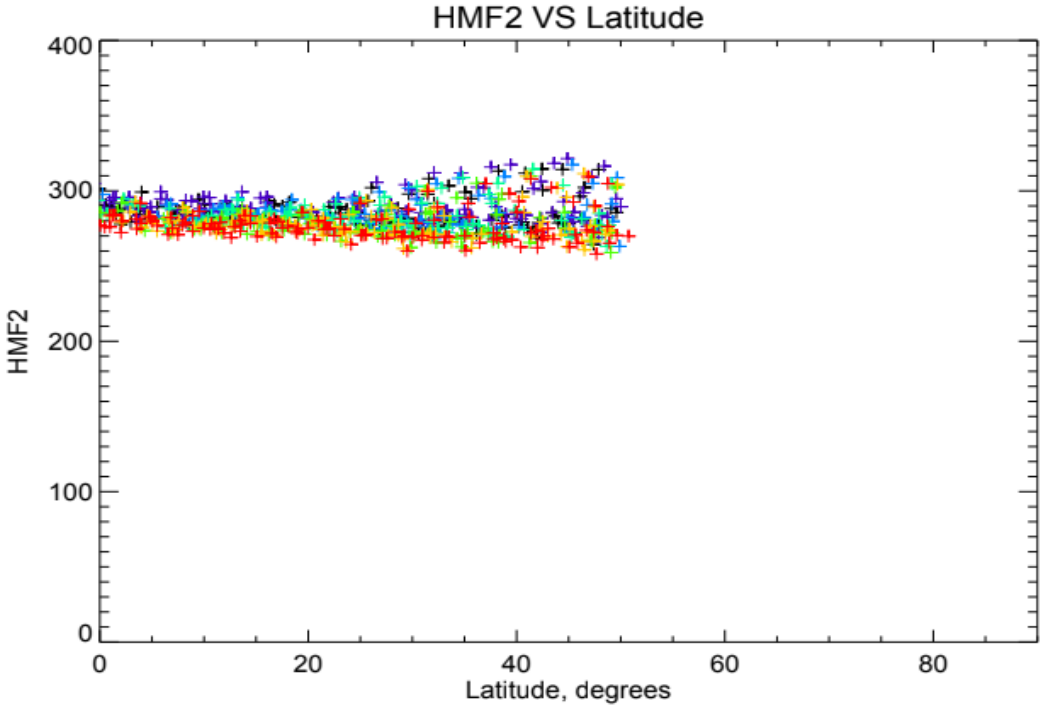

Figure 65: The figure shows how the IRI HmF2 changes with latitude for the chosen days. The different color in the graph represent data from different days.

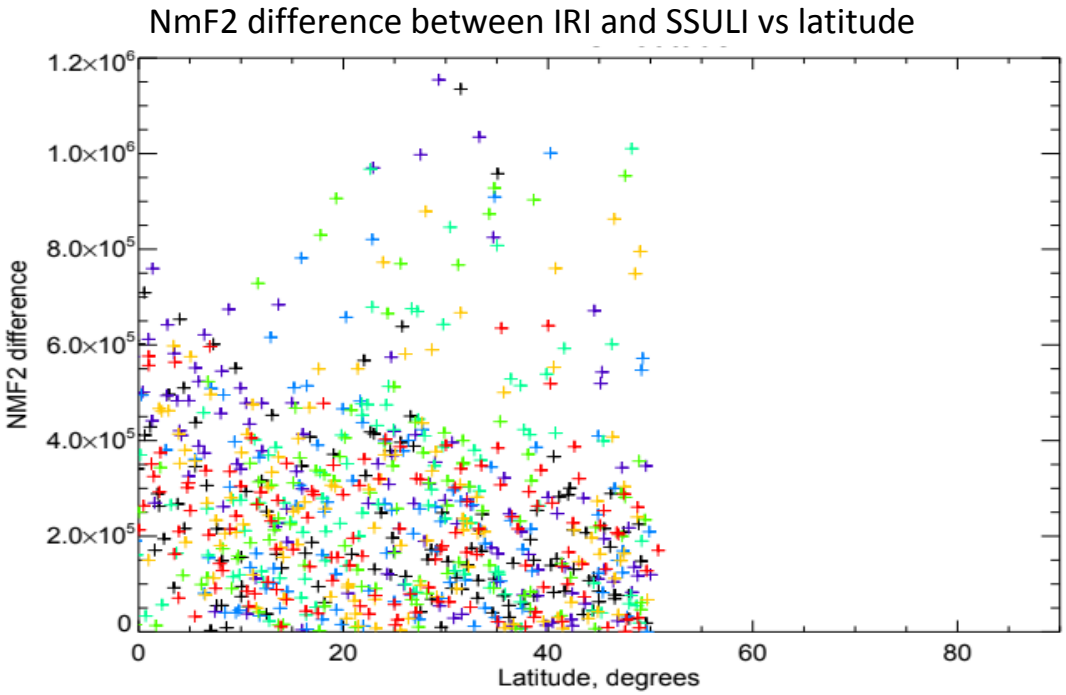

Figure 66: The figure shows the difference of NmF2 between IRI and SSULI data with latitude for the chosen days. The different color in the graph represent data from different days.

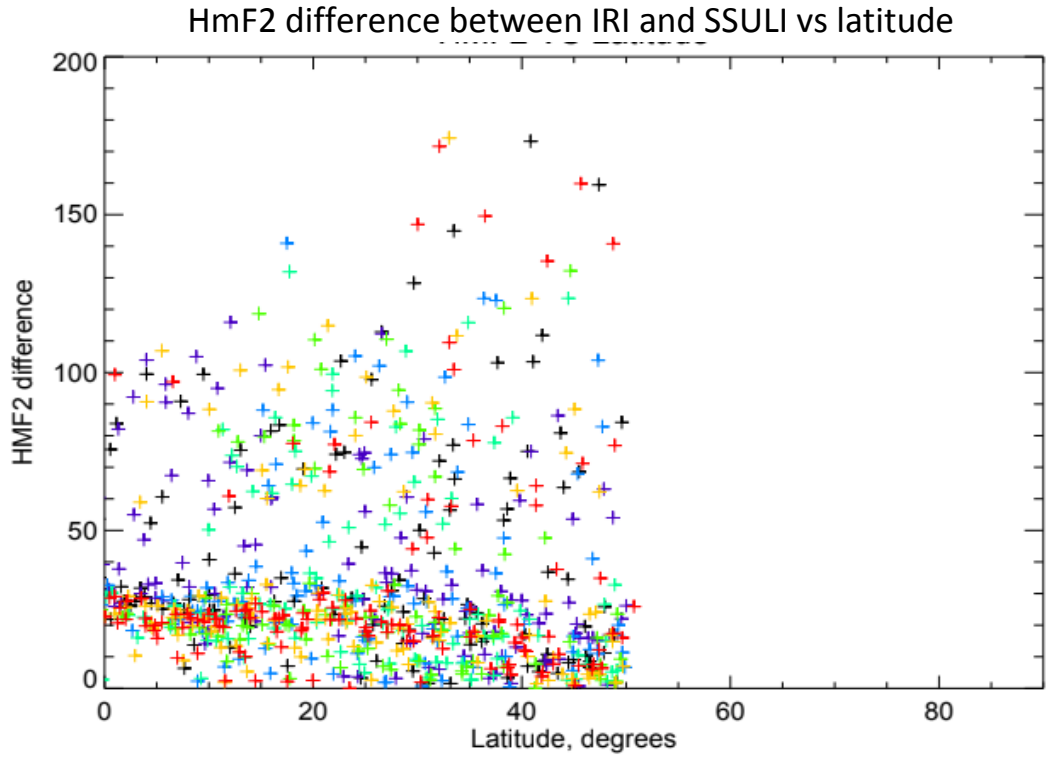

Figure 67: The figure shows the difference of HmF2 between IRI and SSULI data with latitude for the chosen days. The different color in the graph represent data from different days.

3.4.2.2.2Comparison of sunset data

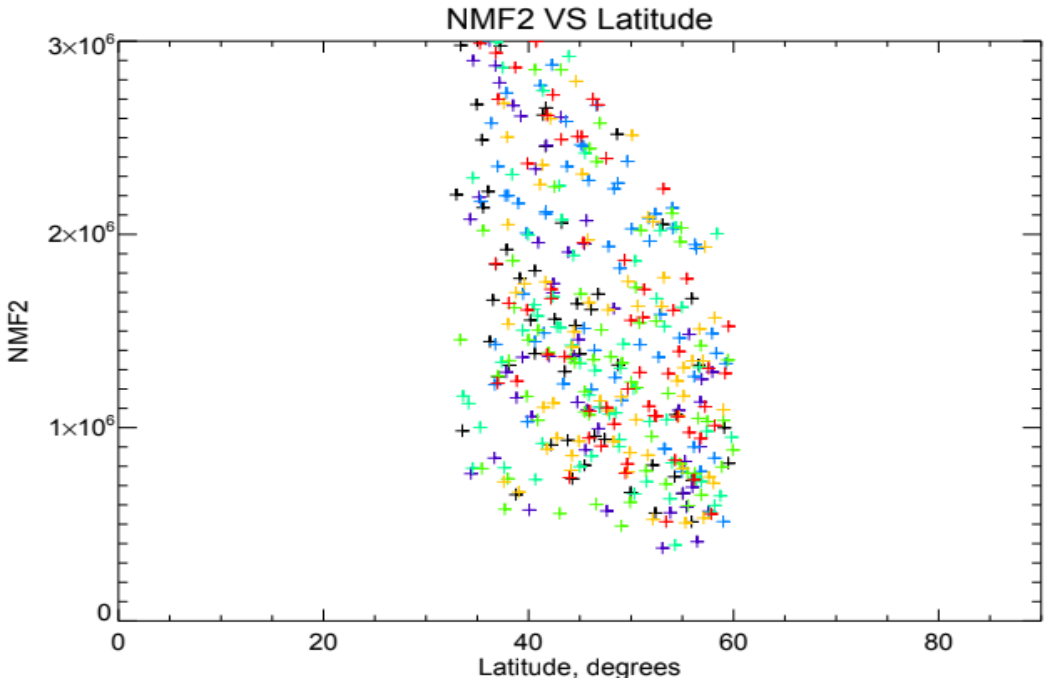

Figure 68: The figure shows how the SSULI NmF2 changes with latitude for the chosen days. The different color in the graph represent data from different days.

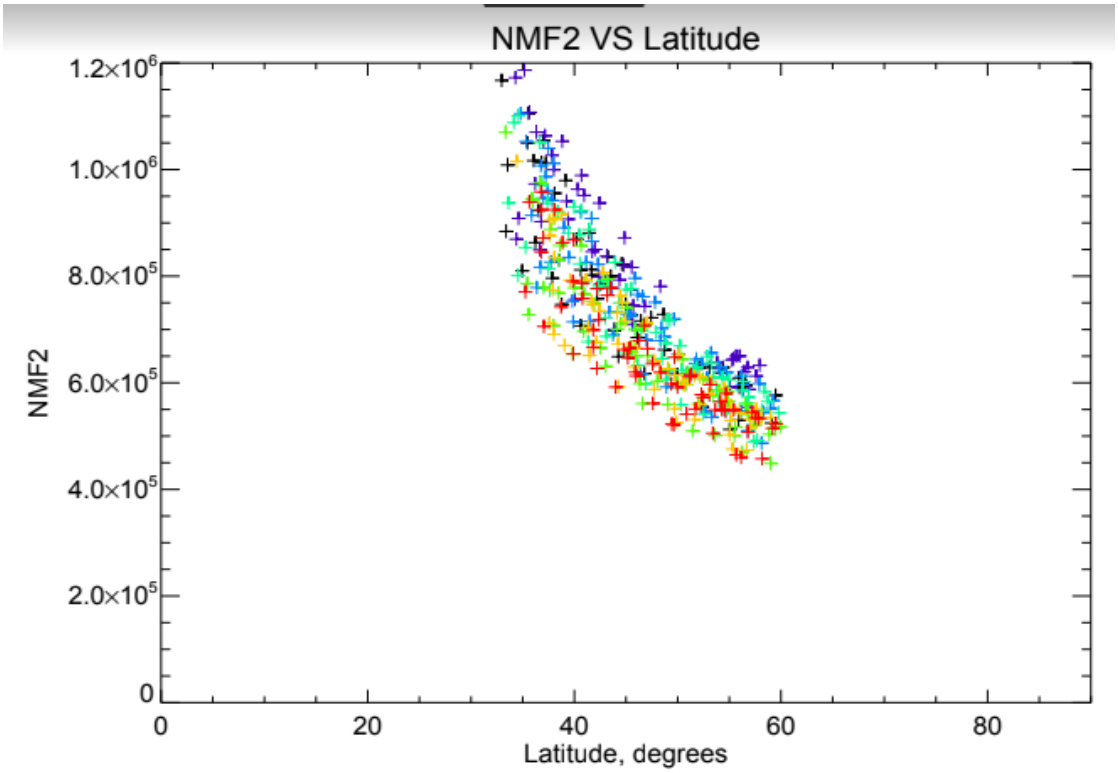

Figure 69: The figure shows how the IRI NmF2 changes with latitude for the chosen days. The different color in the graph represent data from different days.

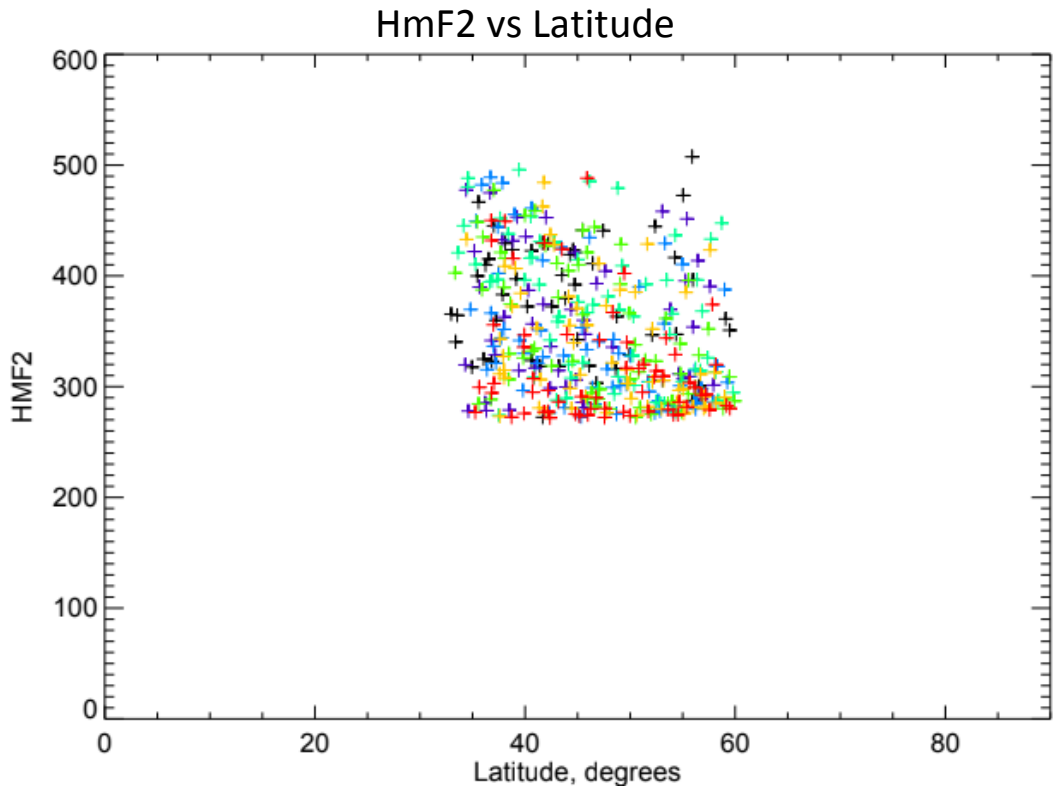

Figure 70: The figure shows how the SSULI HmF2 changes with latitude for the chosen days. The different color in the graph represent data from different days.

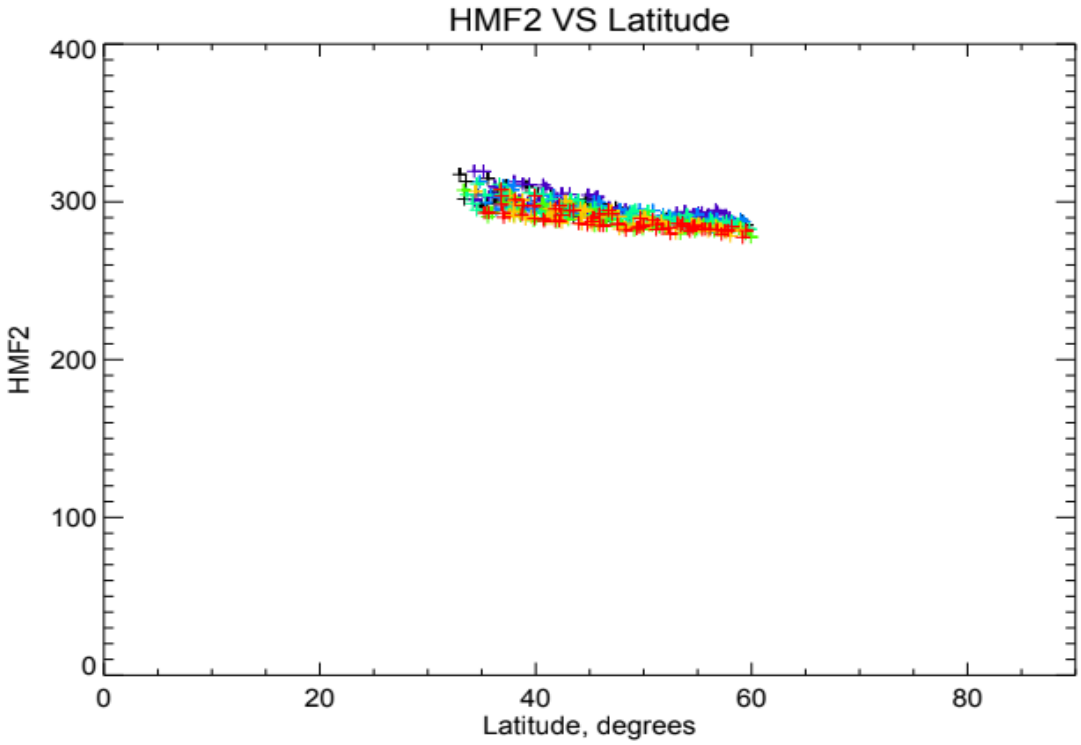

Figure 71: The figure shows how the IRI HmF2 changes with latitude for the chosen days. The different color in the graph represent data from different days.

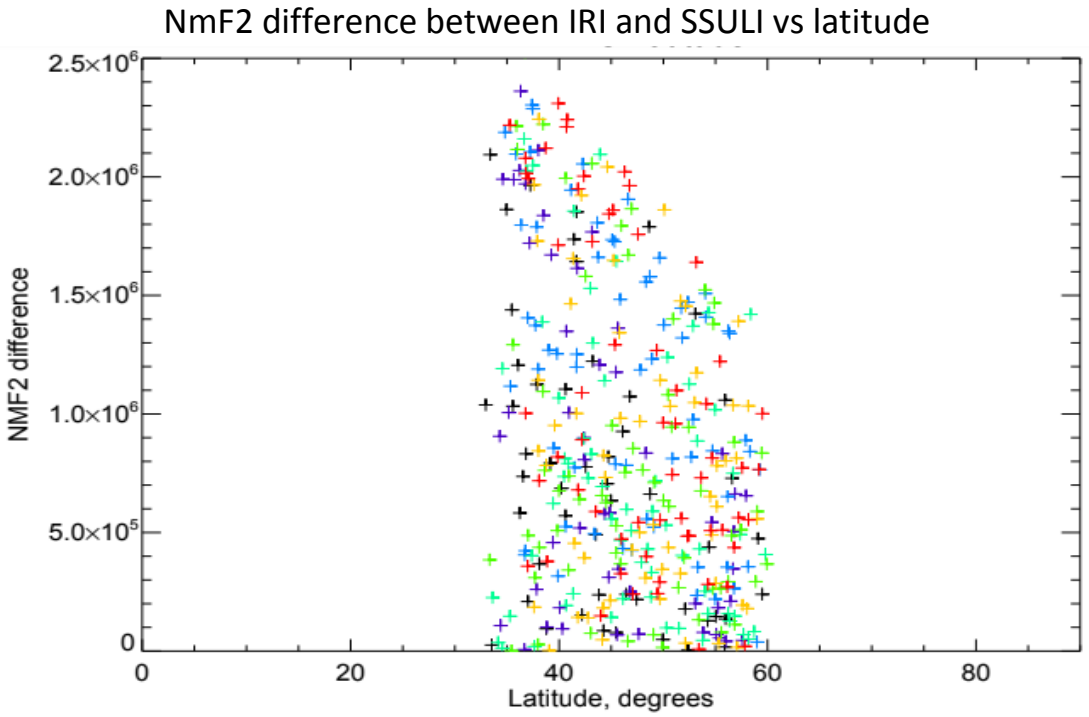

Figure 72: The figure shows the difference of NmF2 between IRI and SSULI data with latitude for the chosen days. The different color in the graph represent data from different days.

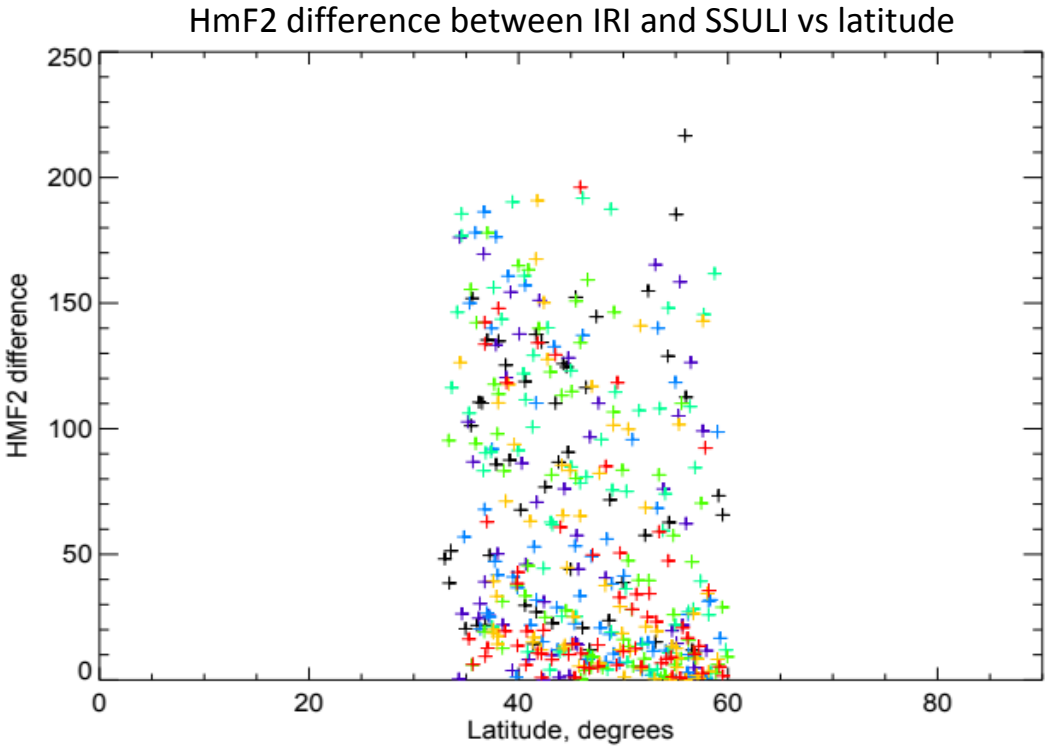

Figure 73: The figure shows the difference of HmF2 between IRI and SSULI data with latitude for the chosen days. The different color in the graph represent data from different days.

From the above figures it can be observed that both the data (SSULI and IRI) matches quite well especially during sunrise. During sunset the two data do not agrees closely with each other compared to the sunrise data.

3.4.3Comparison of SSULI and TIEGCM data

In this section, the data obtained from SSULI is compared with TIEGCM model to check how consistent the data is. Again, for the comparison we have divided the data into two parts. In the first part, we took the data from one orbit. In the second part we included data from all the seven days.

3.4.3.1Comparison of data from one orbit

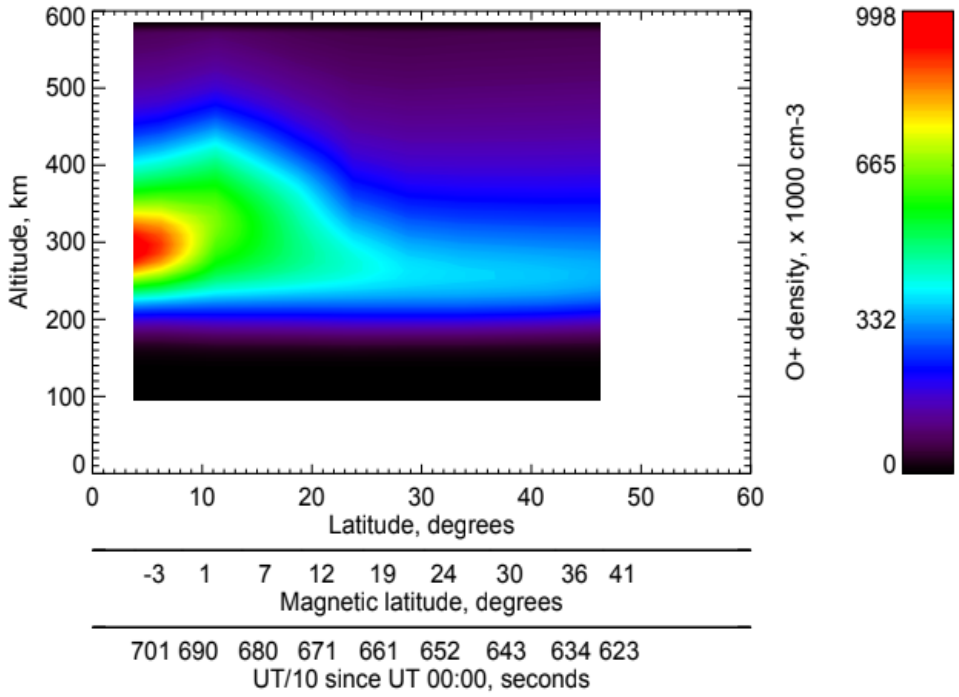

Figure 74: This figure is a contour plot which shows how the O^+ density varies with altitude as well as latitude for the chosen orbit.

In order to compare the data TIEGCM model we have used the same orbit which we chose to

represent the SSULI data. But unlike the SSULI data the TIEGCM contour plot does not have two peaks even though the densities match quite well. So, get deeper understanding of whether the two data is agreeing or not we took three more orbits to compare. The first orbit is chosen from the first day and the next two from the fourth day.

Orbit 2

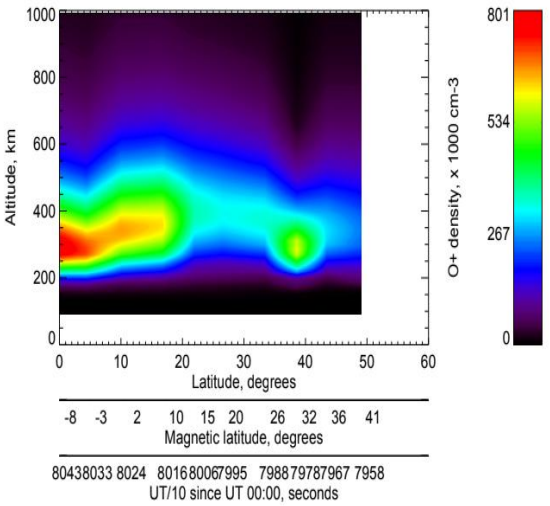

Figure 75: O^+ density contour plot for SSULI data

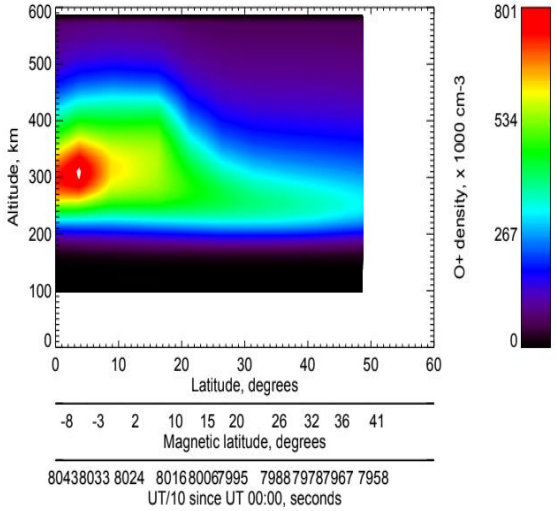

Figure 76: O^+ density contour plot for TIEGCM data

Orbit 3

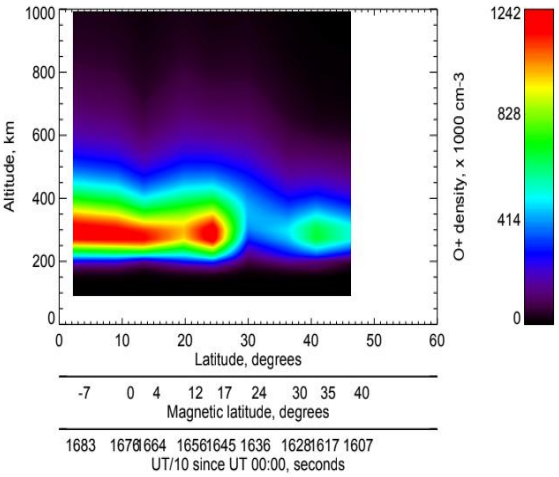

Figure 77: O^+ density contour plot for SSULI data

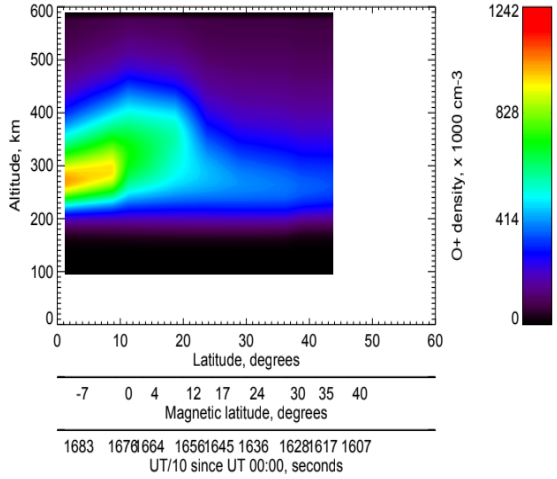

Figure 78: O^+ density contour plot for TIEGCM data

Orbit 4

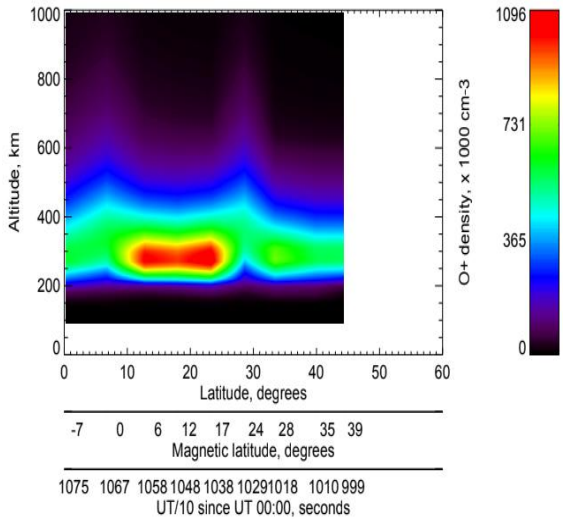

Figure 79: O^+ density contour plot for SSULI data

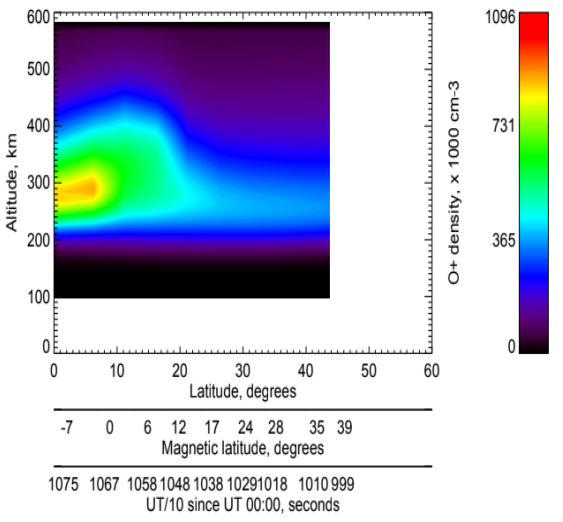

Figure 80: O^+ density contour plot for TIEGCM data

Figures 75, 77 and 79 represents the SSULI data and Figures 76, 78 and 80 represents the TIEGCM data for the corresponding SSULI orbits. Almost in all the orbit, the TIEGCM data is quite like the SSULI data especially the altitude corresponding to the peak density. Yes, there is some difference in the latitude where the peak density is measure but it is mainly because while retrieving the TIEGCM data we have rounded off the UT secs of SSULI to the nearest hour for TIEGCM data. SSULI O^+ density is also consistent with the TIEGCM O^+ density for all the orbits.

3.4.3.2Comparison of data from all seven days

In order to compare the SSULI data with TIEGCM data we divided the data from seven days into two parts. One for the sunrise and the other for the sunset just like we did it while analyzing the SSULI data.

3.4.3.2.1Comparison of sunrise data

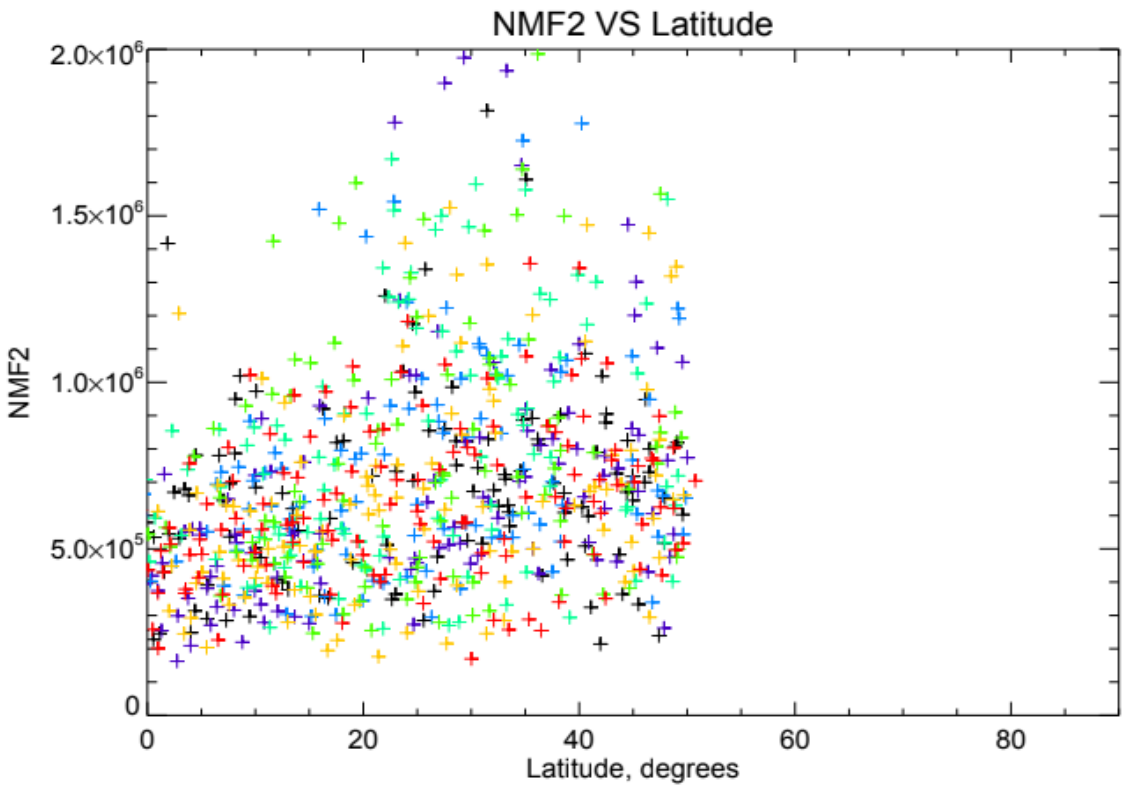

Figure 81: The figure shows how the SSULI NmF2 changes with latitude for the chosen days. The different color in the graph represent data from different days.

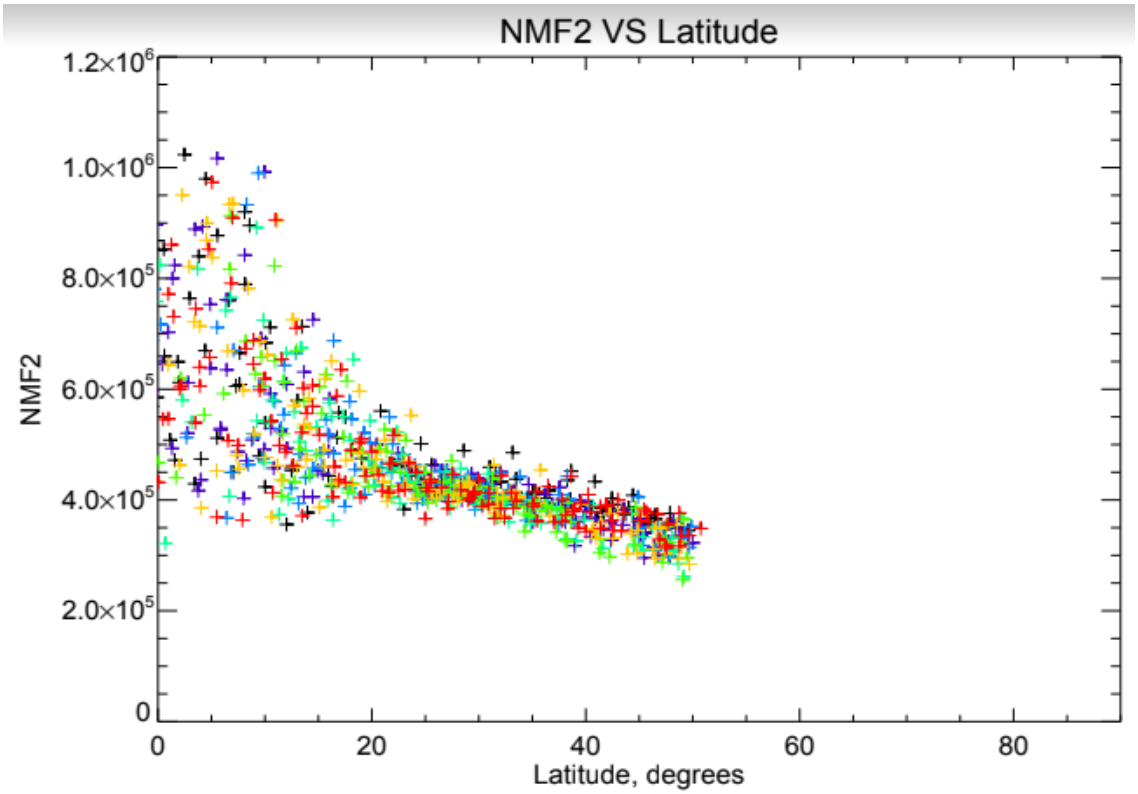

Figure 82: The figure shows how the TIEGCM NmF2 changes with latitude for the chosen days. The different color in the graph represent data from different days.

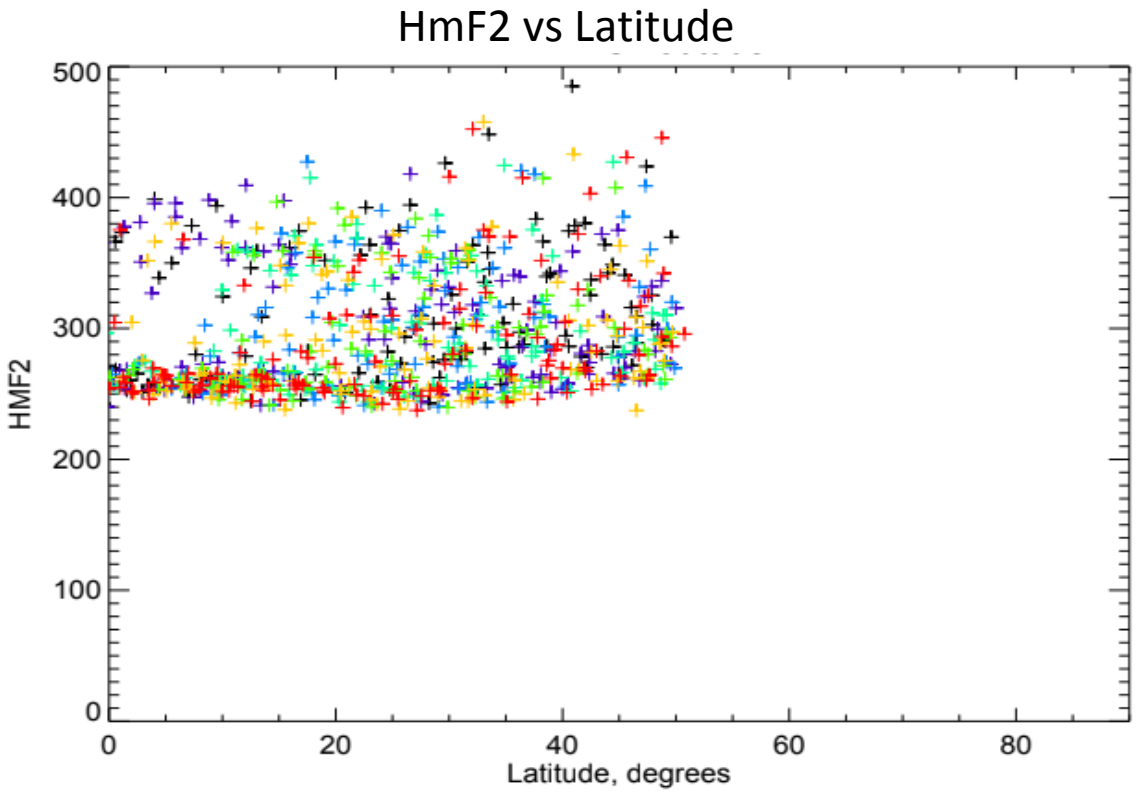

Figure 83: The figure shows how the SSULI HmF2 changes with latitude for the chosen days. The different color in the graph represent data from different days.

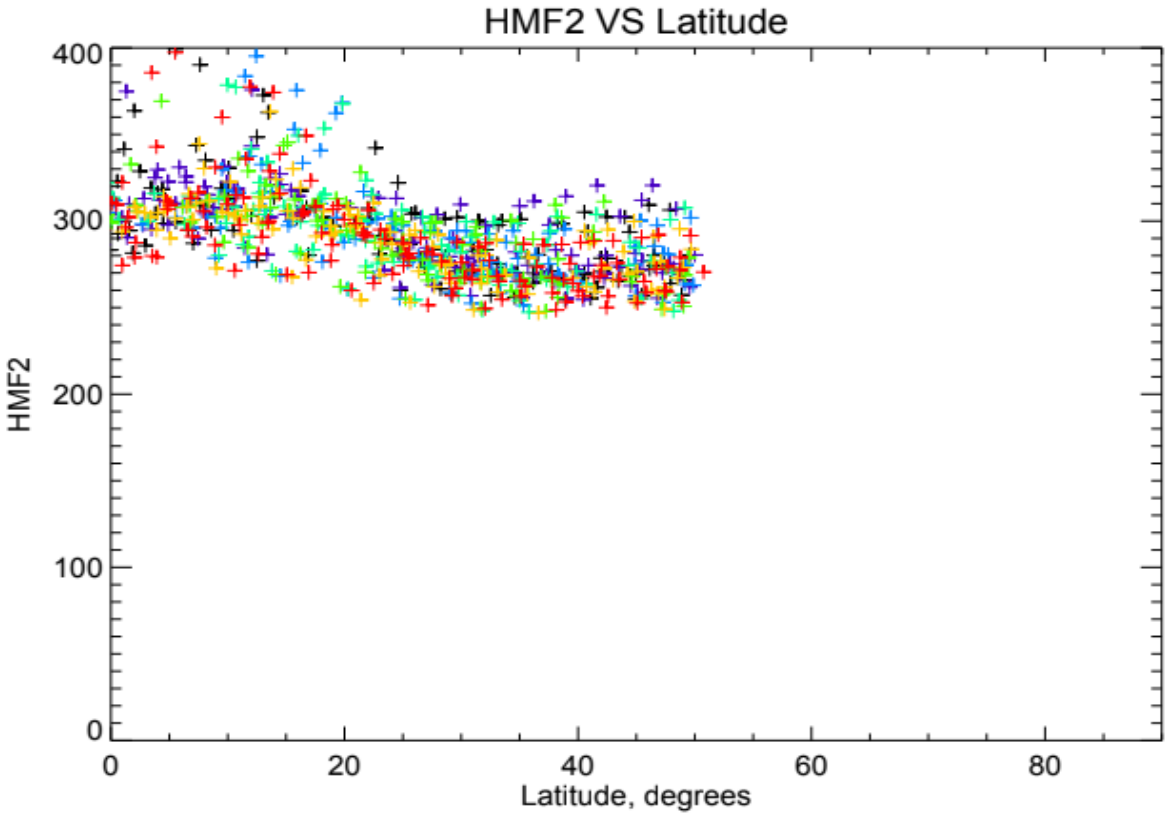

Figure 84: The figure shows how the TIEGCM HmF2 changes with latitude for the chosen days. The different color in the graph represent data from different days.

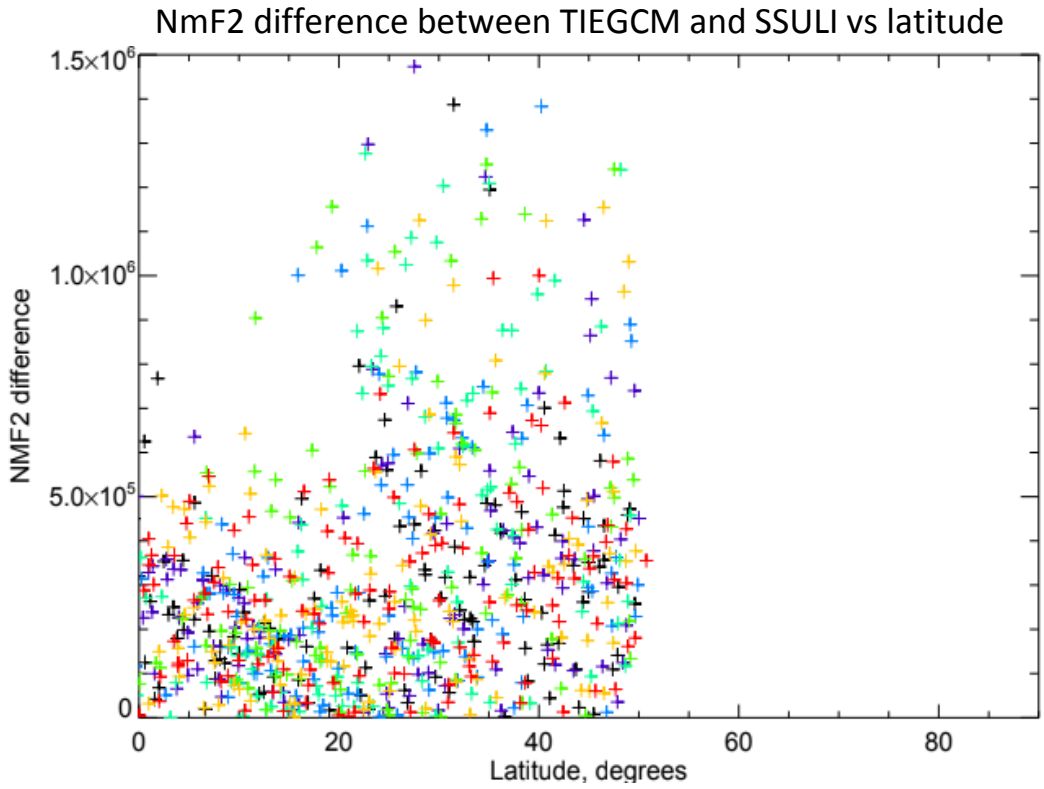

Figure 85: The figure shows the difference of NmF2 between TIEGCM and SSULI data with latitude for the chosen days. The different color in the graph represent data from different days.

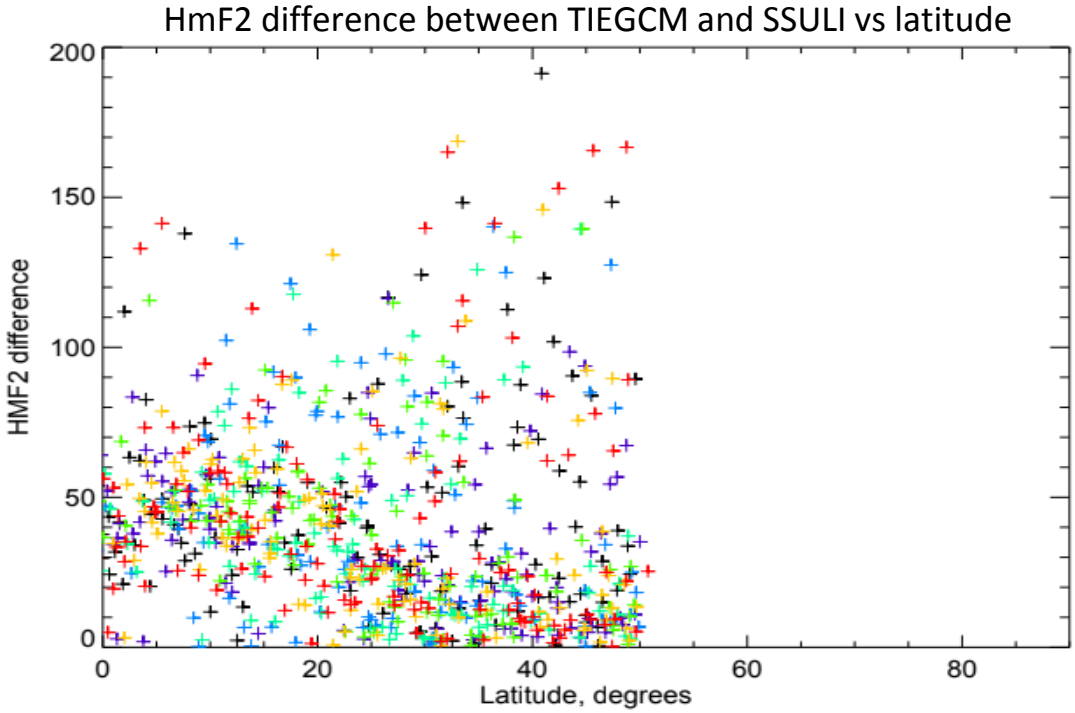

Figure 86: The figure shows the difference of HmF2 between TIEGCM and SSULI data with latitude for the chosen days. The different color in the graph represent data from different days.

3.4.3.2.2Comparison of sunset data

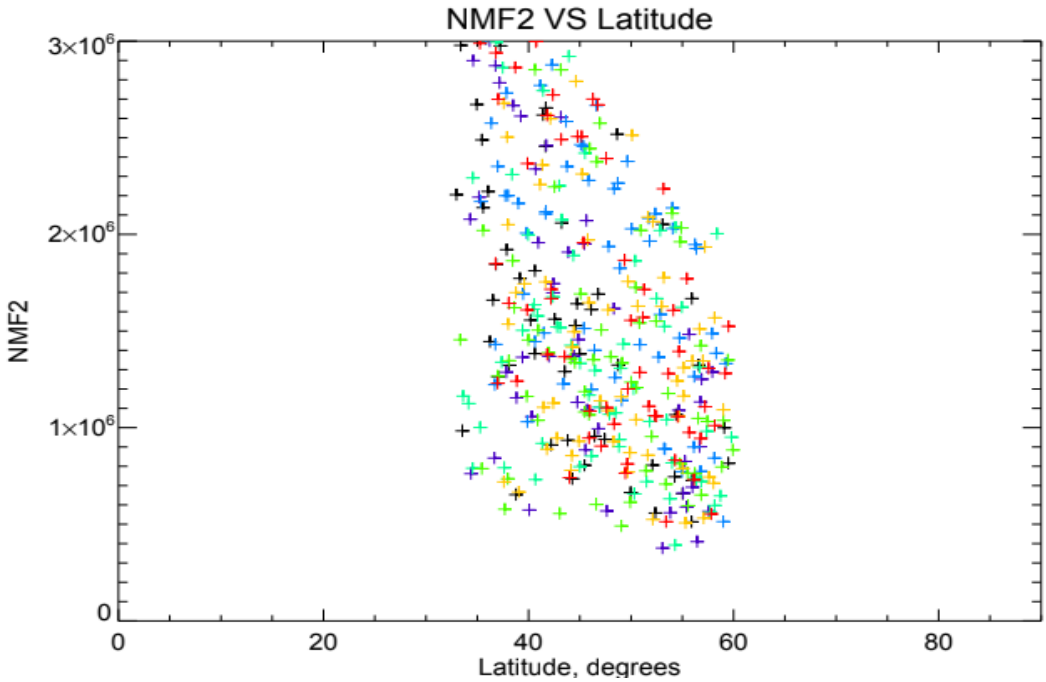

Figure 87: The figure shows how the SSULI NmF2 changes with latitude for the chosen days. The different color in the graph represent data from different days.

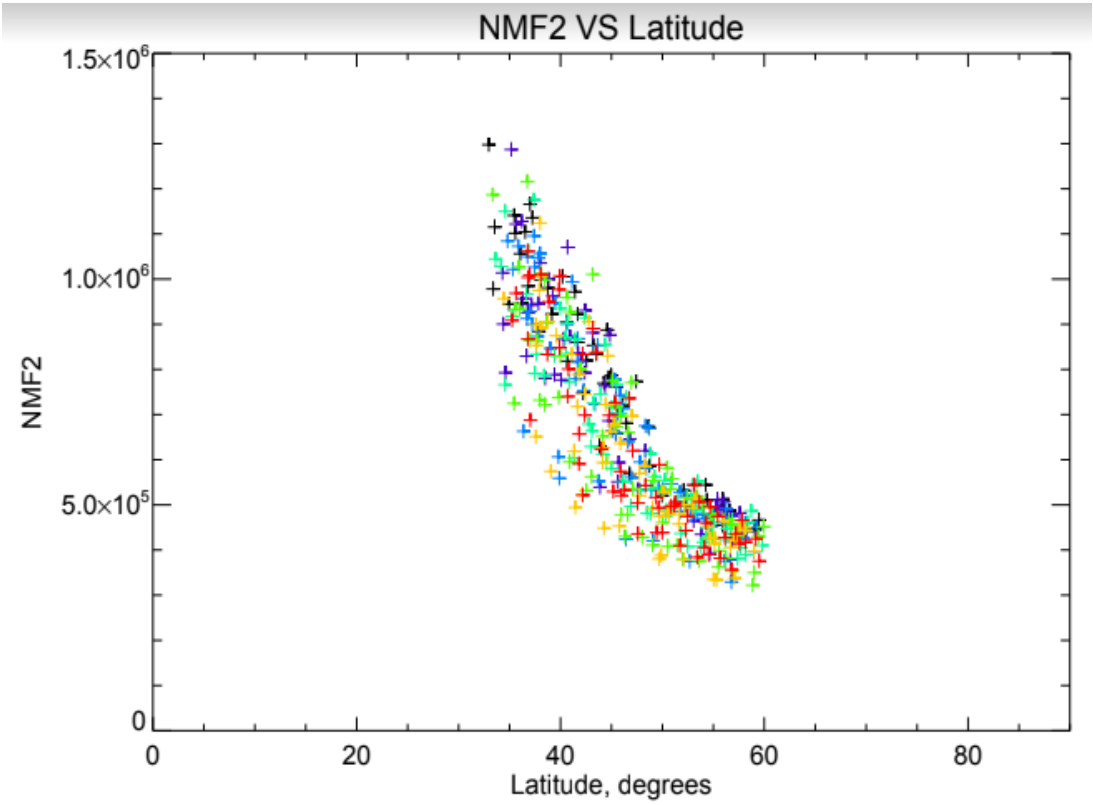

Figure 88: The figure shows how the TIEGCM NmF2 changes with latitude for the chosen days. The different color in the graph represent data from different.

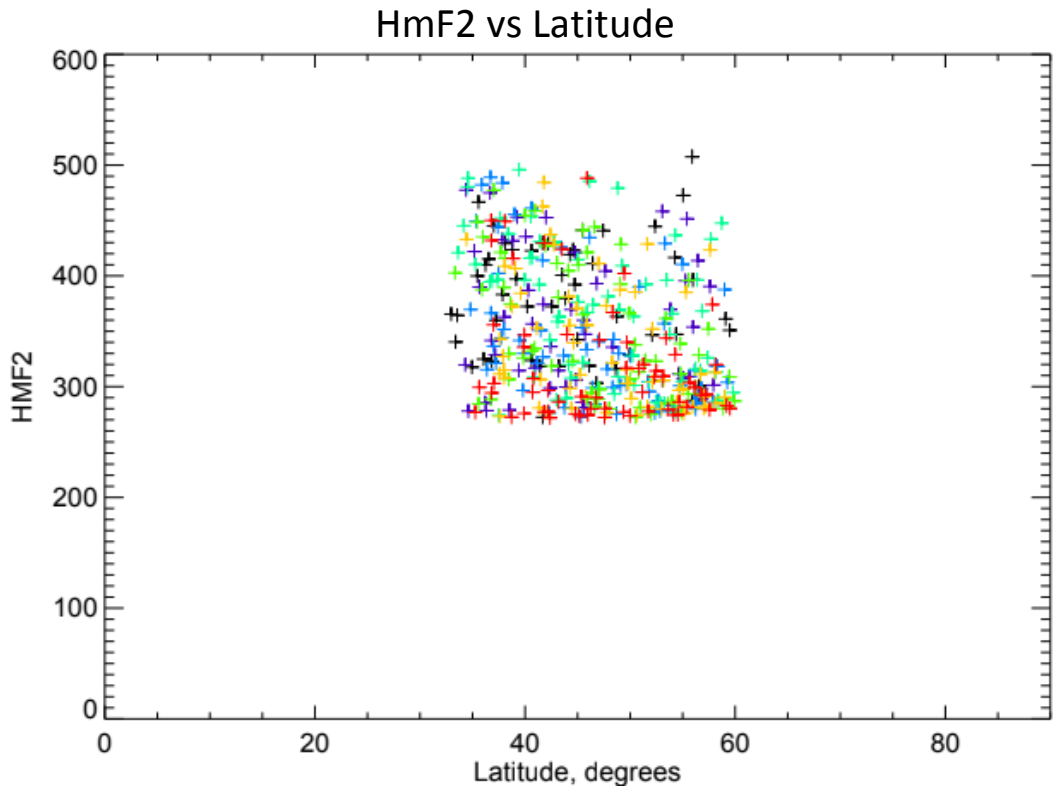

Figure 89: The figure shows how the SSULI HmF2 changes with latitude for the chosen days. The different color in the graph represent data from different days.

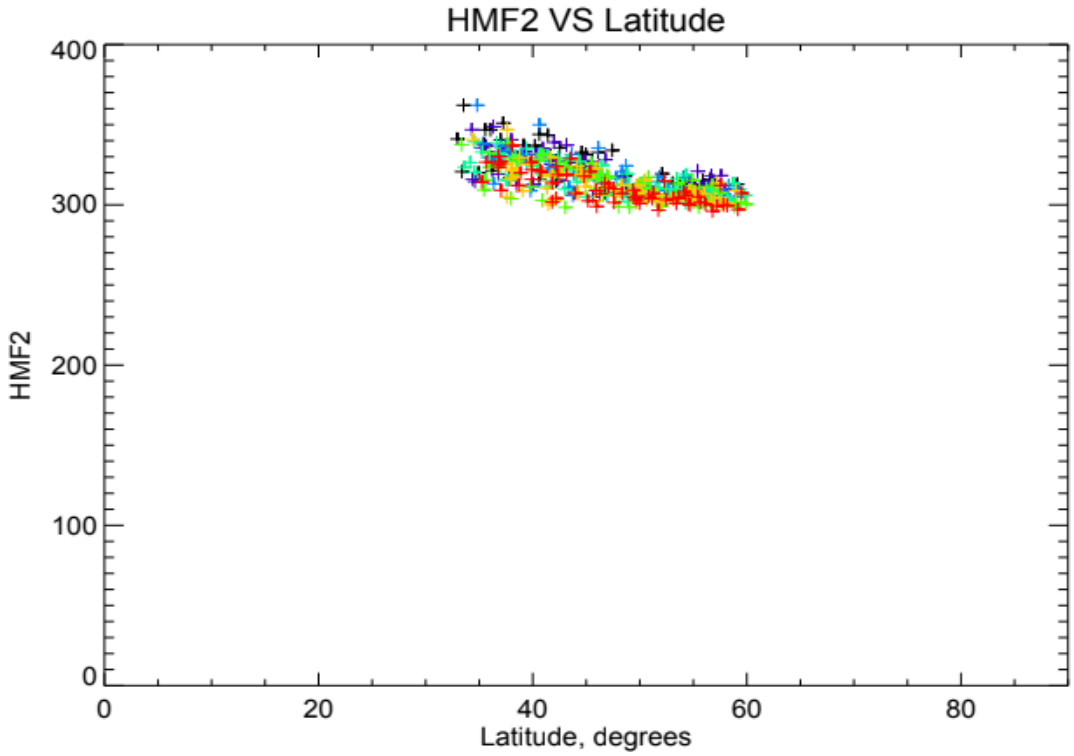

Figure 90 The figure shows how the TIEGCM HmF2 changes with latitude for the chosen days. The different color in the graph represent data from different days.

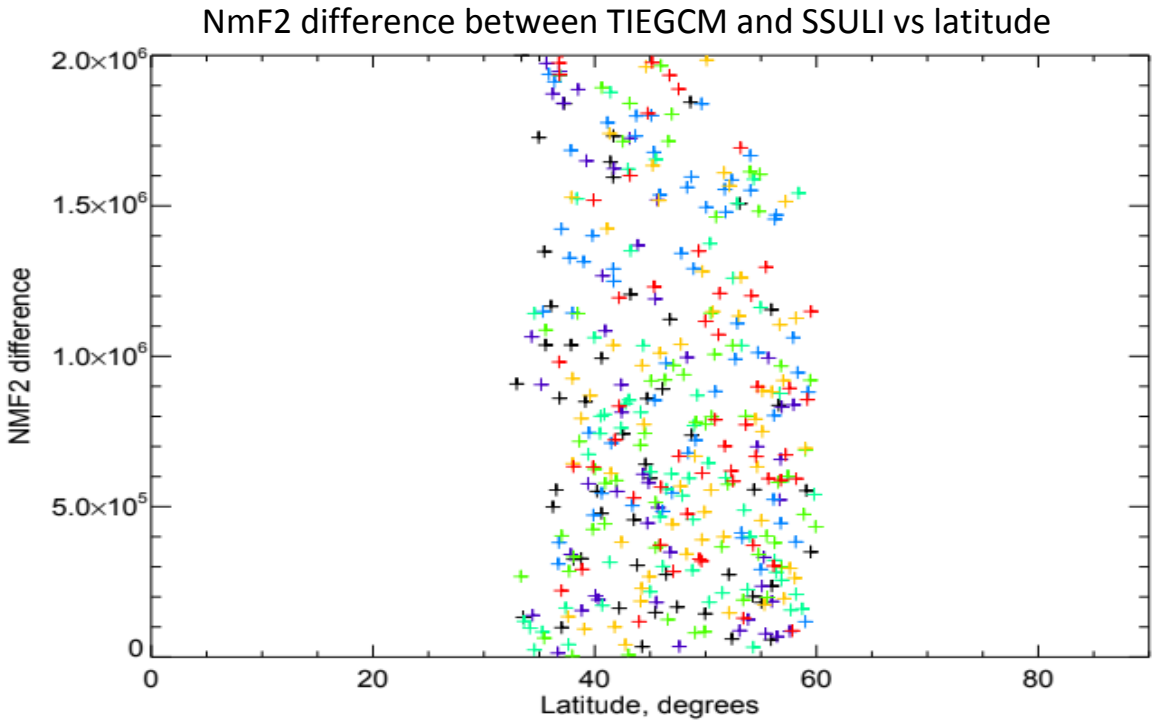

Figure 91: The figure shows the difference of NmF2 between TIEGCM and SSULI data with latitude for the chosen days. The different color in the graph represent data from different days.

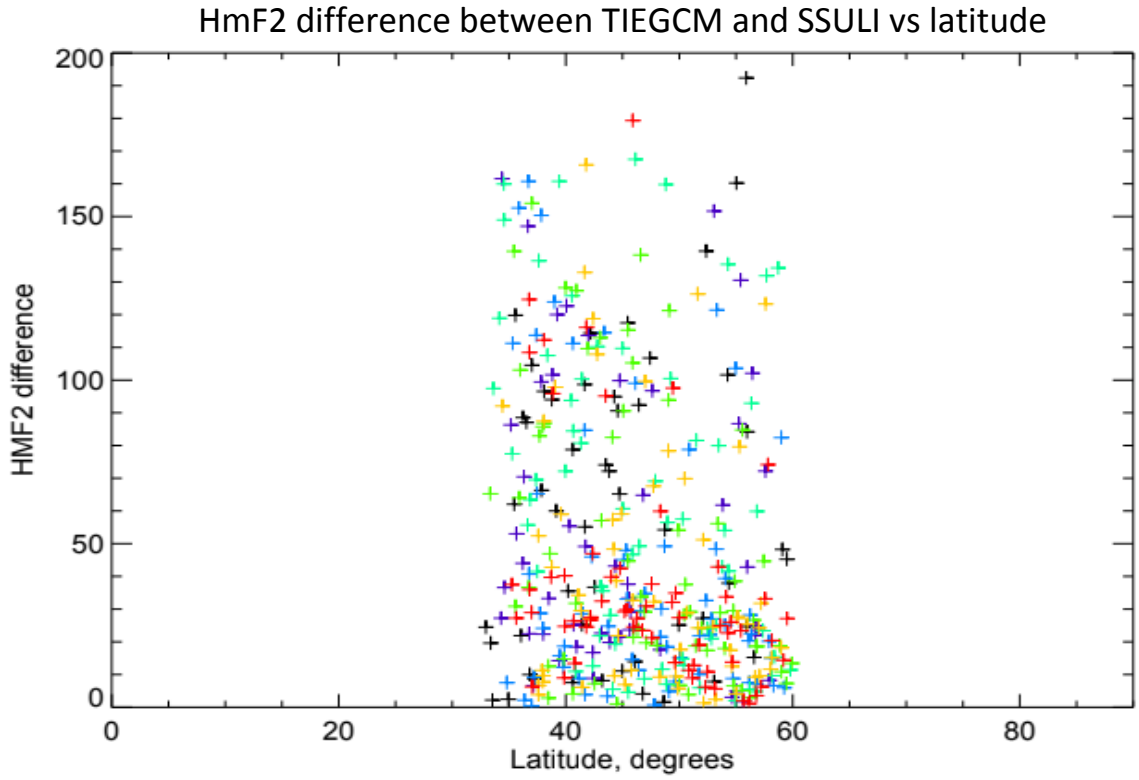

Figure 92: The figure shows the difference of HmF2 between TIEGCM and SSULI data with latitude for the chosen days. The different color in the graph represent data from different days.

By observing the above figures, we can see that during sunrise, the NMF2 and HmF2 for TIEGCM data is less scattered compared to the SSULI data. The same thing can be observed for the data taken during local sunset as well, but it is not that prominent like the sunrise data. Also, for the sunrise data the NmF2 and HmF2 values are quite consistent in both the data and the difference for NmF2 between the two models are mostly below 5e5 cm^{-3}. The HmF2 difference between the two data are mostly below 40 kms which tells the two data match well. During sunset, the NmF2 difference is quite high and so the HmF2 compared to the sunrise data. We can see the same thing happening for IRI data as well and this suggests there is some other activities going on in those days especially during the day which change the spread of O^+ ions over the altitude. The mean density of O^+ ions for the three models are given below. Even though the TIEGCM value is on the higher side but the mean density obtained in the IRI model is very close to the one obtained from SSULI data. It is to be noted that the TIEGCM is at the nearest grid points so that isn't perfect.

Mean density of O^+ ions for SSULI data (cm^{-3})	**Mean density of O^+ ions for IRI data (cm^{-3})**	**Mean density of O^+ ions for TIEGCM data (cm^{-3})**
116120	115574	154144

3.4.4 Comparison of SSULI data with IRI and TIEGCM models in the latitude range of 35^0 N to 50^0 N

After analyzing the data in the previous section, we found that during sunset the latitude spread of the data is less compared to the data observed during sunrise. In order to overcome this bias, we decided to analyze the data in the common latitude range between sunrise data and sunset data i.e. the data that falls between 35 degrees N latitude and 50 degrees N latitude. The plots obtained after applying the criteria are given below:

3.4.4.1 Comparison of sunrise data

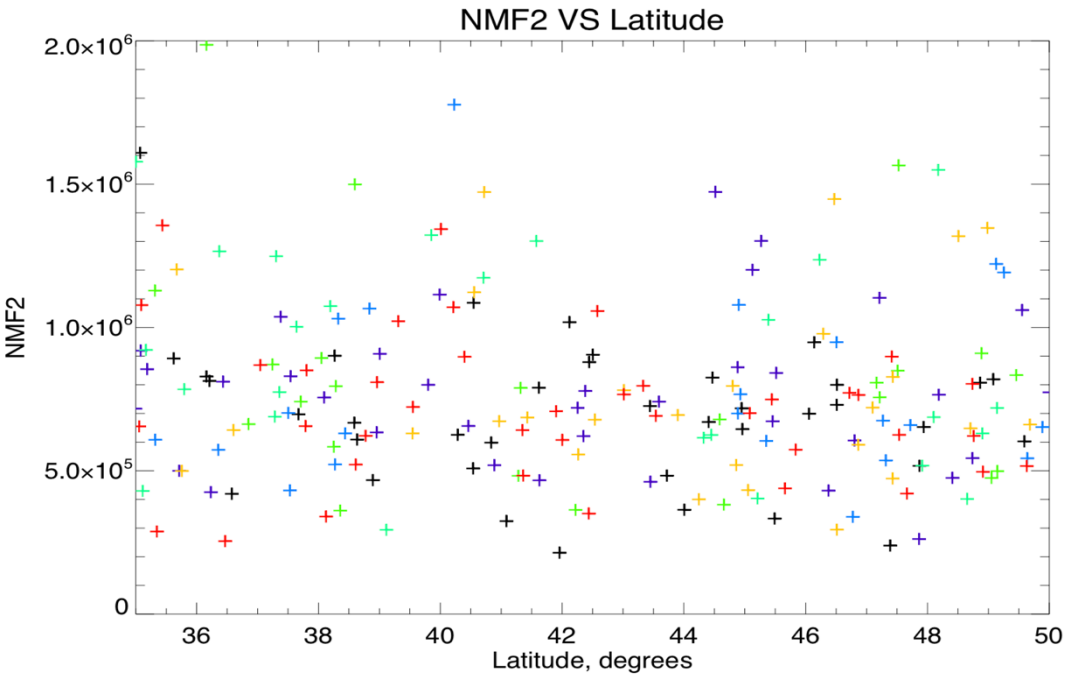

Figure 93: The figure shows how the NmF2 varies with latitude for SSULI data

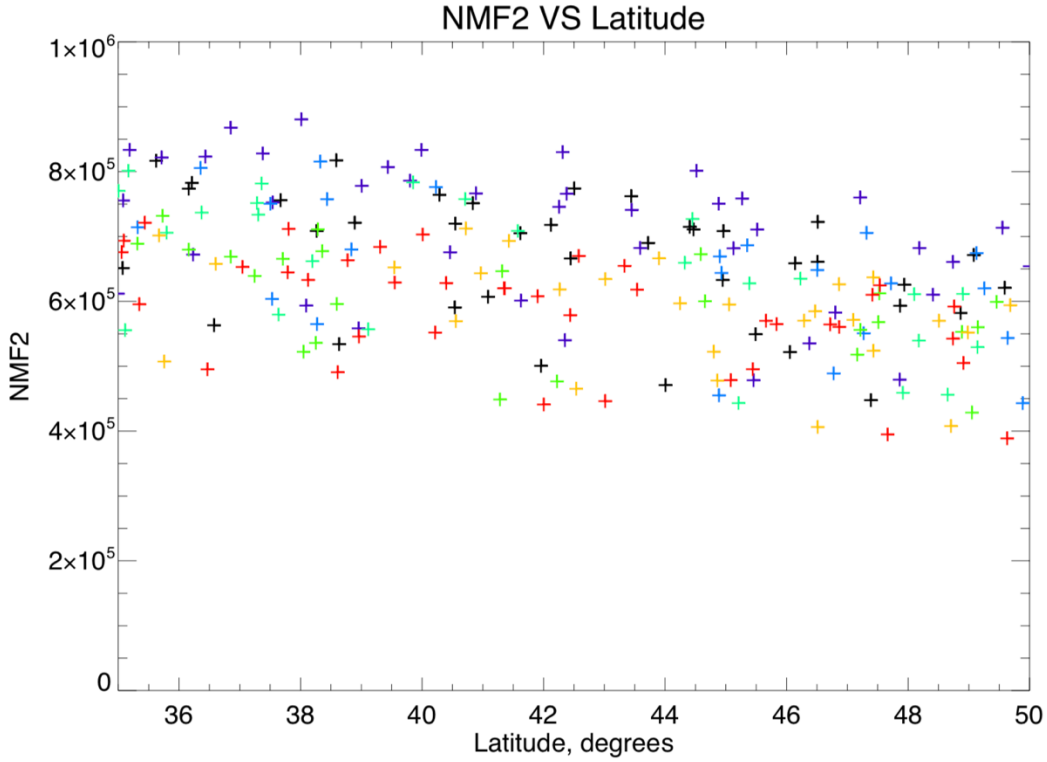

Figure 94: The figure shows how the NmF2 varies with latitude for IRI data

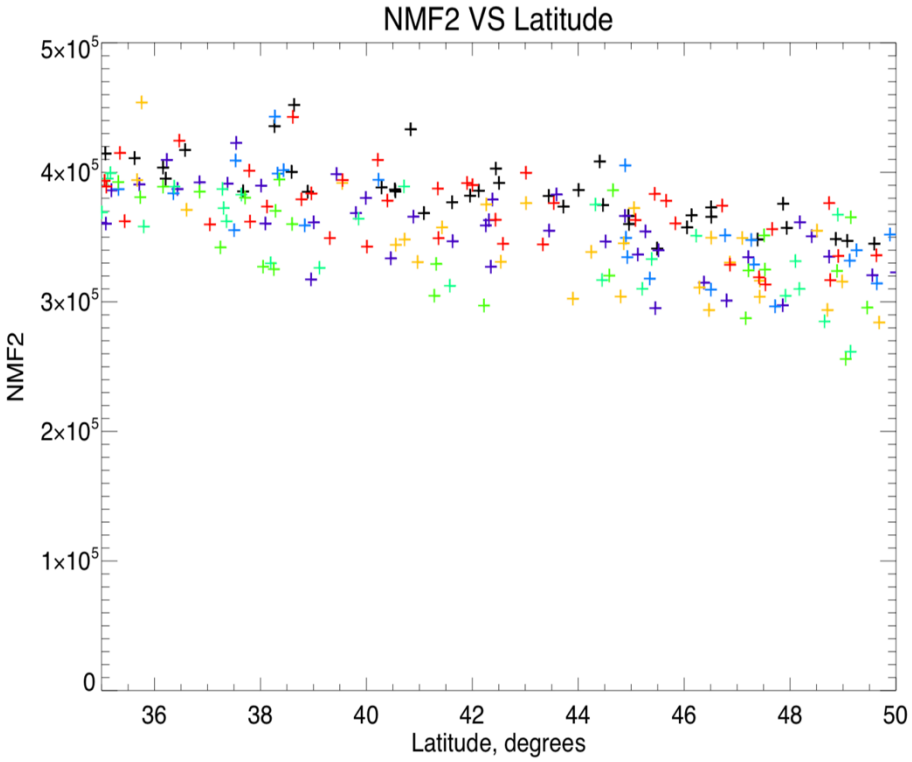

Figure 95: The figure shows how the NmF2 varies with latitude for TIEGCM data

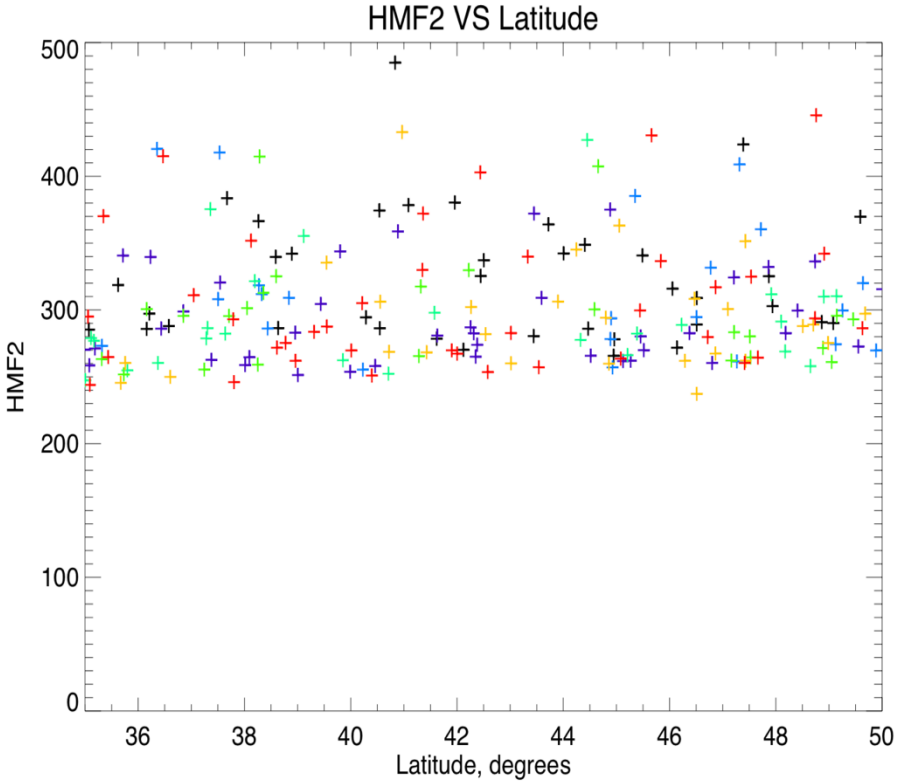

Figure 96: The figure shows how the HmF2 varies with latitude for SSULI data

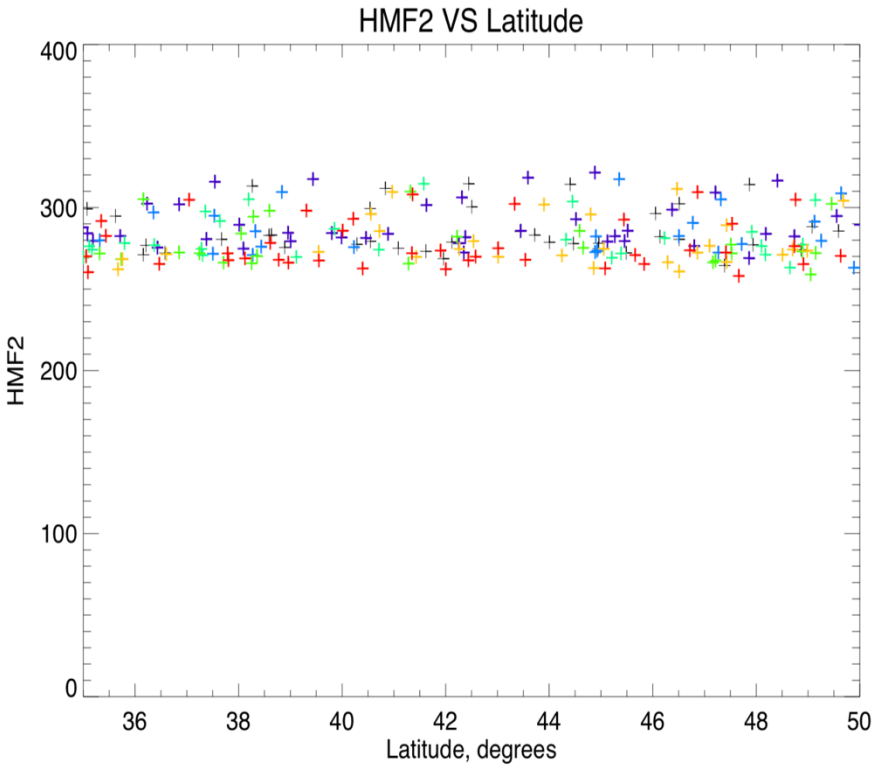

Figure 97: The figure shows how the HmF2 varies with latitude for IRI data

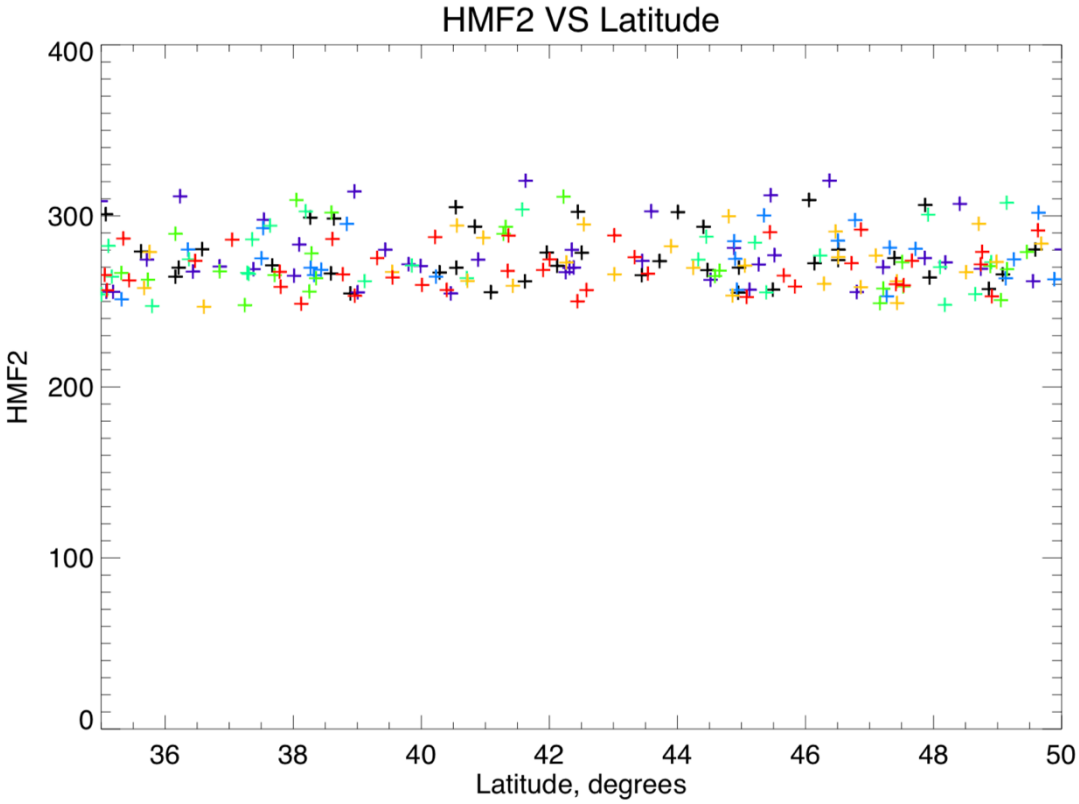

Figure 98: The figure shows how the HmF2 varies with latitude for TIEGCM data

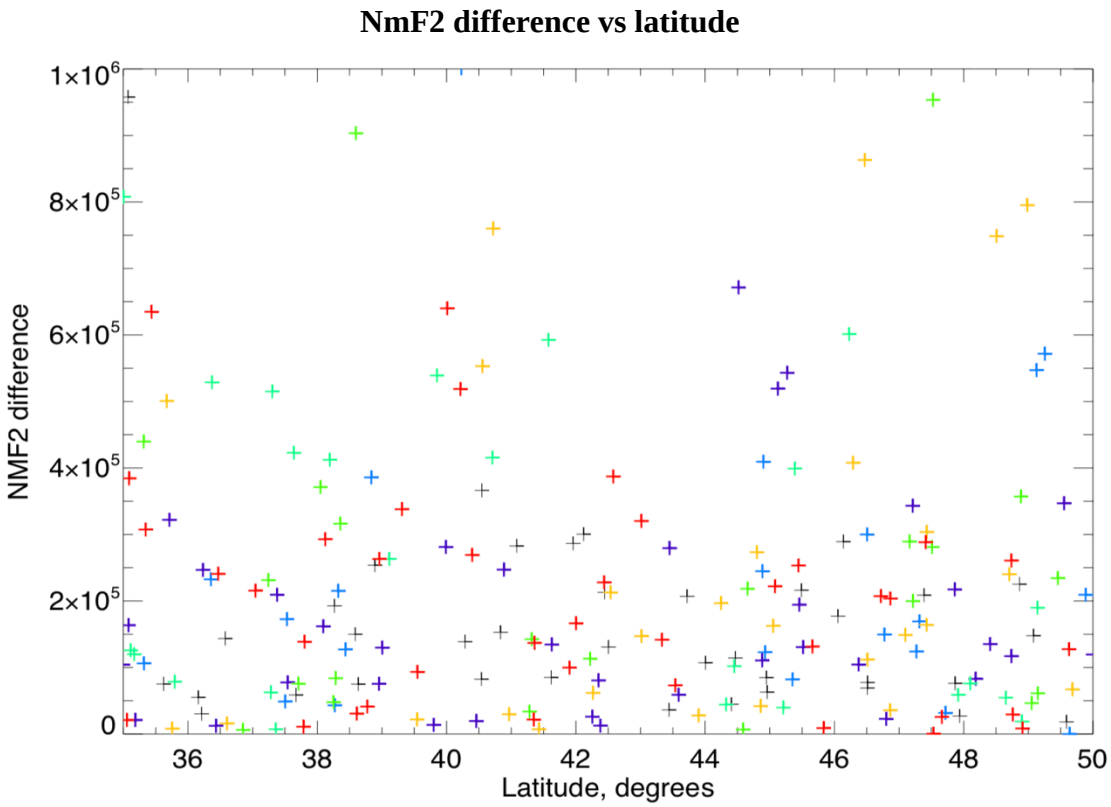

Figure 99: The figure shows how the NmF2 difference between IRI and SSULI data varies with latitude.

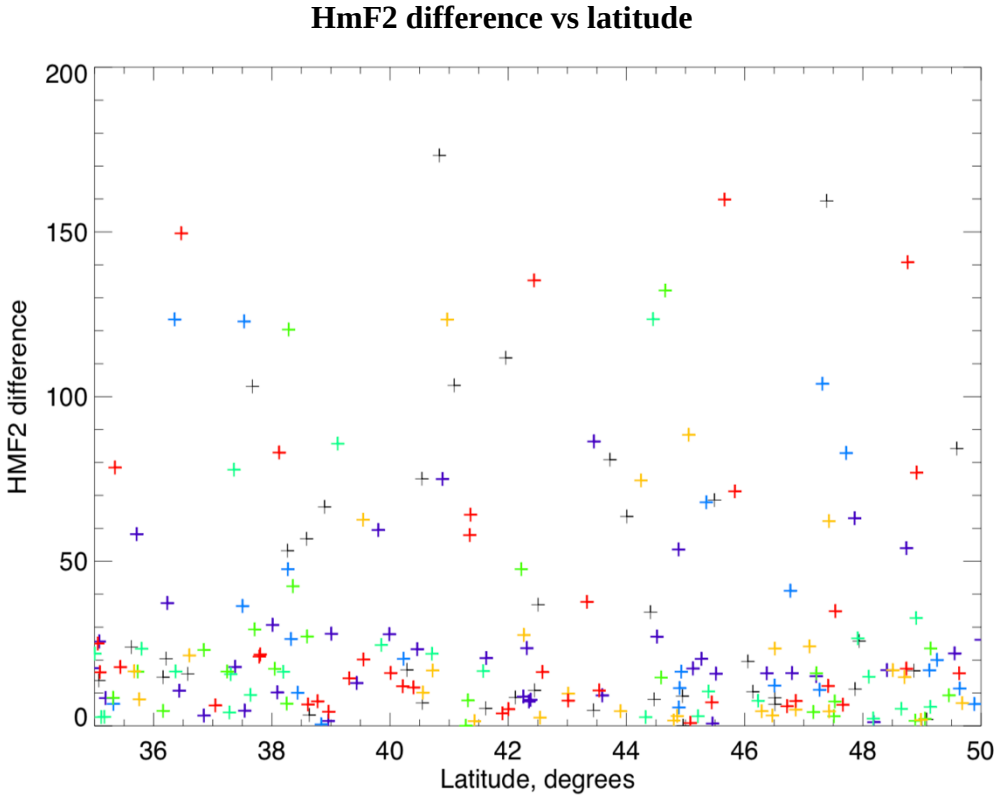

Figure 100: The figure shows how the HmF2 difference between IRI and SSULI data varies with latitude.

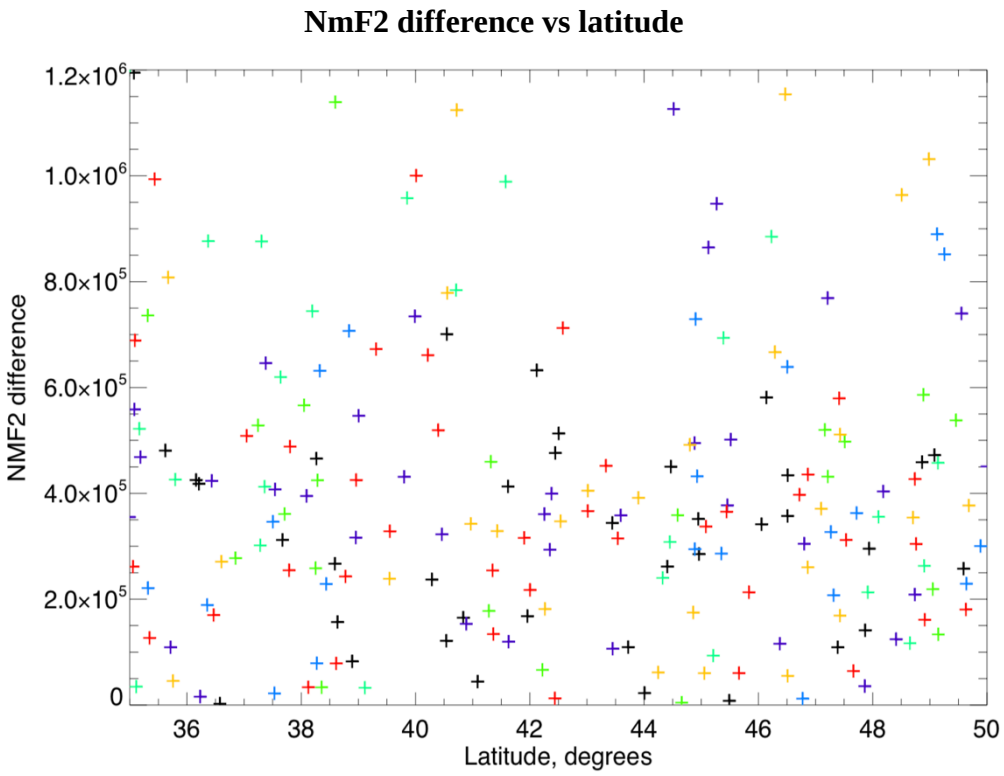

Figure 101: The figure shows how the NmF2 difference between TIEGCM and SSULI data varies with latitude.

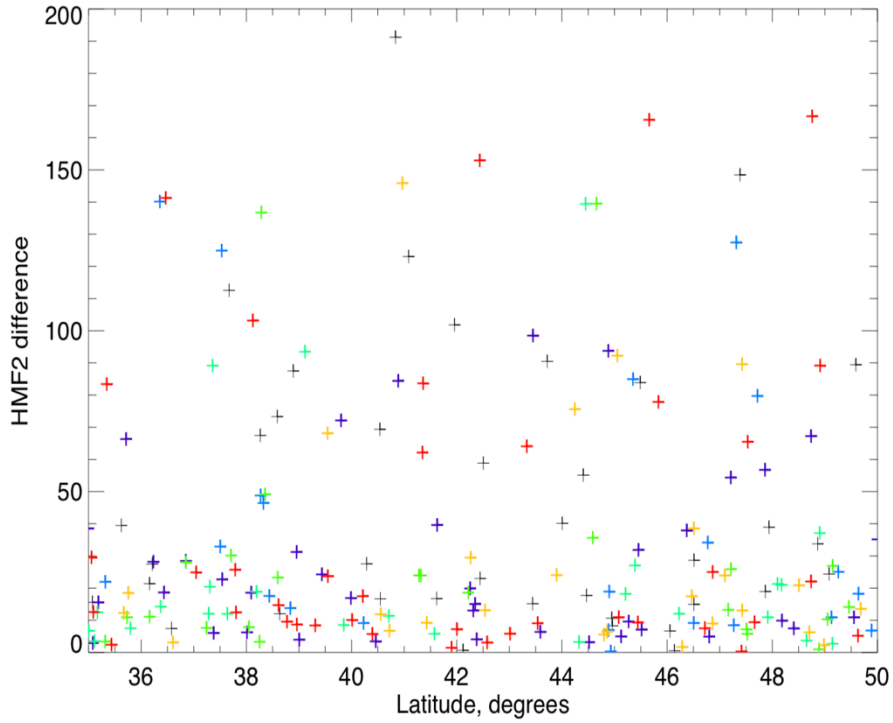

Figure 102: The figure shows how the HmF2 difference between TIEGCM and SSULI data varies with latitude.

3.4.4.2 Comparison of sunset data

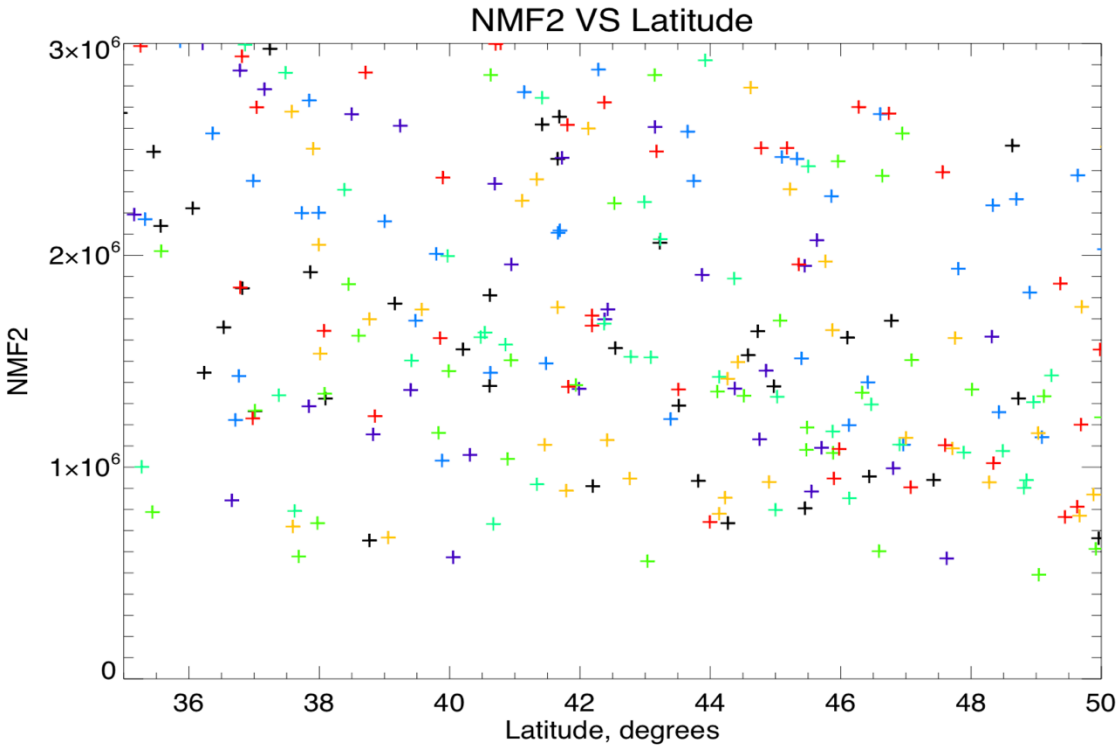

Figure 103: The figure shows how the NmF2 varies with latitude for SSULI data

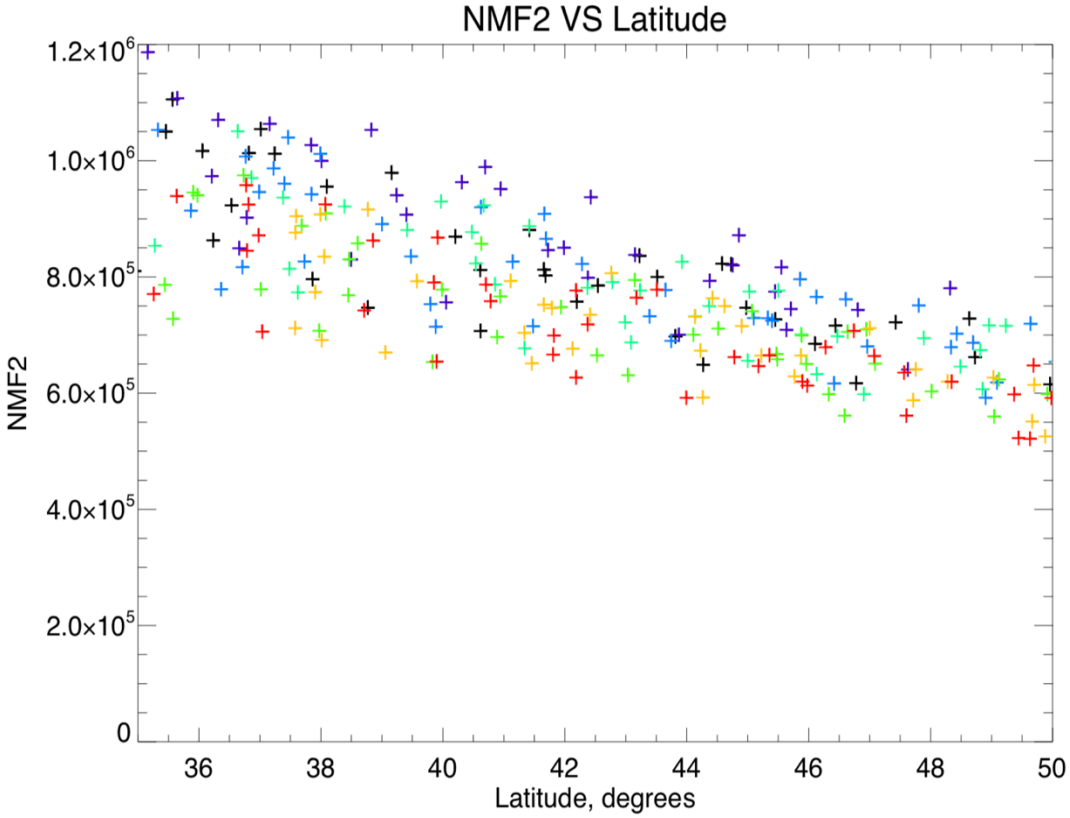

Figure 104: The figure shows how the NmF2 varies with latitude for IRI data

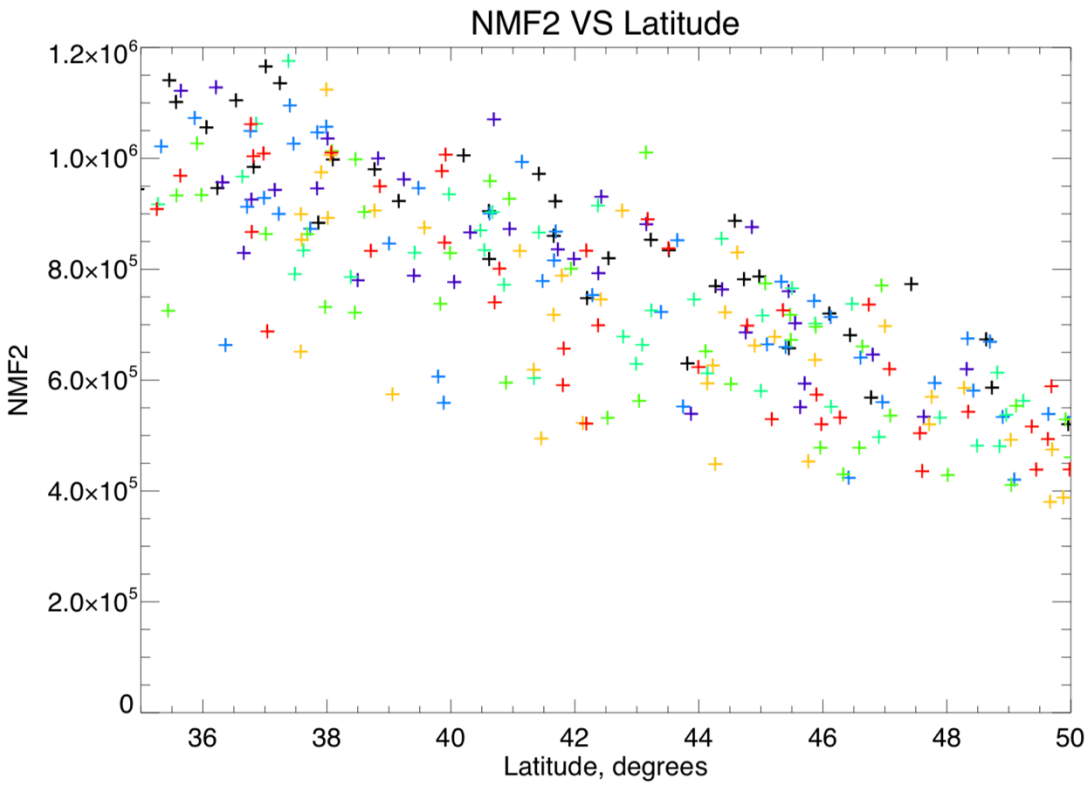

Figure 105: The figure shows how the NmF2 varies with latitude for TIEGCM data

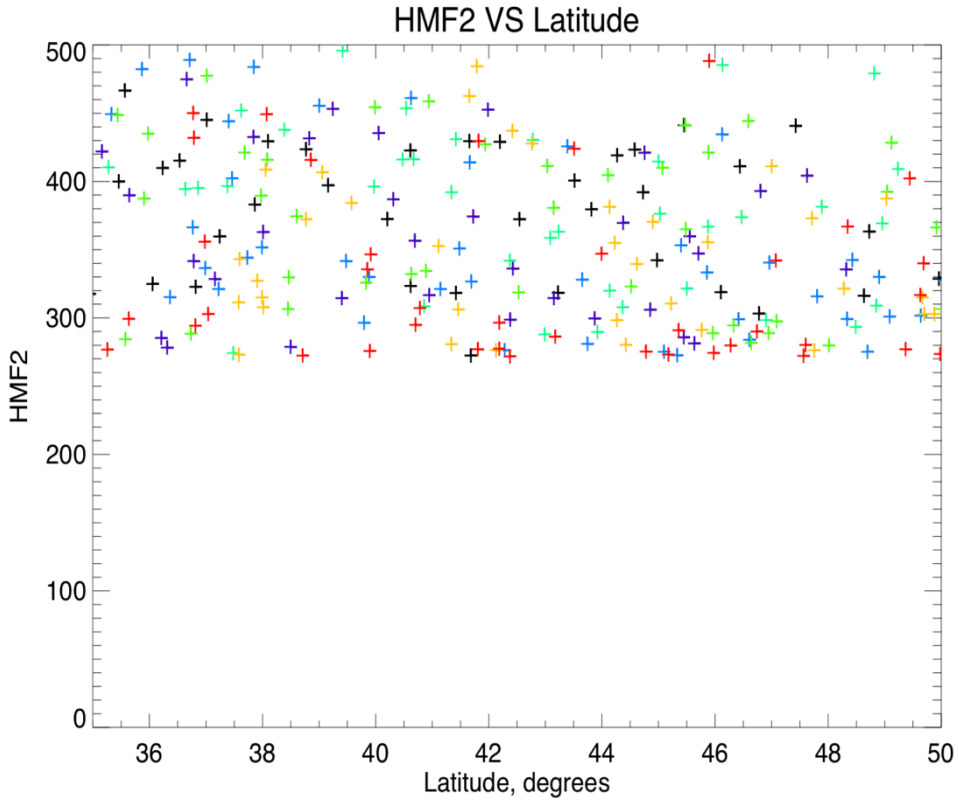

Figure 106: The figure shows how the HmF2 varies with latitude for SSULI data

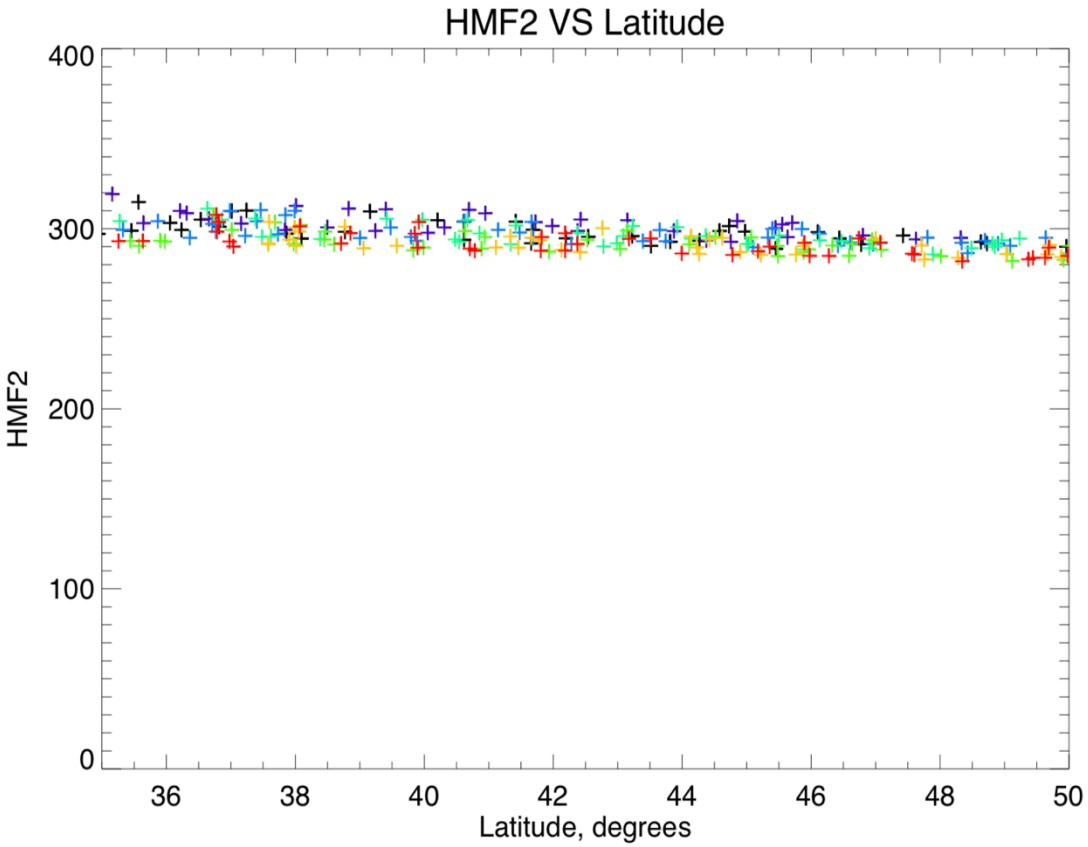

Figure 107: The figure shows how the HmF2 varies with latitude for IRI data

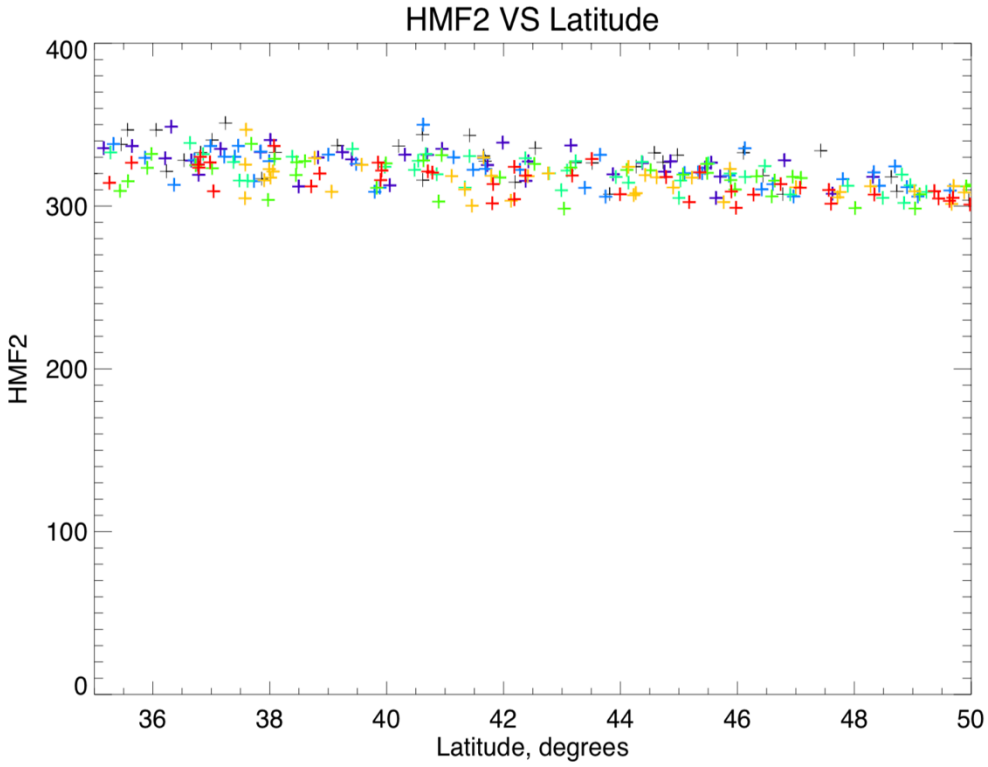

Figure 108: The figure shows how the HmF2 varies with latitude for TIEGCM data

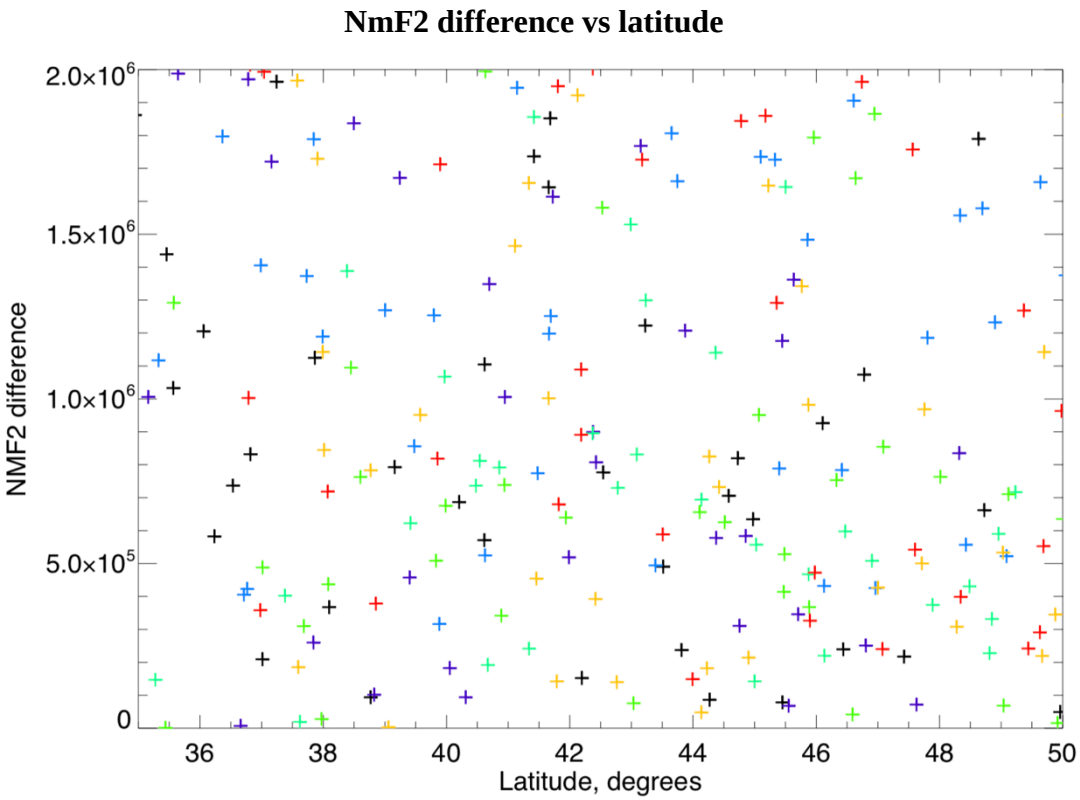

Figure 109: The figure shows how the NmF2 difference between IRI and SSULI data varies with latitude.

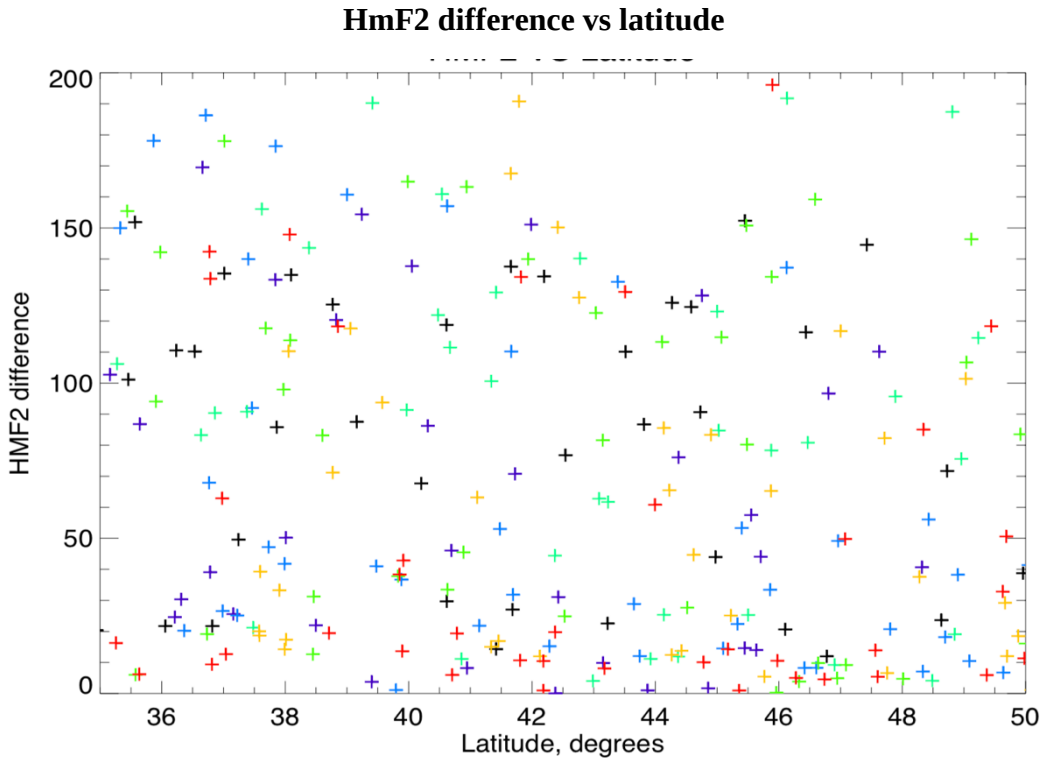

Figure 110: The figure shows how the HmF2 difference between IRI and SSULI data varies with latitude.

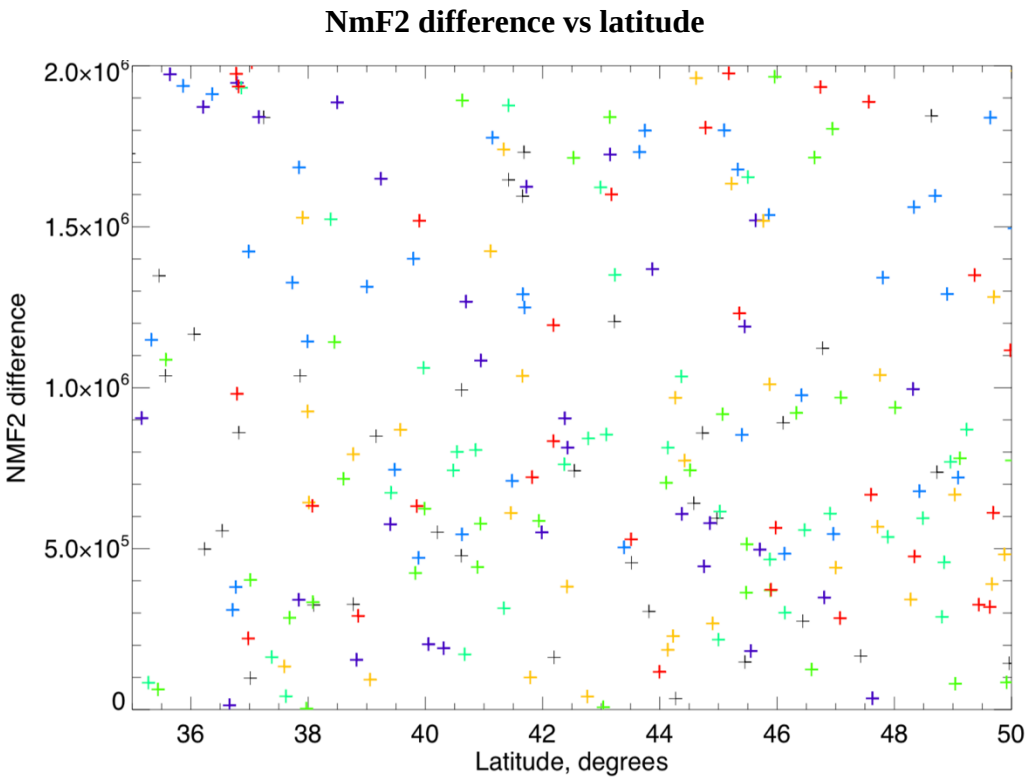

Figure 111: The figure shows how the NmF2 difference between TIEGCM and SSULI data varies with latitude.

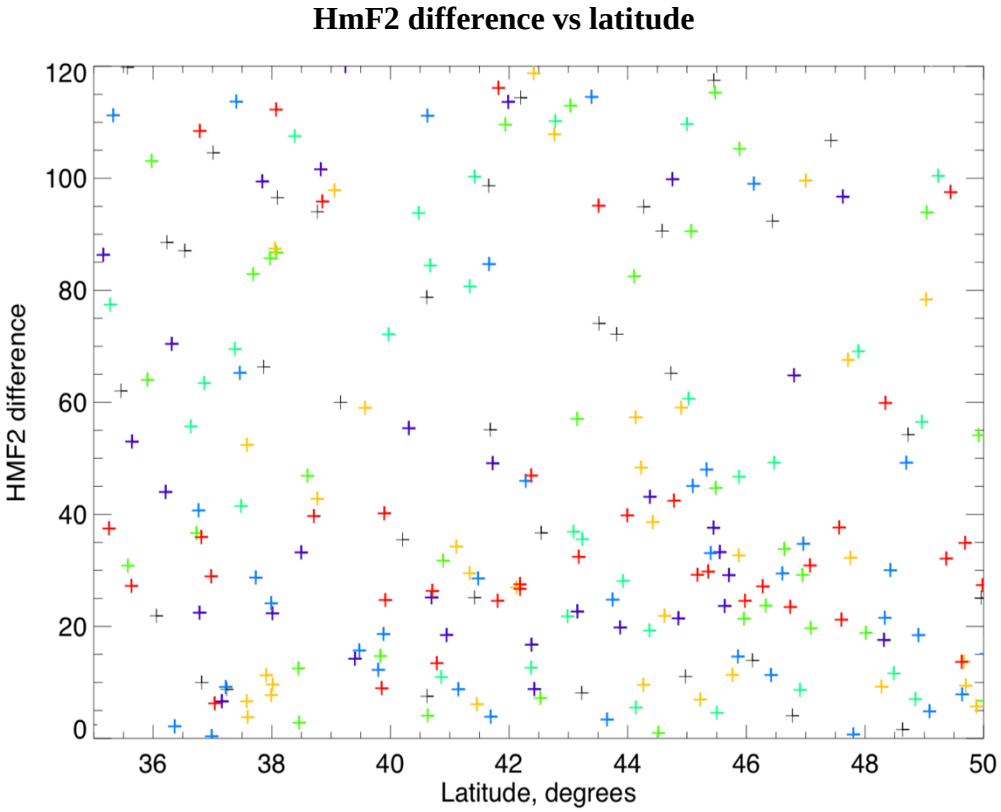

Figure 112: The figure shows how the HmF2 difference between TIEGCM and SSULI data varies with latitude.

From the above graphs we can see that the HmF2 values are higher in the mid latitude region during the sunset time compared to the sunrise time for the SSULI data and so do the NmF2 values. It can also be seen that the SSULI NmF2 values agrees better with the IRI values compared to the TIEGCM values during sunrise but the does not match that well with both the models during the sunset. In case of HmF2, irrespective of the time of observation, the values are quite scattered over the altitudes for SSULI data in the mid latitude region compared to the obtained from IRI and TIEGCM models.

3.5 Conclusions

- The HmF2 does not change much with magnetic latitude compared to geographic latitude.

- The NmF2 value is higher during sunset compared to sunrise.

- Higher the solar flux, more will be the HmF2 value.

- Natural day to day variability is greater than that caused by just a 30-point change in F107 index.

- During sunrise as the ionosphere is dominated by photoionization, SSULI data agrees better with IRI and TIEGCM models than sunset. But during sunset as the ionosphere is more dominated by the impact of motion resulted from (E×B), which is known to be highly variable, SSULI data disagrees with IRI and TIEGCM models.

- The mean density of SSULI data agrees with IRI data more closely than TIEGCM data.

In the mid latitude region, where there is good overlap between the SSULI sunrise and sunset data, we can separate latitudinal effects from sunrise-sunset differences. In this region, we find:

- The mean NmF2 value is highest during sunset.

- The mean HmF2 value is highest during sunset.

- The difference between the SSULI data and both IRI and TIEGCM models is greatest during sunset.

The above conclusions are quite similar to what we have expected from what has been seen with other datasets. Following this approach, if we performed a similar analysis with the ICON EUV dataset, and found similar results, this would confirm the basic reliability of the ICON EUV Level 2 dataset. Naturally, extending this analysis to a wider range of conditions may also yield new understanding, either of the data, the models, or both. Several such ideas are described in the next section.

3.6 Ideas for Future Work

As ICON is yet to be launched, in future when real time data is available from the EUV instrument, we have to use the same algorithms and codes described in chapter 2 of this section to retrieve the data from the instrument and compare it with different ground based and space based proxies. As EUV observes data every 12 seconds and throughout the day, in this case we will have the entire day's profile and not just sunrise and sunset data. The data obtained from EUV should match during the sunset with IRI and TIEGCM models but if the E×B drift is high then we will observe a variation of the of the EUV data with that of the model during the other times in the day.

Bibliography

Bowyer S, J. Edelstein, M. Lampton, Very high sensitivity extreme ultraviolet spectrometer for diffuse radiation. Astrophysics. J. 485(2), 523 (1997).

Charles Y. Johnson, 1966. Ionospheric composition and density from 90 to 1200 kilometers at solar minimum.
https://doi.org/10.1029/JZ071i001p00330

Cleary, D., R. Meier, E. Gentieu, P. Feldman, and A. Christensen (1989), An analysis of the effects of N2 absorption on the O^+ 834-A emissionfrom rocket observations, J. Geophysics. Res., 94(A12), 17,281–17,285, doi:10.1029/JA094iA12p17281.

Coley, W.R., Heelis, R.A., 1989. Low-latitude zonal and verticaldrifts seen by DE-2. Journal of Geophysical Research, 94,6751.

Dymond, K. F., A. C. Nicholas, S. A.Budzien, C. Coker, A. W. Stephan, and D.H. Chua (2017), The Special SensorUltraviolet Limb Imager instruments,J. Geophysics. Res. Space Physics, 122,doi:10.1002/2016JA022763.

Eccles, J.V., Maynard, N., Wilson, G., 1999. Study of the eveningplasma drift vortex in the low-latitude ionosphere using SanMarco electric field measurements. Journal of GeophysicalResearch 104, 28133.

Eccles, J.V., 1998a. Modeling investigation of the eveningpre-reversal enhancement of the zonal electric field in theequatorial ionosphere. Journal of Geophysical Research 103,26709.

Eccles, J.V., 1998b. A simple model of low-latitude electric fields.Journal of Geophysical Research 103, 26699.

Fejer, B.G., dePaula, E.R., Gonzalez, S.A., Woodman, R.F.,1991. Average vertical and zonal F region plasma drifts overJicamarca. Journal of Geophysical Research 96, 13901.

Feldman, P. D., D. E. Anderson Jr., R. R. Meier, and E. P. Gentieu (1981), The ultraviolet dayglow. IV: The spectrum and excitation of singlyionized oxygen, J. Geophysics. Res., 86(A5), 3583–3588, doi:10.1029/JA086iA05p03583.

Forbes, J.M., 1995. Tidal and planetary waves. In: Johnson,R.M., Killeen, T.L. (Eds.), The Upper Mesosphere and LowerThermosphere: A Review of Experiment and Theory, Vol. 87, AGU, Washington, DC.

Hagan M E, C. McLandress, J. M. Forbes, 1997. Diurnal tidal variability in the upper mesosphere and lower thermosphere.
https://link.springer.com/article/10.1007/s00585-997-1176-x

Heelis, R.A, Kendall, P.C., Moffett, R.J., Windle, D.W., Rishbeth,H., 1974. Electrical coupling of the E- and F-regions and itseffect on F-region drifts and winds. Planetary and Space Science22, 743.

Heelis R A, 2004. Electrodynamics in the low and middle latitude ionosphere: a tutorial. Journal of atmospheric and solar-terrestial physics, Volume 66, Issue 10, July 2004, Pages 825-838.https://doi.org/10.1016/j.jastp.2004.01.034.

Immel T J, S. L. England, 2017. The Ionospheric Connection Explorer Mission:Mission Goals and Design. Doi: 10.1007/s11214-017-0449-2.

Kamalabadi F, J. Qin, B. Harding, D. Iliou, J. Makela, R.R. Meier, S.L. England, H.U. Frey, S.B. Mende, T.J. Immel, Inferring nighttime ionospheric parameters with the Far Ultraviolet Imager onboard theIonospheric Connection Explorer. Space Sci. Rev. (2017).

Martin W C, V. Kaufman, A. Musgrove, A compilation of energy levels and wavelengths for the spectrum ofsingly-ionized oxygen (OII). J. Phys. Chem. Ref. Data 22, 1179 (1993). doi:10.1063/1.555928.

Maute, 2017. Thermosphere-Ionosphere-Electrodynamics General Circulation Model for the Ionospheric Connection Explorer: TIEGCM-ICON.
Volume 212, Issue 1–2, pages 523–551.

Meier, R. (1990), The scattering rate of solar 834 Å radiation by magnetospheric O^{+} and O^{++}, Geophysics. Res. Lett., 17(10), 1613–1616,doi:10.1029/GL017i010p01613.

Meier R R, 1991. Ultraviolet spectroscopy and remote sensing of the upper atmosphere.
Volume 58, Issue 1, pp 1–185.

Mende S B, Observing the magnetosphere through global auroral imaging: 2. Observing techniques. J. Geophysics. Res. 121, 10 (2016). doi:10.1002/2016JA022607

Mende S B, H. Heetderks, H.U. Frey, M. Stock, M. Lampton, S.P. Geller, R. Abiad, O.H.W. Siegmund, S.Habraken, E. Renotte, C. Jamar, P. Rochus, J.-C. Gérard, R. Sigler, H. Lauche,Far ultraviolet imagingfrom the IMAGE spacecraft. 3. Spectral imaging of Lyman-α and OI 135.6 nm. Space Sci. Rev. 91,287–318 (2000).

Picone J M, R. R. Meier, 1997. Investigation of ionospheric 0+ remote sensingusing the 834-A airglow.
Journal of Geophysical Research, vol. 102, no. A2, pages 2441-2456.

Rishbeth, H., 1971b. Polarization fields produced by winds in theequatorial F region. Planetary and Space Science 19, 357.

Sirk M M, E.J. Korpela, Y. Ishikawa, J. Edelstein, E.H. Wishnow, C. Smith, J. McCauley, J.B. McPhate, J.Curtis, T. Curtis, S.R. Gibson, S. Jelinsky, J.A. Lynn, M. Marckwordt, N. Miller, M. Raffanti, W. VanShourt, A.W. Stephan, T.J. Immel, Design and performance of the ICON EUV spectrograph. Space Sci.Rev. (2017), this issue. doi:10.1007/s11214-017-0384-2

Stephan A W, E.J. Korpela, M.M. Sirk, S.L. England, T.J. Immel, Daytime ionosphere retrieval algorithm for the Ionospheric Connection Explorer (ICON). Space Sci. Rev. (2017a), this issue.doi:10.1007/s11214-017-0385-1

Stephan A W, R.R. Meier, S.L. England, H.U. Frey, S.B. Mende, T.J. Immel, Daytime O/N_2 retrieval algorithm for the Ionospheric Connection Explorer (ICON). Space Sci. Rev. (2018).

Stephan A W, (2016), Advances inremote sensing of the daytime ionosphere with EUV airglow, J. Geophysics. Res.Space Physics, 121, 9284–9292,doi:10.1002/2016JA022629.

Wharton, L.E., Spencer, N.W., Mayr, H.G., 1984. The Earth'sthermospheric super rotation from Dynamics Explorer 2.Geophysical Research Letters 11, 531.